12-14-2016

A Study of Mineral Impurities within the Georgia Kaolins

Daniel J. Gardner
Georgia State University

A STUDY OF MINERAL IMPURITIES WITHIN THE GEORGIA KAOLINS

by

DANIEL GARDNER

Under the Direction of W. Crawford Elliott, Ph.D.

ABSTRACT

The mining industry located along the fall line region of central Georgia has been and remains as one of the largest global exporters of the clay mineral kaolinite. Among the kaolin deposits in that region, the Cretaceous Buffalo Creek formation and the Eocene Jeffersonville member contain the most commercially viable kaolin to extract and process for resale. The minerals of the sand and silt fractions of these kaolin units were separated via dense liquid separation and analyzed for comparison by X-ray diffraction, scanning electron microscopy, and elemental analysis. The dense fractions are enriched in select heavy minerals (zircon and rutile) and trace elements (rare earth). These elemental enrichments and the differences in the mineral maturity of these gangue (grit) fractions suggest differences in the provenance of the gangue minerals between these two different kaolins.

INDEX WORDS: Kaolinite, Gangue, Grit, Buffalo Creek, Jeffersonville,

A STUDY OF MINERAL IMPURITIES WITHIN THE GEORGIA KAOLINS

by

DANIEL GARDNER

A Thesis Submitted in Partial Fulfillment of the Requirements for the Degree of

Master of Science

in the College of Arts and Sciences

Georgia State University

2016

A STUDY OF MINERAL IMPURITIES WITHIN THE GEORGIA KAOLINS

by

DANIEL GARDNER

Committee Chair: W. Crawford Elliott

Committee: Brian K. Meyer

Daniel M. Deocampo

Electronic Version Approved:

Office of Graduate Studies

College of Arts and Sciences

Georgia State University

December 2016

DEDICATION

This thesis is dedicated above all to my family and friends who provided constant support during my time at Georgia State University. It is further dedicated to the many students who enjoyed my teaching style and showed interest in the many interdisciplinary aspects of geology which I emphasize so extensively. Without the support and interest from my students, this thesis would not have been possible.

ACKNOWLEDGEMENTS

I acknowledge the constant support, contributions, and suggestions provided by my academic advisor Dr. W. Crawford Elliott. I thank my committee members Dr. Brian Meyer and Dr. Daniel Deocampo for contributions and support in the writing of this thesis. I thank Ed Riley of the Thiele Kaolin Company for the production of the grit samples analyzed in this thesis. I thank Dr. Prakash Malla of the Thiele Kaolin Company for the support of this research. I thank the Thiele Kaolin Company for supporting and hosting this research. I thank Dr. Robert Simmons for the SEM analyses conducted for this thesis. I thank Nathan Rabideaux and David Davis from the GSU department of Geosciences for the XRD analyses conducted for this thesis.

TABLE OF CONTENTS

LIST OF TABLES

LIST OF FIGURES

1 INTRODUCTION

1.1 The Georgia Kaolins

The kaolin mining industry in Georgia is located geographically along the fall line region of central Georgia. The Georgia Kaolin District is centered in Sandersville, GA. It has been, and remains, as one of the largest global exporters of kaolinite (Schroeder and Erickson, 2014). The Cretaceous Buffalo Creek Formation and the Eocene Jeffersonville Member of the Huber Formation contain the most commercially viable kaolin to extract and process among the kaolin bearing units in the Georgia Kaolin district. Kaolinite mined in this region has many industrial uses and can be found in numerous household products including, paper coating, ceramics, rubber, plastics, pharmaceuticals, paints, cosmetics, medical supplies, and electronic hardware (Schroeder and Erickson, 2014; Elzea-Kogel et al., 2002). Although the Buffalo Creek Formation and Jeffersonville Member are both extensively mined, these kaolin bearing units differ in color, brightness, composition, and mineralogy. The following subsections give descriptions of the Buffalo Creek and Huber Formation. Following the descriptions of the formations, the geologic history of the Georgia Kaolins is summarized. The primary focus of this study is on the occurrences of the lanthanide rare earth metals in these two formations of the Georgia Kaolins. The potential for reserves of these rare earth elements and the hypotheses explaining their presence in the Georgia Kaolins are stated at the end of this introduction.

1.1.1 Buffalo Creek Formation

The Buffalo Creek Formation was deposited during the late Cretaceous Period. The kaolins within this formation are relatively soft, coarse-grained (approximately 55-65% <2 μm), and laterally discontinuous (Elzea-Kogel, 2002). The Buffalo Creek Formation contains many fining upward sand sequences and is capped by characteristic, soft kaolin lenses (Pickering and

Avant, 1999; Elzea-Kogel et al, 2002). A freshwater origin was suggested by Kesler (1963). This origin explains the lack of marine fossils and the random orientation of kaolin crystals (Murray, 1980). Cramer (1974) and Elzea-Kogel (2002) observed characteristic deltaic subsurface facies patterns in Buffalo Creek kaolin-bearing sediments and concluded that the kaolin-bearing formations were of deltaic nature. Pickering and Linkous (1997) observed similarities between the Upper Cretaceous Brazilian Capim kaolins and the Buffalo Creek kaolins of Georgia. These similarities were consistent with Cramer's conclusions that the soft kaolins formed in a freshwater deltaic location (Elzea-Kogel et al, 2002).

Buffalo Creek Formation kaolins are cream in color and contain low concentrations of organic material. They exhibit conchoidal fracture in outcrop. These kaolins are mostly composed of large concentrations of kaolinite and, smaller concentrations of muscovite and quartz (Figure 1; Cheshire, 2011). Elser (2004) also noted thumb-nail sized muscovite grains in the Buffalo Creek kaolins.

Figure 1: Buffalo Creek Kaolin in outcrop showing conchoidal fracture

Trace minerals found within the Buffalo Creek kaolins include anatase, rutile, and zircon. Cheshire (2011) noted a sizable concentration of the rare earth element bearing phosphate mineral, monazite, within Buffalo Creek kaolins. As shown later in this thesis, the Buffalo Creek kaolins contain sizable amounts of rare earth elements. Unlike Cheshire's observation however, the rare earth elements seen in this study are believed to be sequestered in the zirconium bearing mineral grains. The thickness of the Buffalo Creek Formation varies from zero to approximately ten meters (Cheshire, 2011). The Buffalo Creek Formation was sampled from Washington County in this study. Cheshire (2011) reported exposures of the Buffalo Creek Formation in Wilkinson County as well. Cheshire also reported that no exposures of the Buffalo Creek Formation were observed east of Washington County. Buffalo Creek kaolins have however been reported west of Wilkinson County and are believed to extend to the Ocmulgee River as shown below (Figure 2) (Cheshire, 2011).

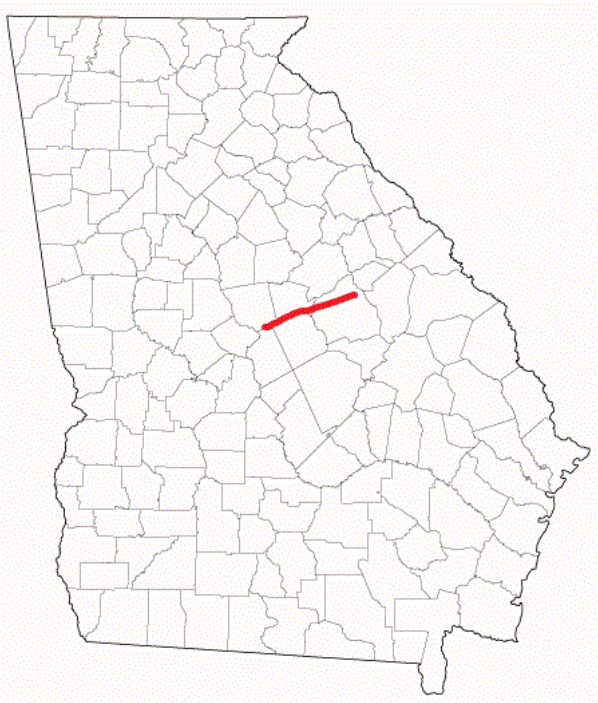

Figure 2: Map showing lateral extent of Buffalo Creek Formation in red. Image modified from Vilsack, 2009

1.1.2 Huber Formation

The Tertiary Huber Formation uncomfortably overlays the Buffalo Creek Formation in the Georgia Kaolin District. The Huber Formation is sub-divided into two members, the Paleocene Marion member and the Eocene Jeffersonville member. The Paleocene Marion Member contains soft, unoxidized, kaolins which are gray to black in color (Figure 3) (Pickering and Avant, 1999). The Marion Member is similar to the Buffalo Creek in many ways such as kaolin concentration and age as suggested by palynology data (Prowell and Christopher, 2000). The primary difference is that the Marion Member contains higher amounts of organics, lignite, and an abundance of iron sulfides (Cheshire, 2011). Since the Marion Member is not commercially viable to mine and process, it was not sampled during this study. Lignite bearing Marion Member kaolins can be seen in the figure below.

Figure 3: Dark colored Marion Member kaolins in foreground, lighter colored Jeffersonville Member kaolins can be seen in the background

The Eocene Jeffersonville Member of the Huber Formation contains what is often referred to as “hard kaolin”. These hard kaolins differ from the Buffalo Creek in hardness, particle size, iron content, and presence of Eocene age trace fossils (Pickering and Avant, 1999). The grain size of the Jeffersonville Member kaolins is finer (approximately 80-90% <2 μm) than the Buffalo Creek kaolins (Cheshire, 2011). The Jeffersonville Member contains abundant trace fossils as well as having a much higher iron and silica content compared to the Buffalo Creek Formation (Cheshire, 2011). The Jeffersonville Member is also more laterally continuous than the Buffalo Creek Formation. It extends as far west as the Ocmulgee River and east to Aiken, South Carolina (Huddlestun and Hetrick, 1991; Figure 4).

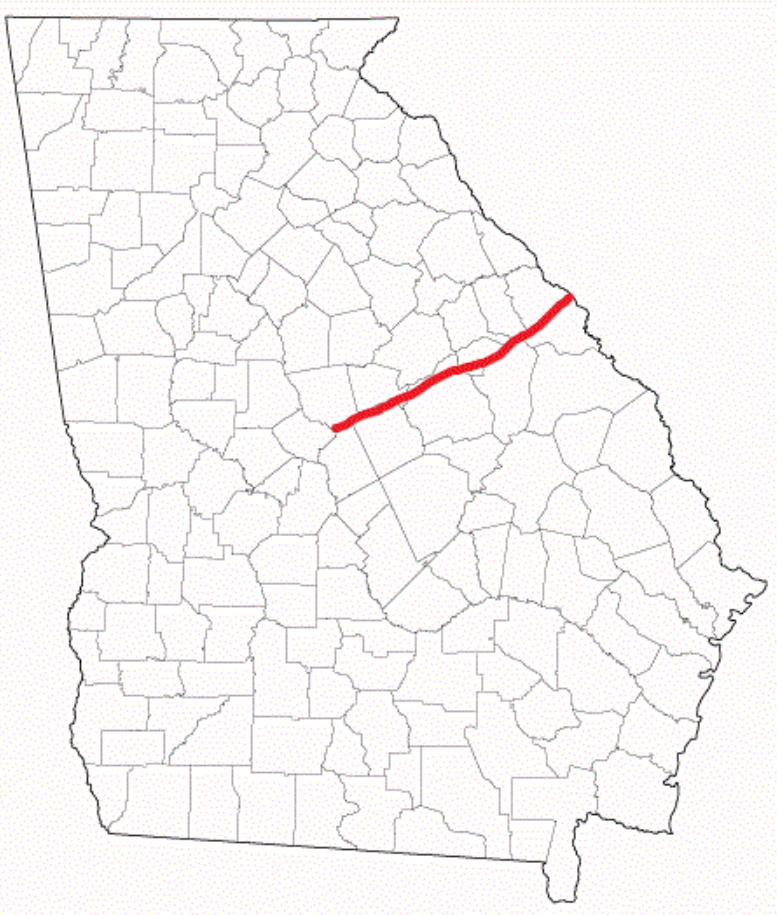

Figure 4: Map showing lateral extent of Jeffersonville Member kaolins in red. Image modified from Vilsack, 2009

The Jeffersonville Member is near-white to gray in color. Many trace fossils can be observed in outcrop samples of Jeffersonville Member kaolin. It is primarily composed of kaolinite and quartz. Trace minerals found within the Jeffersonville member include rutile, anatase, pyrite, tourmaline, zircon, and ilmenite. Similarly to the Buffalo Creek Formation, trace amounts of rare earth elements were also found within Jeffersonville Member kaolins as detailed later in this study. As will be shown, the concentrations of rare earth elements are less than the amounts of rare earth elements in the Buffalo Creek.

1.2 Geologic History of the Georgia Kaolins

Although the complex geologic history of the Georgia Kaolins has been extensively studied, disagreements and confusion pertaining to the provenance, alteration, and stratigraphy of the clay minerals in the Georgia Kaolins remain among researchers (Cheshire, 2011). Recent studies (Cheshire, 2011; Elzea-Kogel et al, 2002) suggest that three separate "super-greenhouse" events were responsible for the majority of the "kaolinization" of primary minerals such as micas and feldspars. These micas (muscovite) and feldspars were deposited by sedimentary processes forming the Cretaceous Buffalo Creek Formation and the Tertiary Huber Formation. Although these "super-greenhouse" events were likely responsible for the majority of kaolinization, the kaolinization process most likely began as the mica and feldspar were weathered from felsic bedrock by chemical and mechanical weathering. These weathering processes continued during fluviatile transport. These sediments were weathered by in-situ chemical processes after deposition. The following subsection describes the complex geologic history of the Georgia Kaolins in more detail.

1.2.1 Paleogeography and Paleoclimate

Beginning in the Cambrian, modern-day Georgia was located on the edge of the Laurentian Craton. The Laurentian Craton was part of the Rodina Supercontinent that formed in the latter part of the Precambrian Era. As a result of the breakup of the supercontinent Rodinia, global temperatures increased during the later Precambrian and into the Cambrian Period (Prothero and Dott, 2004). The increase in global temperatures resulted in increased sea levels transgressing onto the continents. These transgressive seas lead to the sedimentary deposits found on many passive margins along the Laurentian Craton (Prothero and Dott, 2004). Without the influence of terrestrial plants, rates of physical weathering were much higher and thus these passive margins became hosts to an abundance of sand and silt deposition (Prothero and Dott, 2004). The mass of clastic sediments accumulated east of the edge of the Laurentian Craton causing subsidence east of the Craton. Part of this leading edge later was subducted beneath an island arc located further east of the Craton (Figure 5).

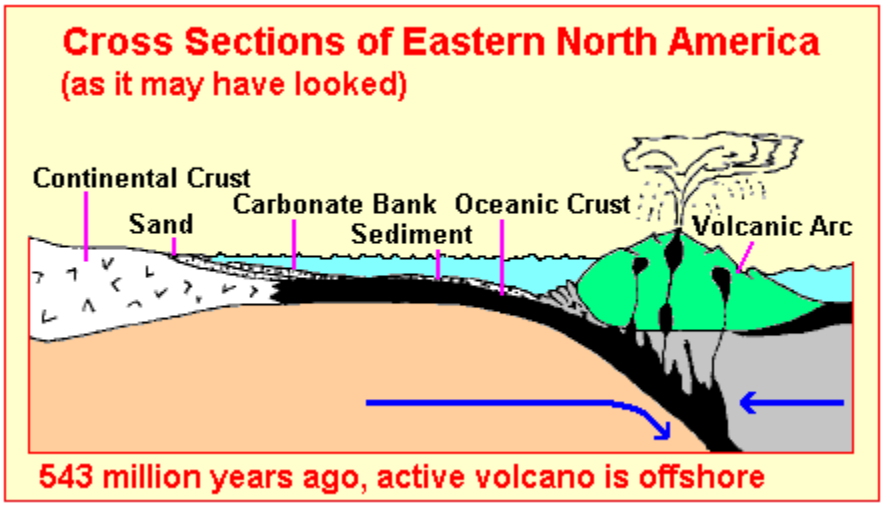

Figure 5: An offshore subduction formed as a result of the mass of accumulated sediments on the continental shelf. Image modified from Plank and Shenck 1998

In the Ordovician Period, this region was affected by the Taconic Orogeny. The Taconic Orogeny thrusted the shallow carbonate bearing sea and granitic island arc up onto the

Laurentian Craton (Figure 6; Miller et al., 2006). In addition to thrusting these rocks onto the craton, the orogeny metamorphosed the carbonate rocks and the granitic island arc. These granites docked onto North America and are now the Piedmont and Blue Ridge rocks of Georgia. The sedimentary sands were minimally metamorphosed to sandstones. These sandstones and carbonate rocks are seen in the Valley and Ridge Province of modern day northwestern Georgia. The Acadian Orogeny of the Devonian Period featured the docking of the metamorphic island arc material onto the North American craton. This docking further contributed to the metamorphism and weathering of the Blue Ridge Mountains and Piedmont Province. Based on the thickness of the post-orogenic sediments (e.g. Devonian Clastic Sequence, Ohio Black Shales, Chattanooga Shale), the Acadian Orogeny had a stronger impact on the New England region than the southeastern United States (Prothero and Dott, 2004). In the Carboniferous Period the craton, including the region to become Georgia, underwent the Alleghenian Orogeny. This collision was part of a larger assembly of continents leading to the formation of the supercontinent Pangaea (Miller et al., 2006). Piedmont, Blue Ridge, and other micro terranes are viewed as suspect terranes. These terranes were docked onto North America during the Taconic or Acadian Orogeny (Williams and Hatcher, 1982). Following and during the Alleghenian Orogeny, a series of three, post-metamorphic intrusions occurred in the Piedmont province which resulted in the formation of the Sparta Granite [~299 Ma], Siloam Granite [~270 Ma], and Edgefield Granite [~255 Ma] (Jones and Walker, 1973; Fullagar and Butler, 1976; Snoke et al., 1980).

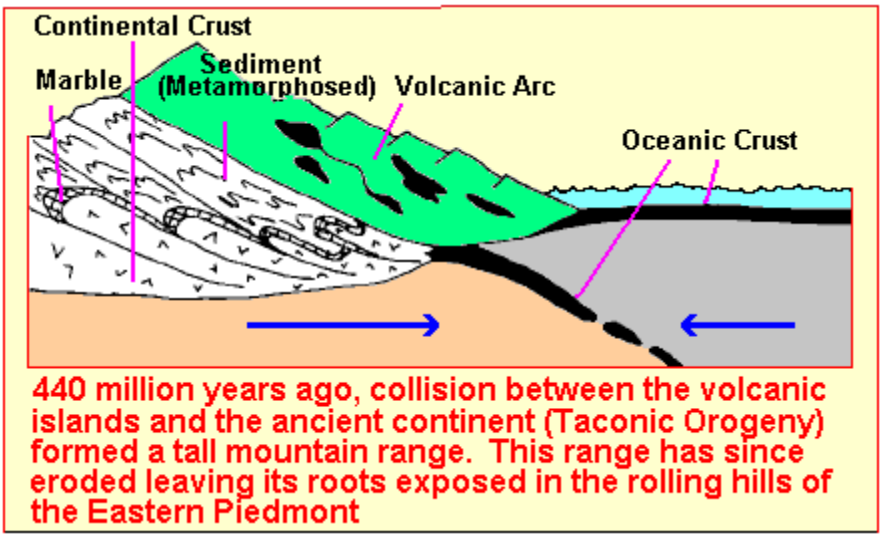

Figure 6: As a result of the Taconic Orogeny, offshore carbonates and the volcanic island arc were thrust upon Laurentia forming the Blue Ridge Mountains and Piedmont Province. Image modified from Plank and Shenck 1998

In the Triassic Period, the supercontinent Pangaea began to rift apart. A passive margin formed at the paleo-coastline located along the Fall Line of the southeastern United States. The rifting of Pangaea was an integral step in the formation of the Georgia Kaolins as it promoted the deposition of weathered felsic sediments in the newly formed continental shelf southeast of the SW-NE trending Fall Line (Cheshire, 2011). An increase in global temperature as suggested by a negative shift in $\delta^{18}O$ values in planktonic foraminifera coincides with the rifting of Pangaea (Frankes et al., 2005). This increase in temperature would have promoted the weathering and erosion of Blue Ridge and Piedmont derived sediments which would contribute to the formation of the Atlantic Coastal Plain (Cheshire, 2011; Frankes et al., 2005). Aside from the increase in global temperatures, the abundance of evaporites which formed in Europe at that time also suggests an arid environment was present (Chamley et al., 1979; Hallam, 1984; Frakes et al., 1992). The arid climate would not favor the kaolinization of micas and feldspars by chemical weathering at that time (Cheshire, 2011). Moving into the early Cretaceous however, the Atlantic

Ocean continued to open which resulted in the climate cooling as well as becoming more humid (Frakes et al., 1992).

Following the rifting of Pangaea, three separate "super-greenhouse" periods occurred from Cretaceous (Albian) to Tertiary (Paleocene). These super-greenhouse periods are times of extensive chemical weathering. It is believed that the sediments eroded from the Blue Ridge and Piedmont were altered to kaolinite during one or all three of these super-greenhouse periods (Cheshire, 2011). The first "super-greenhouse" period occurred during the Albian age of the early Cretaceous period. While the specific cause of this "super-greenhouse" period remains unknown, it is believed that it occurred in response to elevated atmospheric CO_2 concentrations along with increased humidity levels as a result of the opening of the Atlantic Ocean (Poulsen et al., 2003). The second "super-greenhouse" period occurred shortly after, around the time of the Cenomanian-Turonian boundary (91 Ma) in the Cretaceous period. These first two "super-greenhouse" periods are believed to have formed the majority of the Buffalo Creek kaolins by saprolization (Cheshire, 2011). At the time of these first two "super-greenhouse" periods, the area in which the Buffalo Creek Formation would have been deposited would have been around 20-40^{o}N latitude and 70-80^{o}W longitude (Lehman, 1987; Frakes et al., 1992). This tropical-subtropical environment would have greatly accelerated the erosional and saprolization processes (Cheshire, 2011). The deposition of the Buffalo Creek Formation is believed to have continued through the late Cretaceous, at which time global cooling resulted in regressing sea-levels (Norris et al., 2001). Global cooling would have caused a reduction in saprolization as well as kaolinite forming processes. In addition, the regressing sea level would expose deposited portions of Buffalo Creek Formation which would increase physical erosional processes. These increased erosional processes are likely responsible for the unconformity between the Buffalo

Creek and Huber formations as well as the laterally discontinuous nature of the Buffalo Creek kaolins (Cheshire, 2011).

In the Paleocene, the climate began to warm again (Zachos et al., 2001). The Marion Member is believed to have been deposited at this time (Cheshire, 2011). Despite belonging to a different formation than the Buffalo Creek, similarities can be observed between the two formations. It was hypothesized that they are derived from the same saprolite area of the weathered Piedmont province (Cheshire, 2011). In addition, any differences observed between the two, such as the preservation of higher organic content and finer grain sizes, can be attributed to the difference in depositional environment (Elzea-Kogel et al., 2002; Cheshire, 2011).

Following the deposition of the Marion Member in the mid Paleocene, global temperatures greatly increased during the Paleocene-Eocene Thermal Maximum (PETM) and Early Eocene Optimum (Zachos et al., 2001). These extreme temperatures would have further promoted the kaolinization and saprolization processes. Palynology data provided by Prowell and Christopher (2000) suggests that the Jeffersonville Member was deposited during the early-mid Eocene. Cheshire (2011) further suggests that the third "super-greenhouse" period would have occurred during the Early Eocene Optimum. Following this third "super-greenhouse" period and the deposition of the Jeffersonville Formation, another major transgression submerged the southeastern United States (Cheshire, 2011). It was during this time that the Barnwell Group was deposited (Cheshire, 2011). The Barnwell Group includes the Late Eocene Clinchfield Sand Formation and the Twiggs Clay Formation (Pickering and Avant, 1999). Following the Eocene, sea level dropped in response to the formation of polar ice caps. This drop in sea level resulted in the erosion of coastal plain sediments which exposed Piedmont igneous and metamorphic rocks and uncovered the fall line where it currently exists (Cheshire, 2011).

1.3 Rare Earth Element Mining and Consumption in the United States

Although domestic reserves of rare earth elements are estimated at approximately 1,300,000 metric tons, the United States remains a net importer of the rare earth elements (Gambogi, 2016). In 2015 the United States consumed approximately 17,000 tons of rare earth elements and produced approximately 4,100 tons of rare earth elements (Gambogi, 2016). The cost of imported rare earth elements in 2015 was estimated at $150,000,000 (Gambogi, 2016). Few companies domestically mined rare earth elements in 2015 and those who did focused primarily on the fluorocarbonate mineral, bastnasite, which was mined from reserves located in Mountain Pass, California (Gambogi, 2016).

1.3.1 Alternative Sources of Rare Earth Elements

Due to industrial and technological advancement in recent years, the demand for rare earth elements has greatly increased and less conventional sources of rare earths are being explored for economic viability. Previously, four primary types of deposits were known for containing rare earth elements (Van Gosen, 2014). These deposits include carbonatites, alkaline igneous rocks, ion-adsorption clays, and monazite-xenotime-bearing placer deposits (Van Gosen, 2014). Recent studies however suggest the potential of rare earth extraction from alternative sources such as coal, ocean water, and regoliths associated with coastal plain clays (Rozelle et al, 2016; Drost and Wang, 2016; Foley and Ayuso, 2015). Foley and Ayuso are currently studying such regoliths where they have reported enrichments in the light rare earths as high as 200-800 times higher than chondrite. Enrichments on the order of 20-100 times higher than chondrite were observed for the heavy rare earths (Foley and Ayuso, 2015).

1.4 Goals of this Study

The primary focus of this study is to observe and compare the mineralogy and chemical composition of kaolin gangue (sand and silt fractions, also known as "grit") associated with the Buffalo Creek Formation and Jeffersonville Member of the Huber Formation toward determining provenance of these grit minerals in the Georgia Kaolins. Two hypotheses (H1 and H2) were formulated.

H1: The provenance of the gangue minerals are likely from nearby igneous rocks (Sparta Granite).

H2: Rare earth elements are most likely to be found within the heavy fraction of the gangue. This hypothesis is likely to be possible based on the observations made by Cheshire 2011. Cheshire associated light rare earth elements with the phosphate mineral monazite, a heavy mineral whose density is 4.6 to 5.7 g/cm^3. He also mentions the possibility of the association of the heavy rare earth elements with the mineral zircon in the Georgia Kaolins.

The goal of this study is to test these two hypotheses. In doing so, the thesis results are aimed at determining the provenance of the gangue as well as determining which minerals within the heavy fraction are the most strongly correlated with the presence of rare earth elements.

2 METHODS

2.1 Samples and Locations

Samples analyzed in this study were provided with the permission and assistance of the Thiele Kaolin Company on May 14, 2015. Ed Riley of Thiele Kaolin assisted in the collection and blunging of the samples. The blunging process is described in Section 2.2. The sample of the Cretaceous Buffalo Creek Formation was collected from the Avant Mine. The sample of the Jeffersonville Member of the Tertiary Huber Formation was collected from the Dukes Mine. Location maps of these open pit quarries are shown below.

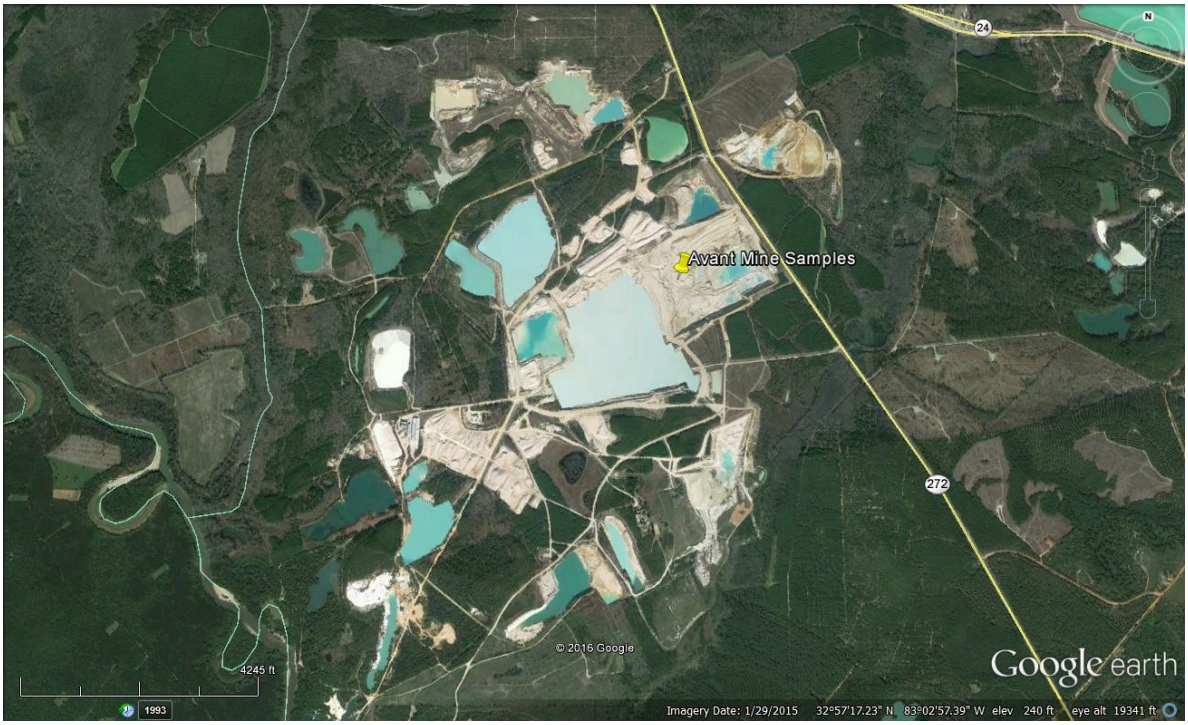

Figure 7: Google Earth map of Avant Mine location, Buffalo Creek kaolins were sampled from the Avant Mine

Figure 8: Google Earth map of Dukes Mine location, Jeffersonville Member kaolins were sampled from the Dukes Mine

2.2 Sample Register, Blunging, and Heavy Mineral Separation

This study, unlike many other studies of the Georgia Kaolins, focuses on the mineralogy of the grit fraction. The sand and silt fractions associated with these kaolinites are referred to as gangue or "grit". Grit is separated from the clay fraction via a process known as blunging. In the first step in the separation of grit, the raw kaolinite from outcrop is crushed. The crushed kaolinite is mixed with water, Na-hexametaphosphate, and soda ash (sodium carbonate) solutions and is blunged in a Morehouse Cowles Dissolver, to separate the clays from the sand and silt. The grit then settles and is collected from the clay slurry by decanting the clay fraction. In actual production, the clay fraction separated from grit is processed further to produce kaolin clay for market.

After blunging, the grit fraction was screened with a 325 mesh sieve (45 micron) to collect the sand and silt fraction. The fraction less than 325 mesh (45 micron) was discarded. The

sand and silt fractions from the Buffalo Creek Formation that remained were washed and dried at 50ºC. The grit fraction from the Jeffersonville Formation was taken for a second blunging process in a Waring Blender since this sample contained a significant amount of unblunged clay. Soda ash ($NaCO_3$) and Na-hexametaphosphate solutions were added in the blender to assist in the blunging process. This mixture was then once again screened and washed. The washed material was then oven dried at 50ºC and collected for further study. The two samples obtained from this process were labeled "BC grit" and "JV grit" to indicate that the source of raw kaolins collected from the Cretaceous Buffalo Creek Formation and the Jeffersonville Member of the Eocene Huber Formation.

The two grit samples were then further separated into light and heavy fractions via dense liquid separation. Lithium metatungstate (ρ=2.95Kg/L) was the dense fluid utilized in these separations. This liquid was chosen due to its low price and low volatility relative to other separatory fluids (Totten and Hanan, 2007). The density separation involved mixing grit and lithium metatungstate (LMT) in a 1 liter separatory funnel. This mixture was covered and left overnight to allow mineral grains with densities greater than 2.95Kg/L to settle to the bottom of the funnel, while mineral grains with densities less than 2.95Kg/L floated to the top of the separatory funnel. After settling overnight, the dense grains which settled at the bottom of the separatory funnel were carefully drained into a funnel filter lined with Number 2 filter paper. Number 2 filter paper was used to assure the retention of silt-sized grains. The filter was then covered and given time to allow for any excess Lithium metatungstate to drain out of the collected dense grains. After the drainage of any excess Lithium metatungstate, the funnel containing the dense grains was rinsed three times using deionized water. The rinsed filters were then placed in an oven at 50ºC for approximately two hours or until dry. After drying, the

samples were carefully collected in small sampling jars and labeled as the “heavy fraction”. The light grains which remained within the separatory funnel were then drained, rinsed, and dried using the same procedure. This material was also collected after drying; however it was labeled the “light fraction”. These separations were performed separately on both the Buffalo Creek and Jeffersonville Member grit samples. These separations yielded the four samples which will be referred to throughout this study: Buffalo Creek light, Buffalo Creek heavy, Jeffersonville light, and Jeffersonville heavy. The initial samples of the Buffalo Creek and Jeffersonville Member will be referred to as Buffalo Creek grit and Jeffersonville grit respectively.

2.3 X-Ray Diffractometry

Preliminary X-Ray Diffraction (XRD) analyses were performed prior to density separations in attempt to approximate the bulk mineralogy of the Buffalo Creek and Jeffersonville grit samples. Later analyses of the heavy and light sub fractions were performed after the dense liquid separation. The X-Ray Diffractometer used for these analyses was a Panalytical X’pert (Figure 9).

Figure 9: Georgia State Geosciences Department’s XRD

Grit samples were analyzed on random oriented slide mounts (Figures 10 and 11), prepared via the backfill method as described in Moore and Reynolds (1997). These samples

were not powdered. The amounts of the recovered heavy minerals were not large and needed to be used for chemical or other mineralogic analyses. Samples were analyzed at normal speed ($1^{o}2\theta$/minute) from a range of 0^{o}-70^{o} with a time constant of 1 second. A nickel filter and copper radiation (at approximately 1.54Å) were used in the analysis. The software X'pert HighScore© was used to assist mineral identification.

Figure 10: Buffalo Creek grit in random oriented slide mount

Figure 11: Jeffersonville Member grit in random oriented slide mount

Mounts of the light and heavy separates were prepared by mixing approximately 0.5 g of sample with 2mL of deionized water. The mixture was then stirred and the slurry was dripped

onto a petrographic glass slide using a 10mL disposable pipette. The slide was then heated at 50ºC for approximately an hour until dry.

Figure 12: Buffalo Creek Heavy separate on a slide

Figure 13: Jeffersonville Member Heavy separate on a slide

2.4 Scanning Electron Microscopy

Scanning Electron Microscopy examinations were performed on the light and heavy separates of both grit samples. The intentions of these examinations were to search for unique mineral grains and image mineralogical consistencies with data provided by X-Ray Diffractometry. The microscope used was a LEO 1450vp SEM. A Rontec (SD type) detector along with IXRF software was also utilized to collect and identify characteristic X-Rays for

elemental identification. The Rontec detector was only used during the examinations of the heavy separates. Subsamples of the heavy separates were coated in carbon to a thickness of about 15 nm. Subsamples of the light separates were gold coated to a thickness of about 15 nm prior to examination. The acceleration voltage also varied between analyses of the light and heavy fraction. An acceleration voltage of 15kV was used in the analysis of the light fraction while a voltage of 30kV was utilized in the analysis of the heavy fraction.

2.5 Chemical Analysis

Samples of the grit, heavy fraction, and light fraction for both Buffalo Creek and Jeffersonville Member kaolins were sent to Activation Laboratories for chemical analyses. Major, trace, and rare earth elements were analyzed by Activation Laboratories using ICP-MS. Standards and reproducibility provided by Activation Laboratories are included in Appendix A. The amounts of Lanthanide REE were calculated for a 500 m^3 volume of Buffalo Creek and Jeffersonville Member. The amount of REE (in grams) is the product of the volume of kaolin, density of the kaolin, fraction of grit, and the concentration REE total (ppm or mg/kg). The fraction of grit and density of the Buffalo Creek and Jeffersonville Members were data from Dombrowski (1993).

3 RESULTS

3.1 X-Ray Diffractometry Data

Preliminary diffraction analyses on the grit samples provided bulk mineralogy which are shown in the first diffraction patterns below (Figures 14 and 15). Buffalo Creek diffraction data is shown in Figure 14. Jeffersonville diffraction data is shown in Figure 15. These diffraction patterns permit identification of the prevalent minerals in these samples. The X-Pert Pro software of the XRD provided assistance in identifying minerals present in these samples.

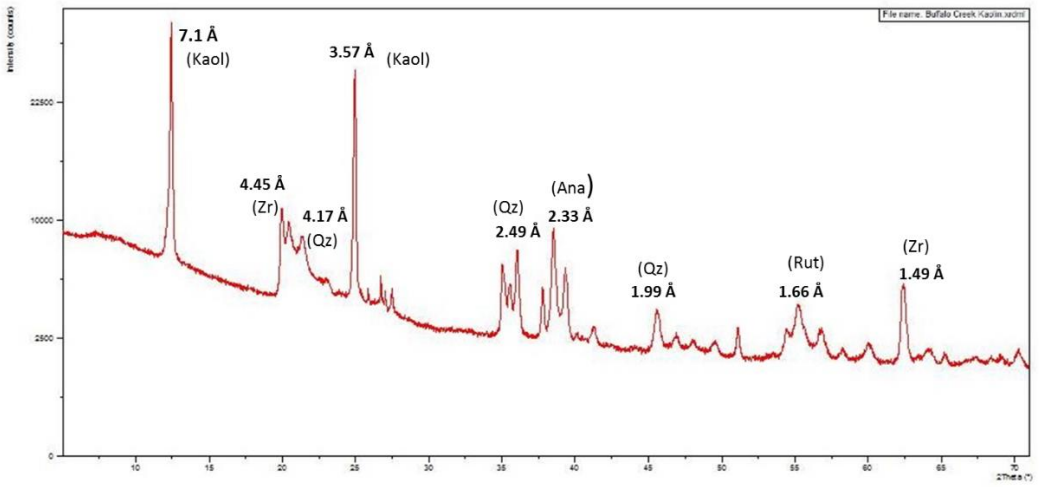

Figure 14: Labelled diffraction scan of Buffalo Creek grit

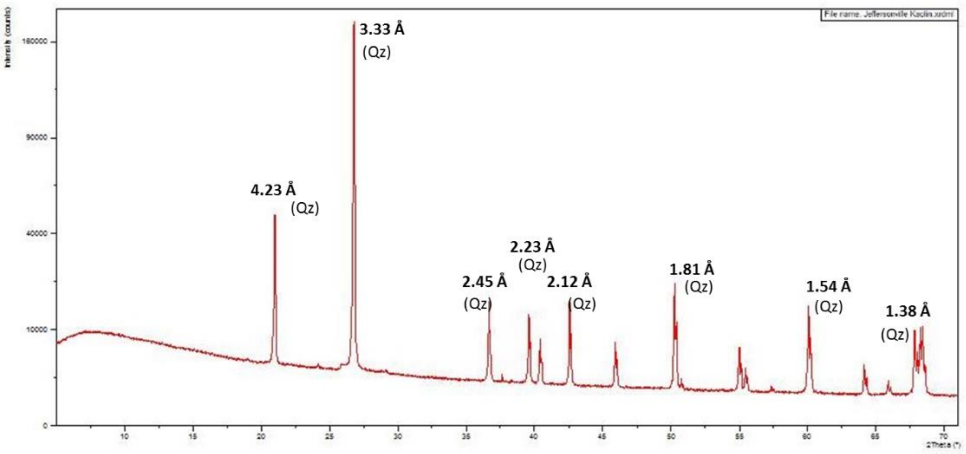

Figure 15: Labelled diffraction scan of Jeffersonville Member grit

The Buffalo Creek grit showed a much more diverse mineralogical composition than the Jeffersonville Grit. Kaolinite, quartz, zircon, and the titanium bearing minerals anatase and rutile were observed in the Buffalo Creek grit. The Jeffersonville grit sample contained almost exclusively quartz. The heavy separates were then analyzed to determine whether the separation process successfully sequestered the dense minerals (Figure 16 and 17).

The diffraction patterns for the heavy separate materials from the Buffalo Creek and Jeffersonville show firstly that the dense liquid separation successfully sequestered the dense and light fractions of the grit. Peaks representing rutile and zircon can be observed on the diffractogram for both Jeffersonville and Buffalo Creek heavy subsamples. The presence of residual kaolinite in the Buffalo Creek Heavy subsample and the absence of kaolinite in the Jeffersonville subsample suggest that the blunging process was more effective in dispersing kaolinite from the Jeffersonville Member grit than from the Buffalo Creek grit. The diffraction patterns for the Buffalo Creek and Jeffersonville light separates further verify that the dense liquid separation was effective in that heavy minerals such zircon were absent.

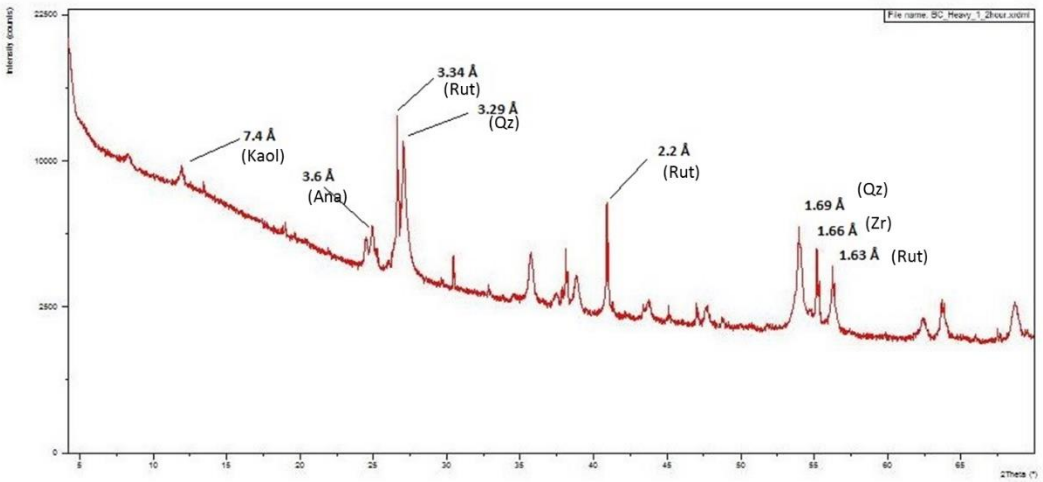

Figure 16: Labelled diffraction scan of Buffalo Creek heavy fraction

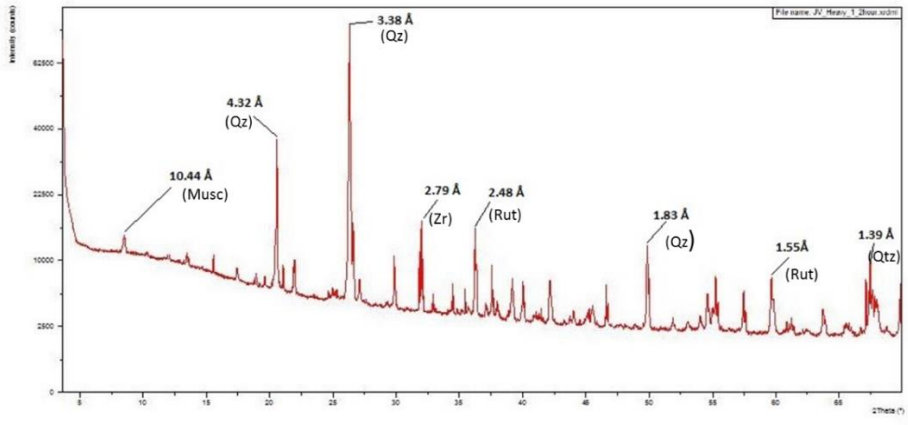

Figure 17: Labelled diffraction scan of Jeffersonville Member heavy fraction

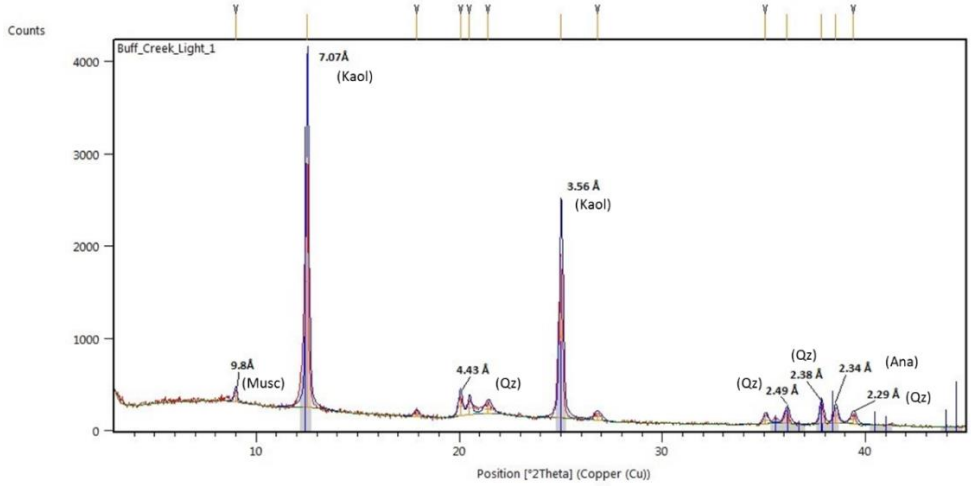

Figure 18: Labelled diffraction scan of Buffalo Creek light fraction

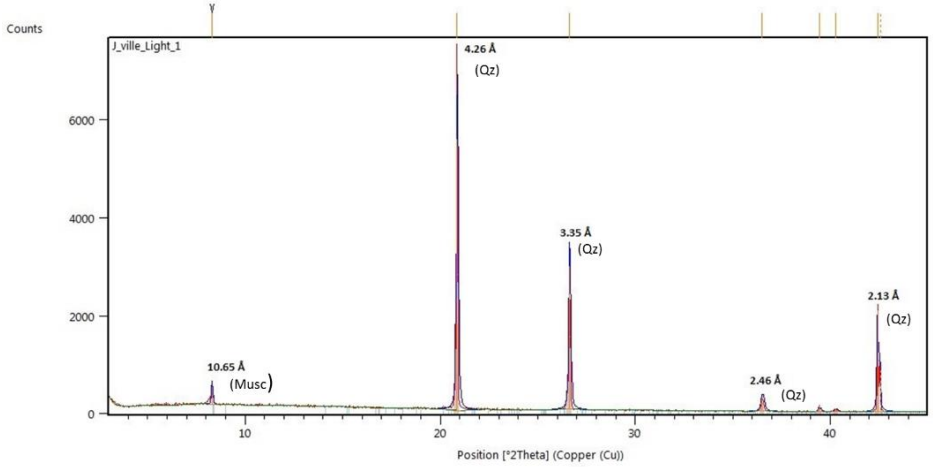

Figure 19: Labelled diffraction scan of Jeffersonville light fraction

3.2 Scanning Electron Microscopy Data

Scanning electron microscopy examinations were performed on the heavy and light separates of both grit samples. The Rontec detector was used only while analyzing the heavy separates in attempt to determine more accurately their mineralogy and elemental composition. Images and elemental spectra for all of the analyzed heavy separates are provided in Appendix B.

Observations varied between the examinations performed on the Buffalo Creek and Jeffersonville samples. Eleven mineral grains of the Buffalo Creek heavy separate were chemically analyzed during the SEM examinations. Among the eleven grains, six showed predominant concentrations of titanium, four exhibited high concentrations of zirconium, and one showed high concentrations of iron and magnesium. Zirconium and titanium bearing minerals within the Buffalo Creek heavy separate are shown in the labeled SEM image below (Figure 21). The grains do not show evidence of extensive physical weathering due to transport. The lack of quartz and kaolinite in the heavy fraction suggests that the dense liquid separation process successfully separated the dense minerals (zircon and rutile) from the light minerals such as quartz.

Ten random mineral grains of the Jeffersonville separate were chemically analyzed during the examinations. Among the ten grains, six showed predominant concentrations of iron and magnesium, three showed high concentrations of zirconium, and one showed a high concentration of titanium. Similarly to the Buffalo Creek heavy separates, few quartz and kaolinite grains were seen in the heavy separate. Unlike the Buffalo Creek heavy separates however, grains of the Jeffersonville show unique signs of physical weathering (Figure 23). During the examinations of the light separates the major difference observed was the

composition. While the Buffalo Creek light separate contained mostly kaolinite, the Jeffersonville light separate was predominantly composed of quartz.

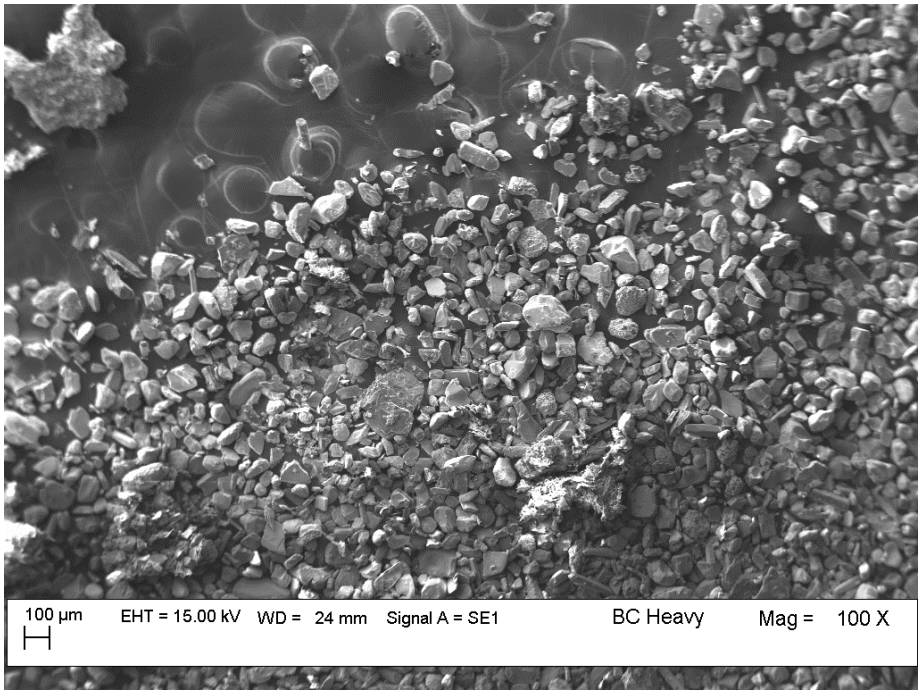

Figure 20: SEM image of the Buffalo Creek heavy fraction

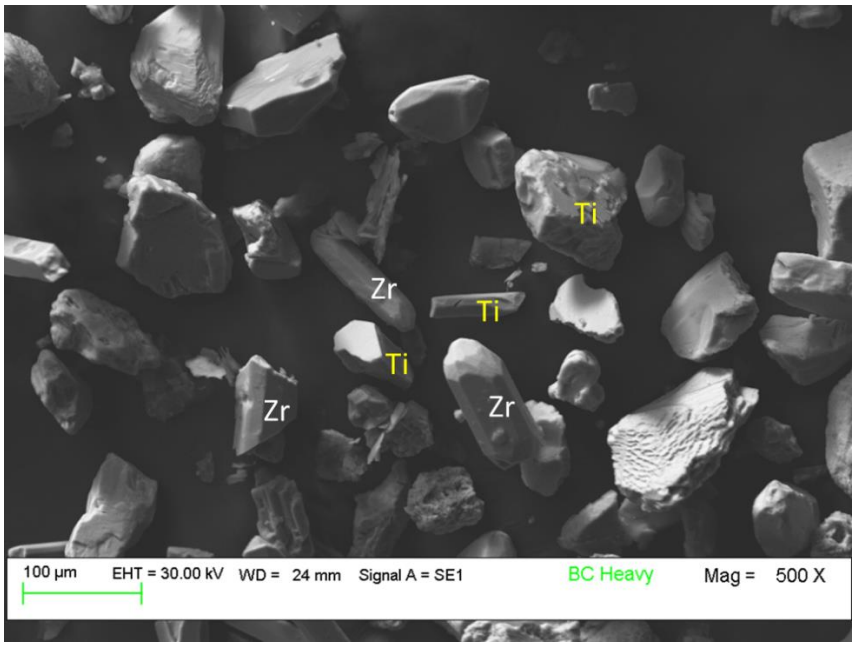

Figure 21: Labelled mineral grains in the Buffalo Creek heavy separate. Ti corresponds to Rutile. Zr corresponds to Zircon

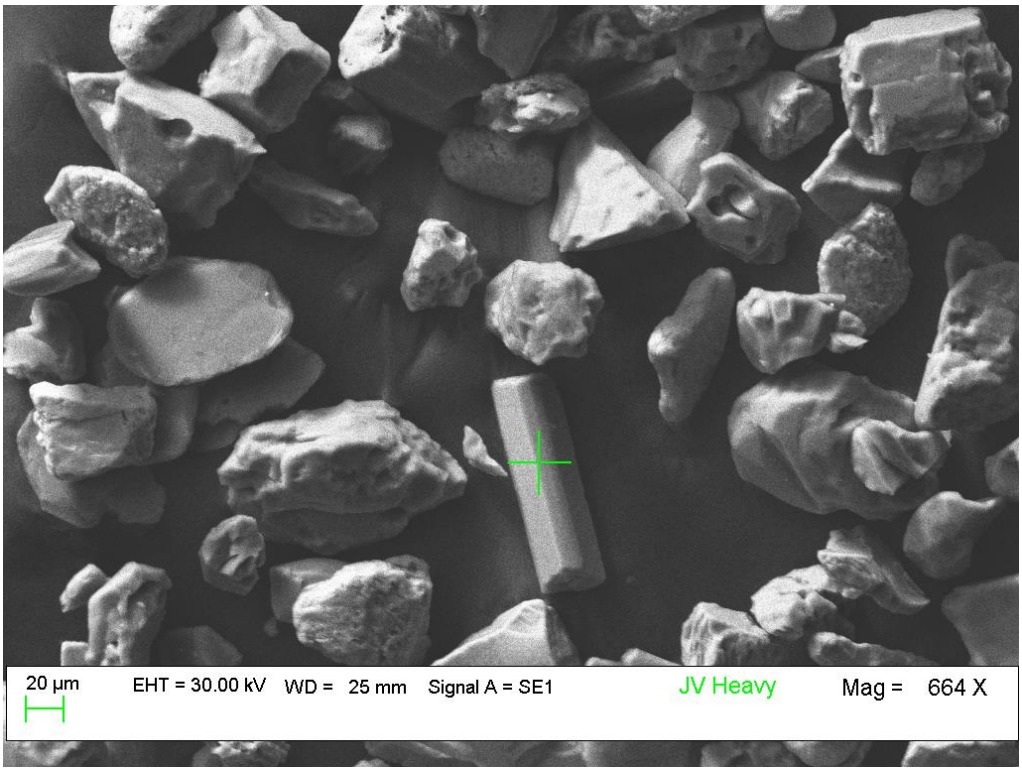

Figure 22: SEM image of Tourmaline within Jeffersonville heavy fraction. The number of weathered mineral surfaces is greater in Jeffersonville compared to Buffalo Creek

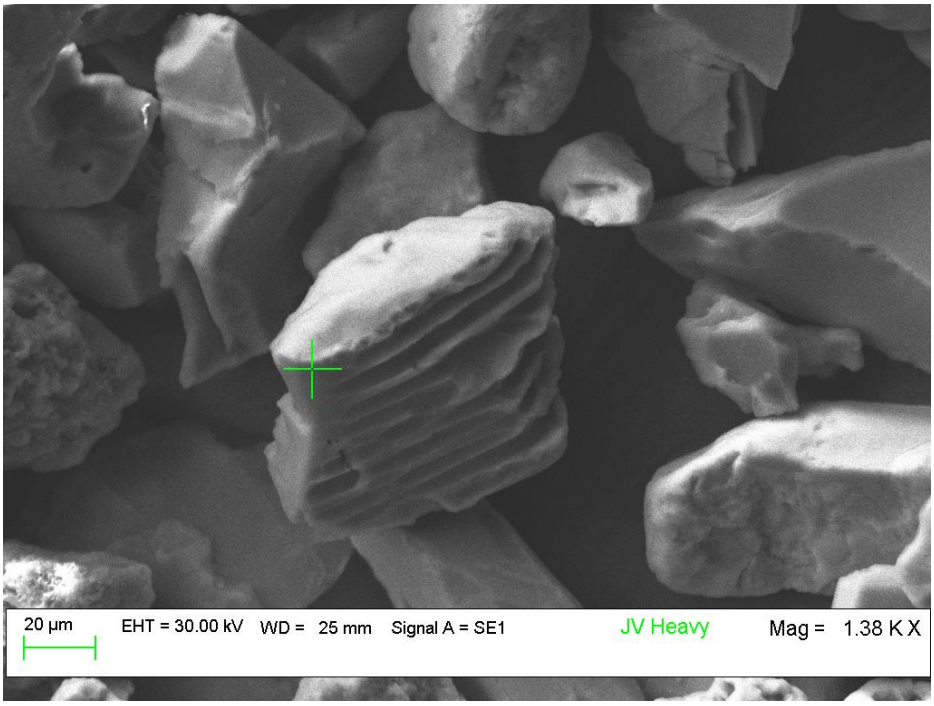

Figure 23: SEM image of physical weathering on Jeffersonville heavy grains

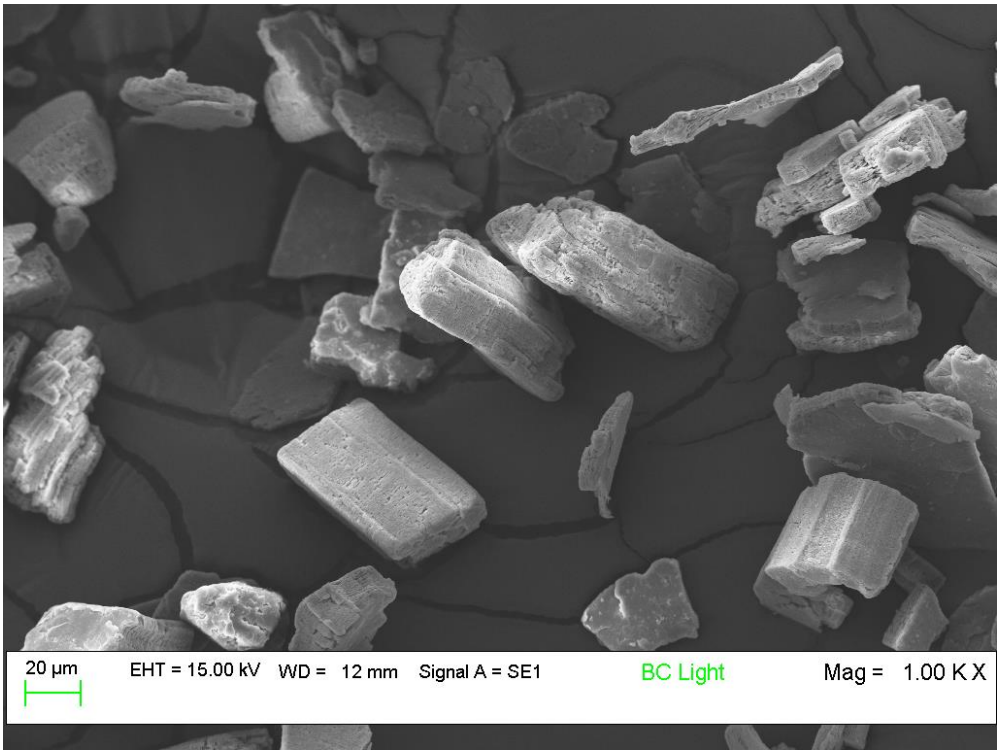

Figure 24: SEM image of Buffalo Creek light fraction

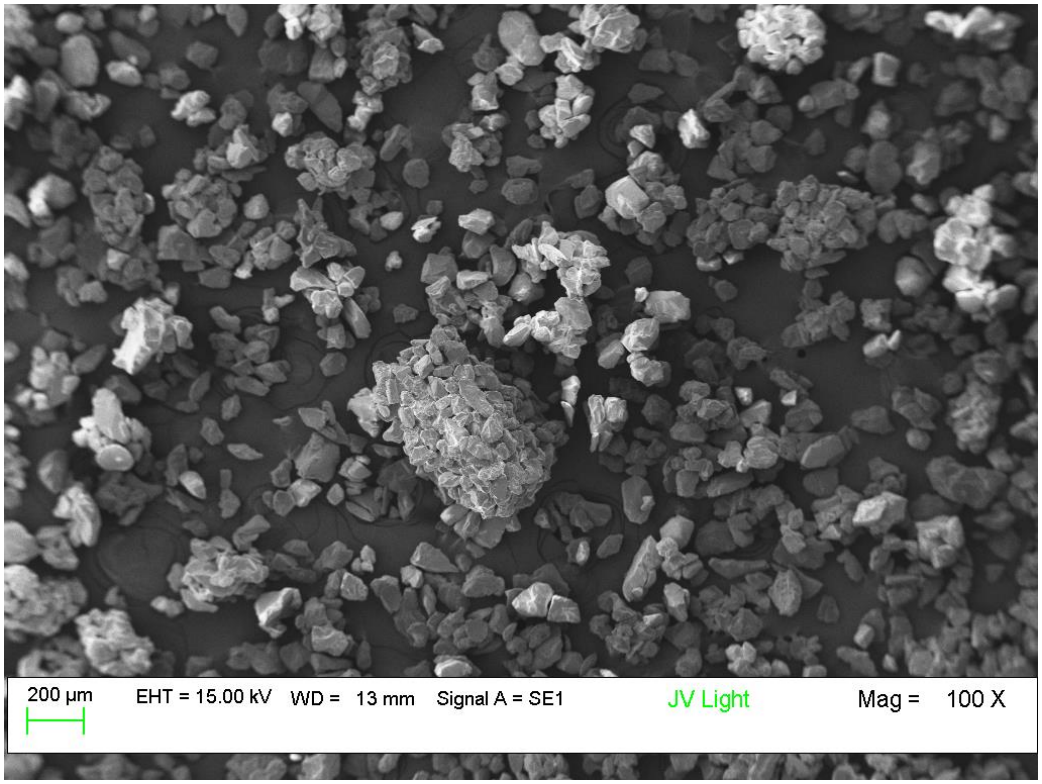

Figure 25: SEM image of quartz grains within Jeffersonville light fraction

3.3 Elemental Data

Major element, trace element, and Lanthanide Rare Earth Element (REE) analyses are summarized in Tables 1-6. For major elements, all reported values represent weight percent (wt%) oxides. Rare earth and trace element values are given in parts per million (ppm). Enrichment data tables which show enrichment and depletion relative to upper continental crust (as provided by Rudnick and Gao 2004) were also compiled. Figures 26 and 27 graphically show rare earth elemental enrichments relative to upper continental crust. The correlation of Zr to REE and TiO_2 to REE are shown in Figures 28 and 29 respectively.

Metal Oxide	BC Grit	JV Grit	BC Heavy	JV Heavy	BC Light	JV Light	Upper Continental Crust
SiO2	42.1	96.65	6.97	40.93	44.82	95.8	66.62
Al2O3	35.43	0.49	3.81	16.59	36.79	0.38	15.4
Fe2O3	0.82	2	6.27	10.1	0.83	2.39	5.04
MnO	0.012	0.016	0.098	0.062	0.007	0.019	0.1
MgO	0.06	0.03	0.24	1.38	0.04	0.01	2.48
CaO	0.08	0.05	0.15	0.18	0.04	0.04	3.59
Na2O	0.11	0.06	0.07	0.39	0.15	0.06	3.27
K2O	0.21	0.05	0.02	0.45	0.26	0.05	2.8
TiO2	7.032	0.168	58.28	19.05	0.801	0.053	0.64
P2O5	0.11	0.01	0.44	0.28	0.03	0.01	0.15

Table 1: Major Elemental Concentrations (Given in Weight Percentage)

Metal Oxide	BC Grit	JV Grit	BC Heavy	JV Heavy	BC Light	JV Light
SiO2	0.63	1.45	0.10	0.61	0.67	1.44
Al2O3	2.30	0.03	0.25	1.08	2.39	0.02
Fe2O3	0.16	0.40	1.24	2.00	0.16	0.47
MnO	0.12	0.16	0.98	0.62	0.07	0.19
MgO	0.02	0.01	0.10	0.56	0.02	0.00
CaO	0.02	0.01	0.04	0.05	0.01	0.01
Na2O	0.03	0.02	0.02	0.12	0.05	0.02
K2O	0.08	0.02	0.01	0.16	0.09	0.02
TiO2	10.99	0.26	91.06	29.77	1.25	0.08
P2O5	0.73	0.07	2.93	1.87	0.20	0.07

Table 2: Major Elemental Enrichments (Relative to UCC)

Element	BC Grit	JV Grit	BC Heavy	JV Heavy	BC Light	JV Light	Upper Continental Crust
La	23.2	2.9	298	178	1.8	1.3	31
Ce	48.7	5.2	612	312	3.8	2.5	63
Pr	5.72	0.61	72.5	37.8	0.44	0.27	7.1
Nd	22.6	2.3	274	133	1.8	0.9	27
Sm	6.6	0.5	75.7	30.2	0.6	0.2	4.7
Eu	0.8	0.08	7.64	5.32	0.11	0.05	1
Gd	12.9	1.3	142	43.7	1.2	0.2	4
Tb	3.5	0.2	35.4	10	0.3	0.1	0.7
Dy	30.1	1.5	308	81.8	2.8	0.3	3.9
Ho	7.6	0.3	76.7	20.1	0.7	0.1	0.83
Er	25.7	1	245	65.6	2.2	0.2	2.3
Tm	4.12	0.16	40.7	11.3	0.37	0.05	0.3
Yb	28.4	1.1	274	81.5	2.5	0.3	2
Lu	4.35	0.16	43	13.4	0.38	0.04	0.31
Sum	224.29	17.31	2504.64	1023.72	19	6.51	148.14

Table 3: Rare Earth Elemental Concentrations (Given in Parts Per Million)

Element	BC Grit	JV Grit	BC Heavy	JV Heavy	BC Light	JV Light
La	0.75	0.09	9.61	5.74	0.06	0.04
Ce	0.77	0.08	9.71	4.95	0.06	0.04
Pr	0.81	0.09	10.21	5.32	0.06	0.04
Nd	0.84	0.09	10.15	4.93	0.07	0.03
Sm	1.40	0.11	16.11	6.43	0.13	0.04
Eu	0.80	0.08	7.64	5.32	0.11	0.05
Gd	3.23	0.33	35.50	10.93	0.30	0.05
Tb	5.00	0.29	50.57	14.29	0.43	0.14
Dy	7.72	0.38	78.97	20.97	0.72	0.08
Ho	9.16	0.36	92.41	24.22	0.84	0.12
Er	11.17	0.43	106.52	28.52	0.96	0.09
Tm	13.73	0.53	135.67	37.67	1.23	0.17
Yb	14.20	0.55	137.00	40.75	1.25	0.15
Lu	14.03	0.52	138.71	43.23	1.23	0.13

Table 4: Rare Earth Elemental Enrichments (Relative to UCC)

Element	BC Grit	JV Grit	BC Heavy	JV Heavy	BC Light	JV Light	Upper Continental Crust
Sc	87	1	333	68	57	8	14
Be	1	1	1	3	1	1	2.1
V	215	8	1559	506	63	8	97
Cr	250	40	1050	390	150	40	92
Co	4	1	5	12	3	2	17.3
Ni	120	20	180	40	50	20	47
Cu	20	10	10	60	20	10	28
Zn	60	30	190	410	30	30	67
Ga	70	1	173	58	56	1	17.5
Ge	2	1	2	3	1	1	1.4
As	6	5	50	17	5	5	4.8
Rb	5	2	2	13	6	2	84
Sr	78	7	26	172	6	5	320
Y	273	7	2175	555	21	2	21
Zr	5778	251	56430	31450	459	72	193
Nb	109	8	1030	361	15	3	12
Mo	24	2	215	18	4	2	1.1
Ag	0	1.5	0	0	2	0.5	53
In	0.8	0.2	5.6	1.2	0.2	0.2	0.056
Sn	28	1	215	35	6	1	2.1
Sb	1.9	0.5	4.5	5.4	0.7	0.5	0.4
Cs	0.5	0.5	0.5	0.5	0.5	0.5	4.9
Ba	57	57	65	216	57	55	624
Bi	1.1	1.1	10.8	5.6	0.4	0.4	0.16
Hf	142	6.1	1380	734	12	1.8	5.3
Ta	8.4	0.4	73.7	29.1	1.1	0.2	0.9
W	9	1	52200	7070	8280	6550	1.9
Tl	0.1	0.1	0.1	0.1	0.1	0.1	0.9
Pb	13	5	136	89	5	5	17
Th	45.5	1.6	418	76.9	5.3	0.4	10.5
U	18.9	0.7	152	56.3	2.8	0.2	2.7

Table 5: Trace Elemental Compositions (Given in Parts Per Million)

Element	BC Grit	JV Grit	BC Heavy	JV Heavy	BC Light	JV Light
Sc	6.21	0.07	23.79	4.86	4.07	0.57
Be	0.48	0.48	0.48	1.43	0.48	0.48
V	2.22	0.08	16.07	5.22	0.65	0.08
Cr	2.72	0.43	11.41	4.24	1.63	0.43
Co	0.23	0.06	0.29	0.69	0.17	0.12
Ni	2.55	0.43	3.83	0.85	1.06	0.43
Cu	0.71	0.36	0.36	2.14	0.71	0.36
Zn	0.90	0.45	2.84	6.12	0.45	0.45
Ga	4.00	0.06	9.89	3.31	3.20	0.06
Ge	1.43	0.71	1.43	2.14	0.71	0.71
As	1.25	1.04	10.42	3.54	1.04	1.04
Rb	0.06	0.02	0.02	0.15	0.07	0.02
Sr	0.24	0.02	0.08	0.54	0.02	0.02
Y	13.00	0.33	103.57	26.43	1.00	0.10
Zr	29.94	1.30	292.38	162.95	2.38	0.37
Nb	9.08	0.67	85.83	30.08	1.25	0.25
Mo	21.82	1.82	195.45	16.36	3.64	1.82
Ag	0.00	0.03	0.00	0.00	0.04	0.01
In	14.29	3.57	100.00	21.43	3.57	3.57
Sn	13.33	0.48	102.38	16.67	2.86	0.48
Sb	4.75	1.25	11.25	13.50	1.75	1.25
Cs	0.10	0.10	0.10	0.10	0.10	0.10
Ba	0.09	0.09	0.10	0.35	0.09	0.09
Bi	6.88	6.88	67.50	35.00	2.50	2.50
Hf	26.79	1.15	260.38	138.49	2.26	0.34
Ta	9.33	0.44	81.89	32.33	1.22	0.22
W	4.74	0.53	27473.68	3721.05	4357.89	3447.37
Tl	0.11	0.11	0.11	0.11	0.11	0.11
Pb	0.76	0.29	8.00	5.24	0.29	0.29
Th	4.33	0.15	39.81	7.32	0.50	0.04
U	7.00	0.26	56.30	20.85	1.04	0.07

Table 6: Trace Elemental Enrichments (Relative to UCC)

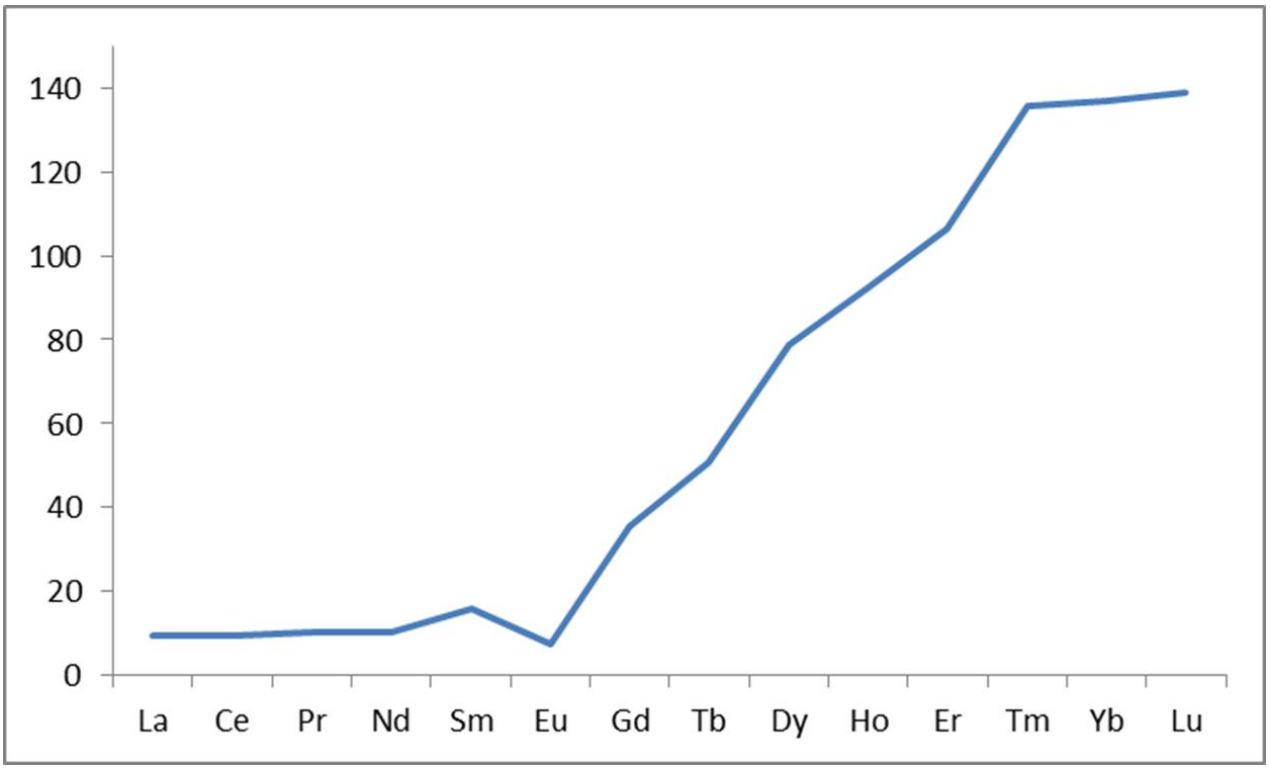

Figure 26: Buffalo Creek rare elemental enrichments relative to UCC

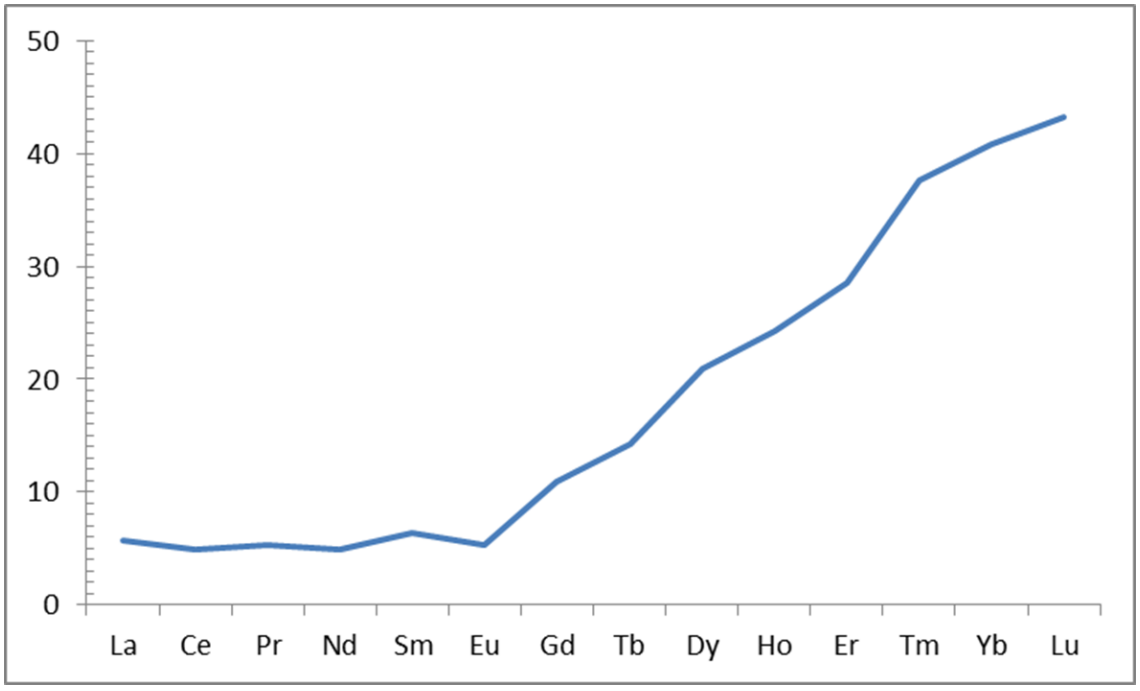

Figure 27: Jeffersonville Member rare elemental enrichments relative to UCC

Trends were observed between the sum of rare earth elements and the concentration of select trace and major elements. To quantify these trends, correlation plots were created and linear regression lines were fit to each plot. The strongest correlations of the rare earth elements were with zirconium and TiO_2.

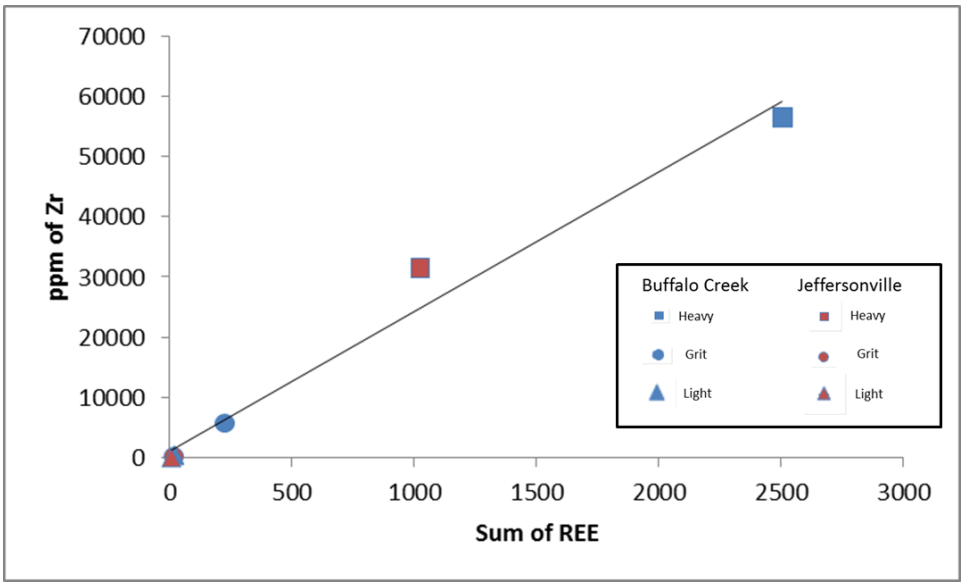

Figure 28: Correlations of sum of rare earths to ppm Zirconium (R^2=0.99)

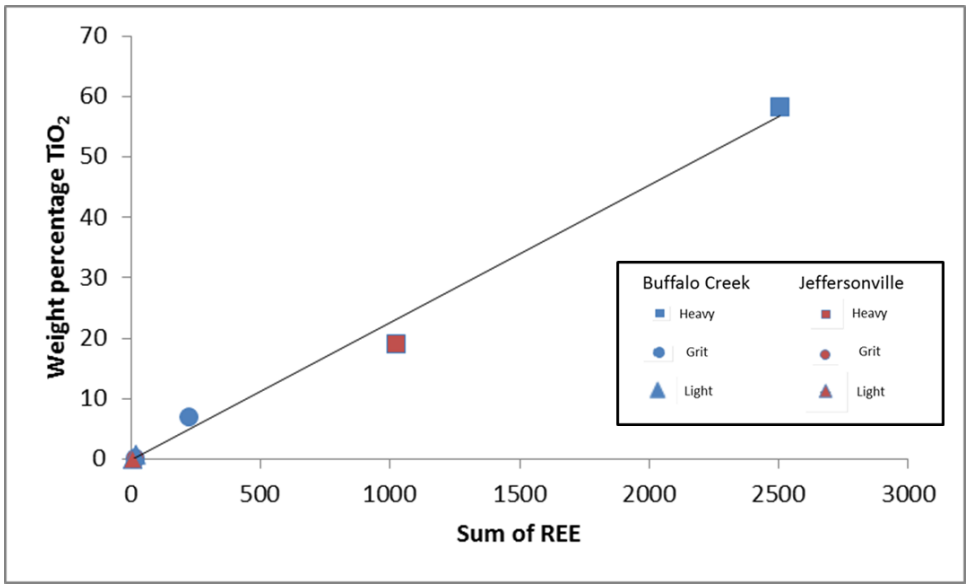

Figure 29: Correlations of sum of rare earths to weight percent TiO_2 (R^2=0.98)

3.4 Amounts of REE in Buffalo Creek and Jeffersonville Member

The amounts of REE were calculated to aid in later economic assessment or REE in the Georgia Kaolins. This model was designed to calculate the approximate amounts of REE within a 500m^3 volume of kaolin. Density and grit percentage values were determined by Dombrowski (1993). Tables showing the calculations of estimated rare earth elements within the grit samples are provided below.

Sample	Area of kaolin (m2)	Depth (m)	Volume (m3)	Volume (cm3)	Density (g/cm3)	Mass of kaolin (g)
BC	100	5	500	500,000,000	1.43	715,000,000
JV	100	5	500	500,000,000	1.70	850,000,000

Table 7: Mass of 500m^3 of Kaolin Approximation

Sample	% Grit	Mass of Grit (g)	ppm REE	REE in Grit (g)
BC	9	64,350,000	224.29	14,433.06
JV	9.6	81,600,000	17.31	1,412.50

Table 8: Concentration of Rare Earth Elements in 500m^3 of Kaolin

4 DISCUSSION

4.1 Mineralogical and Elemental Comparison

4.1.1 XRD

When comparing the preliminary diffraction patterns for the Buffalo Creek and Jeffersonville grit samples, it is evident that there is considerable variation between the mineralogical compositions of these two samples (Figure 14-15). The abundance of quartz in the Jeffersonville Member grit sample is consistent with previous literature stating that it is of a more sedimentary origin (Hurst and Pickerington, 1997). In contrast, more abundant mineralogically mature and heavy minerals (e.g. rutile, anatase, zircon), are found within the Buffalo Creek grit. The variability of these minerals found in the Buffalo Creek shows a less mature mineral suite. The less mature mineral suite may suggest that the mined location of the Buffalo Creek kaolins is closer to the source be it a saprolite or parent rock. The high amounts of quartz and the prevalence of etched mineral surfaces in the Jeffersonville Member are interpreted to be a more mature mineral suite. The distance between the mined location and the source may be much greater for the Jeffersonville member.

Diffraction patterns for the heavy fraction subsamples of the Buffalo Creek and Jeffersonville Member grit suggest that the dense liquid separation fractionated the light and dense minerals from each other (Figures 16-17). The Buffalo Creek heavy subsample primarily contains the dense minerals rutile, anatase, and zircon. In addition to the dense minerals a small peak of kaolinite as well as a peak of quartz is present. The Jeffersonville Member heavy fraction subsample contains the same dense minerals rutile and zircon; however, no kaolinite peak is present. Unlike the Buffalo Creek heavy fraction subsample, the Jeffersonville heavy fraction subsample contains multiple quartz peaks. The presence of light minerals within the dense

subsamples and the high prevalence of quartz within these samples suggests a degree error within the separations; however due to the majority of the heavy minerals sequestered having a density greater than 2.95Kg/L, it can be confidently stated that the dense liquid separation successfully separated the dense minerals from the light minerals of the grit using the LMT liquid.

Diffraction patterns for the light subsamples also suggest a clean separation of the light and heavy minerals. The Buffalo Creek light fraction contains the minerals muscovite, kaolinite, anatase, and quartz. The Jeffersonville light fraction contains the minerals muscovite and quartz. In the case of the light separates, anatase is the only mineral present with a density greater than 2.95Kg/L. The presence of anatase in the Buffalo Creek light subsample suggests error in the separations as stated above, however the predominance of light minerals in the light density fraction further suggests that the LMT dense liquid separation successfully sequestered the light and dense fractions of the grit.

4.1.2 SEM

Elemental compositions were obtained from EDS spectra during SEM examinations. These data were used to further validate the mineralogical composition of the samples. Among the eleven grains of BC heavy which were analyzed, four were abundant in zirconium (and containing silicon), six were abundant in titanium, and one mineral grain contained high concentrations of iron and silicon. This data is consistent with what was expected after the XRD analyses reported abundances of the titanium bearing minerals anatase and rutile as well as the zirconium bearing mineral zircon and silicon (i.e. zircon). The iron rich grain is likely ilmenite. Spectra obtained while viewing Jeffersonville Member heavy grains varied greatly. Among the ten grains analyzed, six were abundant in iron and magnesium, three were abundant in zirconium

and silicon, and one was abundant in titanium. The high concentrations of iron and magnesium in this sample are indicative of minerals such as tourmaline, or ilmenite. This assumption for the identification of tourmaline, or ilmenite is made based on the crystal habit of the minerals, the chemical composition of the minerals, and the sedimentary nature of the parent material of the Jeffersonville Member kaolin.

Physical differences were also observed when comparing the SEM examinations of the Buffalo Creek and Jeffersonville Member heavy separates. The lack of excessive kaolinite and quartz in the heavy fraction suggests that the blunging and dense liquid separation successfully sequestered the dense minerals within both grit samples. The Jeffersonville Member heavy fraction grains show evidence of physical weathering indicating a relatively greater degree of maturity, as observed by SEM specialist Dr. Robert Simmons (Figure 23). Buffalo Creek heavy grains did not show evidence of the same degree of physical weathering.

Although compositional spectra were not collected on the light separates of the samples during analysis, many of the quartz grains were confidently identified by Dr. Robert Simmons. The SEM images of the Buffalo Creek light fraction suggest that it is composed mostly of kaolinite based on the presence of hexagonal or pseudo-hexagonal flakes. In contrast, the Jeffersonville Member light sample is almost exclusively composed of quartz. The few kaolin grains which can be observed in the Jeffersonville Member light sample are much smaller than the kaolin sheets which can be observed in the Buffalo Creek light sample. These observations regarding both subsamples are consistent with Elzea-Kogel et al., (2002) and what was expected after receiving the preliminary XRD data. The large fraction of quartz shows a different source or provenance for the Jeffersonville Member kaolins compared to the Buffalo Creek.

4.1.3 Elemental Analysis

The intent of having the samples chemically analyzed was to determine if any of the samples contained unique trace constituents which may help more confidently assess provenance. Data received from Activation Laboratories was first sorted in the elemental groups of major elements, rare earth elements, and trace elements. Tables of this data were compiled, as provided above. These elemental values were normalized to the Upper Continental Crust standard as provided by Gao and Rudnick (2004). Enrichment tables were then compiled by dividing the measured value for a given element by the concentration of that element in the UCC standard (i.e., normalization). In addition to compiling the enrichment tables, graphs were also made to show enrichments/depletions within each sample as compared to UCC.

The elemental analysis of the grit samples is consistent with the preliminary XRD data. The major and trace element composition for the Buffalo Creek grit sample reflects the mineralogy of zircon, rutile and smaller amounts of quartz and other phases. The major and trace element composition of the Jeffersonville Member shows a considerable amount of SiO_2 (96 wt%). This composition is reflected by the high quartz composition in that sample (Figure 15, Table 1). This data also validates that the blunging process is more effective in separating kaolinite out of Jeffersonville kaolins as opposed to Buffalo Creek kaolins. In addition to a more diverse composition, it was observed that the Buffalo Creek grit contains approximately 224 ppm REE on a whole rock basis (Table 3). This concentration is enriched when normalized to upper continental crustal (UCC) or to North American Shale Composite (NASC, Gromet et al., 1984) values (Table 4).

The elemental analyses of the light and heavy subsamples provide insight on the source of the rare earth elements within the Jeffersonville Member and Buffalo Creek grit samples.

High concentrations of titanium oxide and zirconium are observed in both heavy fraction subsamples. High concentrations of rare earth elements are also observed in both heavy fraction subsamples. Low concentrations of titanium oxide and zirconium are observed in both light subsamples and subsequently, low concentrations of rare earth elements are observed in both light subsamples. The concentrations of phosphorous are low in the grit. Cheshire (2011) and Dombrowski (1993) argue for the presence of REE-phosphate minerals (monazite) in the Georgia Kaolins. Monazite is a source of the Light Lanthanide Rare Earth Elements (La, Ce, Nd). The separation of grit apparently did sequester the REE-phosphates from the Georgia Kaolins into the heavy fraction.

4.1.4 Geologic History and Provenance

Using knowledge of the geologic history of the Georgia Kaolins along with data provided by this study, the provenances of the Buffalo Creek Formation and Jeffersonville Member were determined. The correlation of the first two super greenhouse periods occurring just before the deposition of the Buffalo Creek Formation along with its relatively diverse mineralogical composition suggests that its provenance is proximal to the Georgia Kaolin District. A proximal provenance would have undergone less sedimentary transport, which would explain why many mature constituents such as zircon and Rare Earth Elements remained in the Buffalo Creek Formation. The Jeffersonville Member was deposited later, after the third super greenhouse event, which occurred during the Paleocene-Eocene Thermal Maximum. This super greenhouse event was warmer than the first two and likely altered weathered micas and feldspars in the Blue Ridge and Piedmont provinces of Georgia. These weathered micas and feldspars were transported via fluviatile processes and deposited in the Georgia Kaolin District. Minerals such as zircon and rutile are less prone to sedimentary transportation. As such, these minerals are seen

in much lower concentrations in the Jeffersonville Member kaolins than in the Buffalo Creek Formation.

4.2 Rare Earth Elemental Correlations

Once observed, the exceptionally high rare earth element concentrations were looked at more closely. The sums of rare earths in all six samples were calculated and plotted against select trace elements to determine which elements apparently had the strongest correlation with the total amounts of rare elements (Table 3; Figures 28-29). These figures (Figures 28-29) show a strong correlation coefficient between total rare earths and titanium within the samples (R^2=0.98). Zirconium also had a strong positive correlation (R^2=0.99). The enrichment of rare earths within zircon is consistent with previous findings for REE in zircon (Watson et al, 2006; Trail et al, 2012; Klemme et al, 2005). However, the strong correlation of rare earth elements with titanium bearing minerals is inconsistent with previous findings. A recent study conducted by Klemme et al., 2005 concluded that rare earth metals tend not to partition into rutile directly from a rhyolitic melt.

Another argument to test the association of REEs with rutile is the comparison of the valence and ionic radius of titanium and the elements of the lanthanide series. The ionic radii of the lanthanum series elements ranges from approximately 0.8Å-1.0Å, and all contain a valence of 3+ or 4+ (Bloss, 1965). Titanium occurs in valence states of 3+ and 4+ and has ionic radii of 0.69Å and 0.64Å respectively (Bloss, 1965). The light rare earth elements contain ionic radii greater than 0.9 Å. The REE would not readily partition into rutile by inspection of ionic radii.

The ionic radius of zirconium is approximately 0.82Å (Bloss, 1965). A radius of this size is very close to that of the heavy rare earths and suggests that the lanthanide series would partition much more readily into zircon than in rutile. Aside from this observation, previous

studies of zircon trace elemental chemistry have provided strong evidence to support this hypothesis (Watson et al, 2006; Trail et al, 2012). In addition to previous studies supporting this hypothesis, the highest R^2 value in this study is associated with the correlation between the sum of REE and ppm of Zr. This correlation further validates the association heavy rare earth elements with the mineral zircon. An additional observation to note is that the concentrations of zirconium and titanium are often strongly positively correlated with each other based on density and mineral maturity, within upper continental crustal rocks. This association of REE in rutile is likely coincidental and reflects the co-association of zircon and rutile in the heavy fractions produced by the heavy liquid separation.

5 CONCLUSION

The blunging process in combination with dense liquid separation via Lithium Metatungstate (LMT) successfully produced grit samples and subsamples for this study of the Georgia Kaolins. Images of the heavy and light separates, provided by SEM, show very few kaolin grains, which are easily identifiable by their sheet structure. The only sample which showed significant amounts of kaolin during the SEM examinations was the Buffalo Creek Light fraction. In contrast, the lack of kaolin and predominance of SiO_2 in the Jeffersonville Light subsample, suggests that the blunging process, as performed in this study, is more effective in dispersing kaolinite from the Jeffersonville Member raw kaolin ore than from Buffalo Creek raw kaolin ore.

Using the data provided by this study, many differences in mineralogy can be observed between the Buffalo Creek and Jeffersonville Grit samples. Mineralogically, the Jeffersonville sample's 96% abundance of quartz in addition to evidence of extensive physical weathering suggests a sedimentary, fluviatile origin. The Buffalo Creek grit was composed of various minerals. In terms of chemical compositions, the Buffalo Creek grit samples contain an abundant variety of less soluble elements such as titanium, zirconium, and rare earth metals. This composition suggests that the saprolite or parent source rock for the Buffalo Creek kaolins was closer in proximity to the Georgia Kaolin district than the saprolite or parent source rock for the Jeffersonville kaolins. A further refinement and testing of this idea requires a geochronologic study of the zircon grains found in the Buffalo Creek and Jeffersonville grit.

The two constituents most strongly associated with the presence of the Lanthanide rare earth elements in this study are Zr and TiO_2. These constituents have correlation coefficients of R^2= 0.99 and R^2= 0.98 respectively when plotted against the sum of lanthanide rare earths. Despite

being strongly positive, the correlation of rare earths with the titanium bearing mineral rutile is likely coincidental as a result of the common association of zirconium and titanium oxide. The correlation of the mineral zircon with REE however is consistent with previous findings (Trail et al, 2012). This correlation may indicate a pathfinder element for REE in the Georgia Kaolins. The presence of enrichments in the HREE elements associated with the heavy mineral zircon differs from observations made by Cheshire (2011). Cheshire associated REE within the Georgia Kaolins with the phosphate minerals florencite and monazite. Cheshire also noted stronger enrichments in the LREE, which differs from what was observed in this study. One possible explanation for the inconsistency between these studies is that the blunging process, in particular the reaction of soda ash (NaCO3) and Na-hexametaphosphate solution with grit may have, dispersed phosphate minerals such as monazite. This hypothesis would further explain the low concentrations of phosphate minerals and the low P_2O_5 in the grit as seen in Table 1.

The amounts of the REE in the Buffalo Creek are noteworthy, especially when normalized to Upper Continental Crust. For the Buffalo Creek, the combined effects of the production of grit fraction followed by the heavy liquid separation of that grit produces a heavy fraction that is 35-150 times greater in heavy REE (Eu-Lu) relative to UCC, or a total Lanthanide REE content of 2530 ppm. This concentration of REE is reflective of the presence of zircon in the grit. The total REE concentration comprises a concentration that is clearly mineable (Foley and Ayuso, 2015). For the Jeffersonville Member, the total amount of REE produced by heavy mineral separation of grit fraction is 1038 ppm. This amount is still significant relative toward considering to extract REE further from the Jeffersonville Member. The United States currently imports many of its supplies of the heavy REE from China. Consequently, the technique of

producing grit followed by heavy mineral separation warrants further development as a possible way to extract and co-produce HREE along with kaolinite from the Georgia Kaolins.

WORKS CITED

Chamley, H., Debrabant, P., Foulon, J., d'Argoud, G. G., Latouche, C., Maillet, N., … Sommer, F. (1979). Mineralogy and geochemistry of Cretaceous and Cenozoic Atlantic sediments off the Iberian Peninsula (site 398, leg 47 B, DSDP). *Initial Reports of the Deep Sea Drilling Project, 47*.

Cheshire, M. C. (2011). *Isotopic and geochemical composition of the Georgia kaolins: Insights into formation and diagenetic conditions*. INDIANA UNIVERSITY.

Dombrowski, T. (1992). *The use of trace elements to determine provenance relations among different types of Georgia Kaolins.* INDIANA UNIVERSITY.

Drost, D., & Wang, R. (2016). Rare earth element criticality and sustainable management. Retrieved from http://www.atlantis-press.com/php/download_paper.php?id=25848475

Elser, A. M. (2004). *The provenance and weathering of muscovite from the Georgia kaolin deposits*. Georgia State University.

Elzea-Kogel, J. E., Jr, S. M. P., Shelobolina, E., Chowns, T., & Yuan, J. (2002). *The Georgia Kaolins: Geology and Utilization*. Littleton, Colo: Society for Mining, Metallurgy, and Exploration.

Foley, N., & Ayuso, R. (2015). REE enrichment in granite-derived regolith deposits of the Southeastern United States: Prospective source rocks and accumulation processes. *Geological Survey Paper, 3*, 131–138.

Frakes, L. A., Francis, J. E., & Syktus, J. I. (2005). *Climate modes of the Phanerozoic*. Cambridge University Press. Retrieved from https://books.google.com/books?hl=en&lr=&id=EJlm8WH2lWoC&oi=fnd&pg=PP1&dq=Frakes,+L.A.,+Francis,+J.E.,+and+Syktus,+J.I.+(1992)+Climate+Modes+of+the+Phanerozoic.+Cambridge+University+Press,+pp.+274.&ots=1w-Xiq37nO&sig=Y9MeKeOYJBnGxPMKRP7z_3-CVN4

Fullagar, P. D., & Butler, J. R. (1976). Petrochemical and geochronologic studies of plutonic rocks in the southern Appalachians: II, The Sparta granite complex, Georgia. *Geological Society of America Bulletin*, *87*(1), 53–56.

Gambogi, J. (2016). Rare Earths, 2015. *Mining Engineering*, *68*(7), 30–30.

Gao, R., & Rudnick, R. L. (2003). *Composition of the continental crust, treatise of geochemistry, vol. 3*. Elsevier.

Hallam, A. (1984). Continental humid and arid zones during the Jurassic and Cretaceous. *Palaeogeography, Palaeoclimatology, Palaeoecology*, *47*(3), 195–223.

Huddlestun, P. F., & Hetrick, J. H. (1991). *The stratigraphic framework of the Fort Valley Plateau and the central Georgia Kaolin District*. Georgia Geological Society.

Hurst, V. J., & Pickering Jr, S. M. (1997). *Origin and classification of coastal plain kaolins, Southeastern USA, and the role of groundwater and microbial action* (Vol. 45). Retrieved from http://www.clay.uga.edu/courses/8550/Hurst_Pickering_1997.pdf

Jones, L. M., & Walker, R. L. (1973). Rb-Sr whole-rock age of the Siloam granite, Georgia: A Permian intrusive in the southern Appalachians. *Geological Society of America Bulletin*, *84*(11), 3653–3658.

Klemme, S., & Prowatke, S. (2005). Partitioning of trace elements between rutile and silicate melts: Implications for subduction zones. *Geochimica et Cosmochimica Acta, 69(9),* 2361-2371.

Lehman, T. M. (1987). Late Maastrichtian paleoenvironments and dinosaur biogeography in the western interior of North America. *Palaeogeography, Palaeoclimatology, Palaeoecology, 60*, 189–217.

Miller, B. V., Fetter, A. H., & Stewart, K. G. (2006). Plutonism in three orogenic pulses, eastern Blue Ridge Province, southern Appalachians. *Geological Society of America Bulletin*, *118*(1–2), 171–184.

Moore, D. M., & Reynolds Jr, R. C. (n.d.). *X-ray Diffraction and the Identification and Analysis of Clay Minerals*. Oxford University Press, New York.

Murray, H. H. (1980). Major kaolin processing developments. *International Journal of Mineral Processing*, *7*(3), 263–274. http://doi.org/10.1016/0301-7516(80)90022-8

Norris, R. D., Kroon, D., Huber, B. T., & Erbacher, J. (2001). Cretaceous-Palaeogene ocean and climate change in the subtropical North Atlantic. *Geological Society, London, Special Publications*, *183*(1), 1–22.

Pickering, S. M., & Linkous, M. A. (1997). Comparison of Fine and Coarse Commercial Kaolin Deposits from Georgia (USA) and Brazil. *PREPRINTS-SOCIETY OF MINING ENGINEERS OF AIME*.

Pickering, S. M. P., & Avant, D. (1999). Stratigraphy of the Georgia Kaolin District. SE GSA March, 1999

Plank, M. O., & Schenck, W. S. (1998). Delaware Piedmont Geology. Delaware Geological Survey.

Poulsen, C. J., Gendaszek, A. S., & Jacob, R. L. (2003). Did the rifting of the Atlantic Ocean cause the Cretaceous thermal maximum? *Geology*, *31*(2), 115–118.

Prothero, D. R., & Dott, R. H. (2004). *Evolution of the Earth*. McGraw-Hill Science Engineering.

Prowell, D. C., & Christopher, R. (2000). The last Appalachian orogeny: evidence for Cenozoic tectonism and uplift of mountains in the eastern United States. Geological Society of America, Southeastern Section Meeting. In *Abstracts with Programs* (Vol. 32, p. 67).

Rozelle, P. L., Khadilkar, A. B., Pulati, N., Soundarrajan, N., Klima, M. S., Mosser, M. M., … Pisupati, S. V. (2016). A Study on Removal of Rare Earth Elements from US Coal Byproducts by Ion Exchange. *Metallurgical and Materials Transactions E*, *3*(1), 6–17.

Schroeder, P. A., & Erickson, G. (2014). Kaolin: From Ancient Porcelains to Nanocomposites. *Elements*, *10*(3), 177–182. http://doi.org/10.2113/gselements.10.3.177

Snoke, A. W., Kish, S. A., & Secor, D. J. (1980). Deformed Hercynian granitic rocks from the Piedmont of South Carolina. *American Journal of Science*, *280*(10), 1018–1034.

Totten, M. & Hanan, M. (2007). Heavy Minerals in Shales. *Developments in Sedimentology, 58*, 323-341.

Trail, D., Watson, E. B., & Tailby, N. D. (2012). Ce and Eu anomalies in zircon as proxies for the oxidation state of magmas. *Geochimica et Cosmochimica Acta*, *97*, 70–87.

Van Gosen, B. S., Verplanck, P. L., Long, K. R., Gambogi, J., & Seal, R. R. (2014). The rare-earth elements–Vital to modern technologies and lifestyles. *US Geological Survey Fact Sheet*, *3078*.

Vilsack, T. (2009). 2007 Census of Agriculture United States Summary and State Data. *Census of Agriculture*, *1*(51).

Watson, E. B., Wark, D. A., & Thomas, J. B. (2006). Crystallization thermometers for zircon and rutile. *Contributions to Mineralogy and Petrology*, *151*(4), 413–433.

Zachos, J., Pagani, M., Sloan, L., Thomas, E., & Billups, K. (2001). Trends, rhythms, and aberrations in global climate 65 Ma to present. *Science*, *292*(5517), 686–693.

APPENDICES

Appendix A

Standard and reproducibility data were provided by Activation Laboratories. The dataset was arranged into the three elemental groups observed in this study, major, rare earth, and trace elements.

Analyte Symbol	SiO_2	Al_2O_3	Fe_2O_3	MnO	MgO	CaO	Na_2O	K_2O	TiO_2	P_2O_5
Unit Symbol	%	%	%	%	%	%	%	%	%	%
Lower Limit	0.01	0.01	0.01	0.001	0.01	0.01	0.01	0.01	0.001	0.01
Method Code	FUS-ICP	FUS-ICP	FUS-ICP	FUS-ICP	FUS-ICP	FUS-ICP	FUS-ICP	FUS-ICP	FUS-ICP	FUS-ICP
NIST 694 Meas	11.64	1.94	0.75	0.012	0.35	42.75	0.89	0.58	0.121	30.21
NIST 694 Cert	11.2	1.8	0.79	0.0116	0.33	43.6	0.86	0.51	0.11	30.2
DNC-Meas	47.14	17.93	9.78	0.15	10.14	11.5	1.88	0.22	0.48	0.07
DNC-Cert	47.15	18.34	9.97	0.15	10.13	11.49	1.89	0.234	0.48	0.07
W-2a Meas	52.65	15.36	10.82	0.17	6.39	11.05	2.21	0.63	1.09	0.14
W-2a Cert	52.4	15.4	10.7	0.163	6.37	10.9	2.14	0.626	1.06	0.13
SARM-62 Meas	33.05	0.84			0.05	0.15			0.13	0.14
SARM-62 Cert	32.8	0.88			0.04	0.11			0.13	0.12
SY-4 Meas	50.81	21.26	6.26	0.11	0.52	8.01	7.17	1.76	0.3	0.13
SY-4 Cert	49.9	20.69	6.21	0.108	0.54	8.05	7.1	1.66	0.287	0.131
BIR-1a Meas	47.84	15.67	11.39	0.17	9.71	13.61	1.78	0.02	0.98	0.02
BIR-1a Cert	47.96	15.5	11.3	0.175	9.7	13.3	1.82	0.03	0.96	0.021

Table 9: Major Elemental Standards and Reproducibility

Analyte Symbol	La	Ce	Pr	Nd	Sm	Eu	Gd	Tb	Dy	Ho	Er	Tm	Yb	Lu
Unit Symbol	ppm	ppm	ppm	ppm	ppm	ppm	ppm	ppm	ppm	ppm	ppm	ppm	ppm	ppm
Lower Limit	0.1	0.1	0.05	0.1	0.1	0.05	0.1	0.1	0.1	0.1	0.1	0.05	0.1	0.04
Method Code	FUS-MS	FUS-MS	FUS-MS	FUS-MS	FUS-MS	FUS-MS	FUS-MS	FUS-MS	FUS-MS	FUS-MS	FUS-MS	FUS-MS	FUS-MS	FUS-MS
DNC-Meas				5.4									2.1	
DNC-Cert				5.2									2	
LKSD-3 Meas	48	89.5		46.1	8.3	1.4		0.9	5.4				2.9	0.46
LKSD-3 Cert	52	90		44	8	1.5		1	4.9				2.7	0.4
W2a Meas		24.7		13.4	3.3			0.6		0.8			2.1	0.3
W2a Cert		23		13	3.3			0.63		0.76			2.1	0.33
CTA-AC-1 Meas	2300	3510		1130	163	50.4	124						12.4	
CTA-AC-1 Cert	2176	3326		1087	162	46.7	124						11.4	
BIR-1a Meas	0.6	1.8		2.4	1.2	0.54	1.9		4				1.8	0.26
BIR-1a Cert	0.63	1.9		2.5	1.1	0.55	2		4				1.7	0.3
NCS DC86312 Meas	2360	183		1520				34.9	196	37.6	96.6	14.5	90.4	13
NCS DC86312 Cert	2360	190		1600				34.6	183	36	96.2	15.1	87.79	11.96
NCS DC 70009 Meas	25.8	65.3	8	33	13		15	3.2	21	4.4	13.3	2.2	15.9	2.58
NCS DC 70009 Cert	23.7	60.3	7.9	32.9	12.5		14.8	3.3	20.7	4.5	13.4	2.2	14.9	2.4
OREAS 100a Meas	274	496	50	166	26	4.07	25	4.1	24.4	5.1	16.1	2.4	15.6	2.25
OREAS 100a Cert	260	463	47.1	152	23.6	3.71	23.6	3.8	23.2	4.81	14.9	2.31	14.9	2.6
OREAS 101a Meas	791	1380	130	402	51	8.05		5.6	33.5	6.8	20.8	3	18.9	2.71
OREAS101a Cert	816	1396	134	403	48.8	8.06		5.92	33.3	6.46	19.5	2.9	17.5	2.66
JR-1 Meas	19.4	46.3	6.1	24.4	6	0.27		1				0.72	4.9	0.74
JR-1 Cert	19.7	47.2	5.58	23.3	6.03	0.3		1.01				0.67	4.55	0.71
NCS DC 96318 Meas	1970	426	759	3250	1660	19.1	2240	514	3290	607	1720	277	1860	253
NCS DC 96318 Cert	1960	430	740	3430	1720	18.91	2095	470	3220	560	1750	270	1840	260
USZ 42-2006 Meas	20800	27900	2300	6530	509	86								
USZ 42-2006 Cert	21100	27600	2300	6500	539	87.22								
Method Blank	<0.1	<0.1	<0.05	<0.1	<0.1	<0.05	<0.1	<0.1	<0.1	<0.1	<0.1	<0.05	<0.1	<0.04

Table 10: Rare Earth Elemental Standards and Reproducability

Analyte Symbol	Sc	Be	V	Cr	Co	Ni	Cu	Zn	Ga	Ge	As	Rb	Sr	Y	Zr
Unit Symbol	ppm	ppm	ppm	ppm	ppm	ppm	ppm	ppm	ppm	ppm	ppm	ppm	ppm	ppm	ppm
Lower Limit	1	1	5	20	1	20	10	30	1	1	5	2	2	2	4
Method Code	FUS-ICP	FUS-ICP	FUS-ICP	FUS-MS	FUS-MS	FUS-MS	FUS-MS	FUS-MS	FUS-MS	FUS-MS	FUS-MS	FUS-MS	FUS-ICP	FUS-ICP	FUS-ICP
NIST 694 Meas			1633												
NIST 694 Cert			1740												
DNC-1 Meas	31		155	270	55	250	110	70	15			3	137	16	41
DNC-1 Cert	31		148	270	57	247	100	70	15			5	144	18	38
LKSD-3 Meas					29	50	30				27	71			
LKSD-3 Cert					30	47	35				27	78			
OKA-2 Meas															
OKA-2 Cert															
W-2A Meas	36	< 1	275	90	43	70	110	70	17	1		20	191	20	99
W-2A Cert	36	1.3	262	92	43	70	110	80	17	1		21	190	27	94.9
SARM-62 Meas															476900
SARM-62 Cert															476000
SY-4 Meas	1	3	10										1236	121	532
SY-4 Cert	1.1	2.6	8										1191	119	517
CTA-AC-1 Meas							60	40							
CTA-AC-1 Cert							54	38							
BIR-1a Meas	43	< 1	333	390	50	170		70	17	11	73	516	103	13	17
BIR-1a Cert	44	0.58	310	370	52	170		70	16	11.2	69.9	500	110	16	18
ZW-C Meas								1040	96			8700			
ZW-C Cert								1050	99			8500			
NCS DC 70009 Meas				30	4		1050	110	17						
NCS DC 70009 Cert				30	3.7		960	100	16.5						
OREAS 100a Meas					17		160								
OREAS 100a Cert					18.1		169								
OREAS 101a Meas					46										
OREAS 101a Cert					48.8										
JR-1 Meas					1	< 20			18		16				
JR-1 Cert					0.83	1.67			16.1		16.3				
SARM 3 Meas															
SARM 3 Cert															
Method Blank				< 20	< 1	< 20	< 10	< 30	< 1	< 1	< 5	< 2			

Table 11: Trace Elemental Standards and Reproducability

Analyte Symbol	Nb	Mo	Ag	In	Sn	Sb	Cs	Ba	Bi	Hf	Ta	W	Tl	Pb	Th	U
Unit Symbol	ppm	ppm	ppm	ppm	ppm	ppm	ppm	ppm	ppm	ppm	ppm	ppm	ppm	ppm	ppm	ppm
Lower Limit	1	2	0.5	0.2	1	0.2	0.5	3	0.4	0.2	0.1	1	0.1	5	0.1	0.1
Method Code	FUS-MS	FUS-MS	FUS-MS	FUS-MS	FUS-MS	FUS-MS	FUS-MS	FUS-MS	FUS-MS	FUS-MS	FUS-MS	FUS-MS	FUS-MS	FUS-MS	FUS-MS	FUS-MS
NIST 694 Meas																
NIST 694 Cert																
DNC-1 Meas	1					0.9		105						6		
DNC-1 Cert	3					0.96		118						6.3		
LKSD-3 Meas		< 2	2.8				2.6			4.9	0.6				11.4	5
LKSD-3 Cert		2	2.7				2.3			4.8	0.7				11.4	4.6
OKA-2 Meas															29200	
OKA-2 Cert															28900	
W-2A Meas		< 2	< 0.5			0.9		175	< 0.4	2.5		< 1	< 0.1		2.2	0.5
W-2A Cert		0.6	0.046			0.79		182	0.03	2.6		0.3	0.2		2.4	0.53
SARM-62 Meas										10700						
SARM-62 Cert										11100						
SY-4 Meas								361								
SY-4 Cert								340								
CTA-AC-1 Meas															24.1	4.8
CTA-AC-1 Cert															21.8	4.4
BIR-1a Meas	< 1					0.6		6		0.6				5		
BIR-1a Cert	0.6					0.58		6		0.6				3		
ZW-C Meas							255				83.6	334	34.4			
ZW-C Cert							260				82	320	34			
NCS DC 70009 Meas		974	1.7	1.2	1680							2040	1.9		28.8	
NCS DC 70009 Cert		980	1.8	1.3	1701							2200	1.8		28.3	
OREAS 100a Meas		25													53.7	143
OREAS 100a Cert		24.1													51.6	135
OREAS 101a Meas		20													39.7	424
OREAS 101a Cert		21.9													36.6	422
JR-1 Meas	15		< 0.5	< 0.2	3	1.1	22.7		0.4	4.5	1.7		1.5	19	28.1	9.4
JR-1 Cert	15.2		0.031	0.028	2.86	1.19	20.8		0.56	4.51	1.86		1.56	19.3	26.7	8.88
SARM 3 Meas	990															
SARM 3 Cert	978															
Method Blank	< 1	< 2	< 0.5	< 0.2	< 1	< 0.5	< 0.5		< 0.4	< 0.2	< 0.1	< 1	< 0.1	< 5	< 0.1	< 0.1

Table 12: Trace Elemental Standards and Reproducability

Appendix B

Mineral grains analyzed and photographed during the SEM examinations are shown below. Elemental spectra are provided for mineral grains which were chemically analyzed.

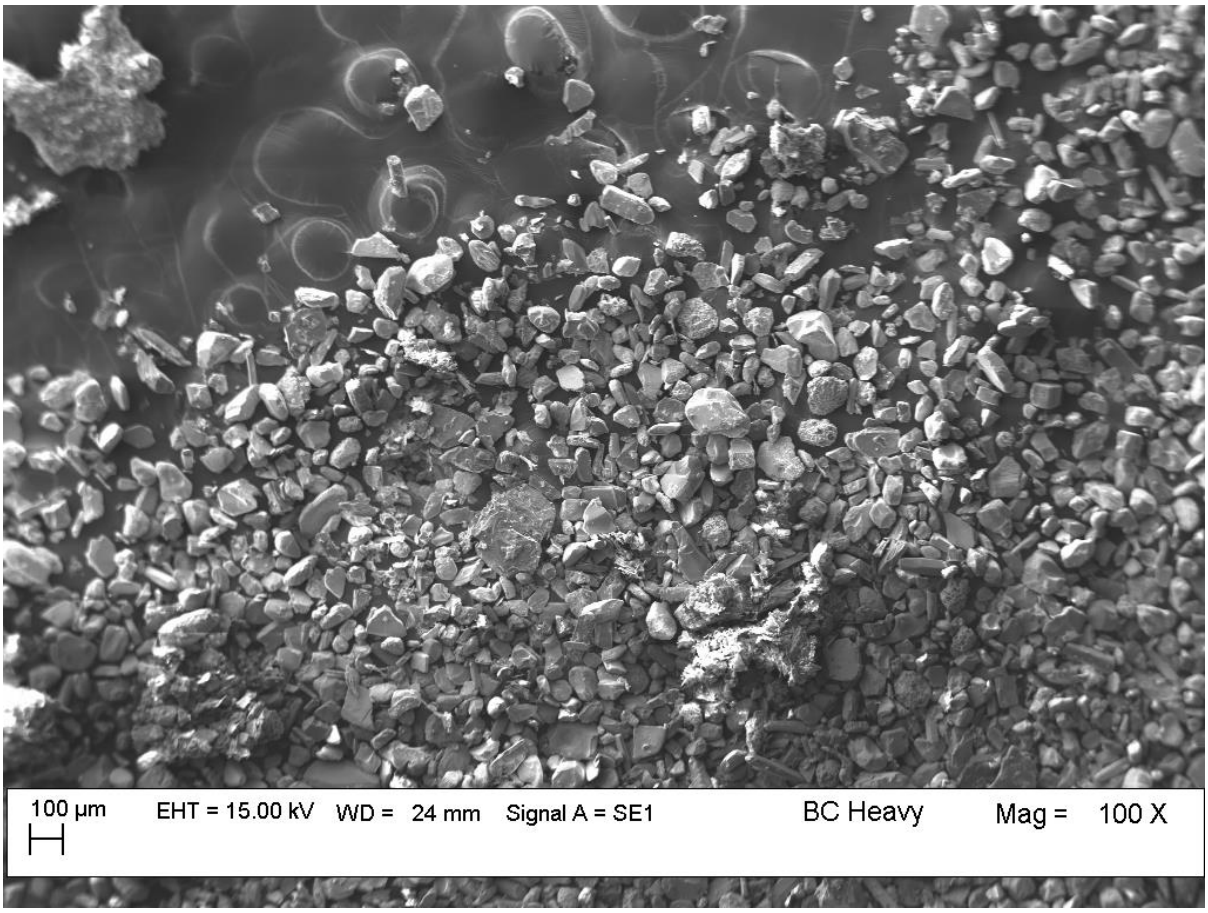

SEM 1

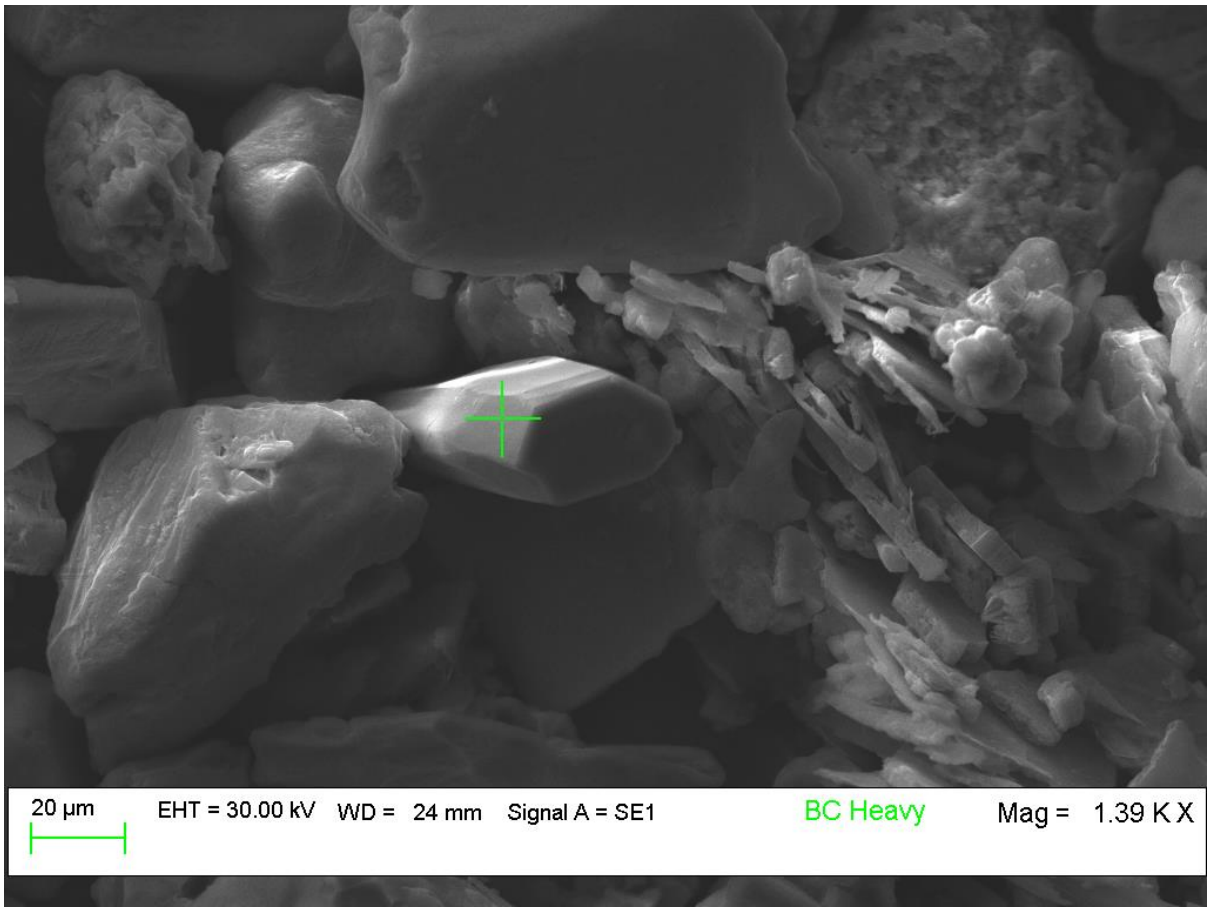
20 µm
EHT = 30.00 kV
WD = 24 mm
Signal A = SE1
BC Heavy
Mag = 1.39 K X

SEM2

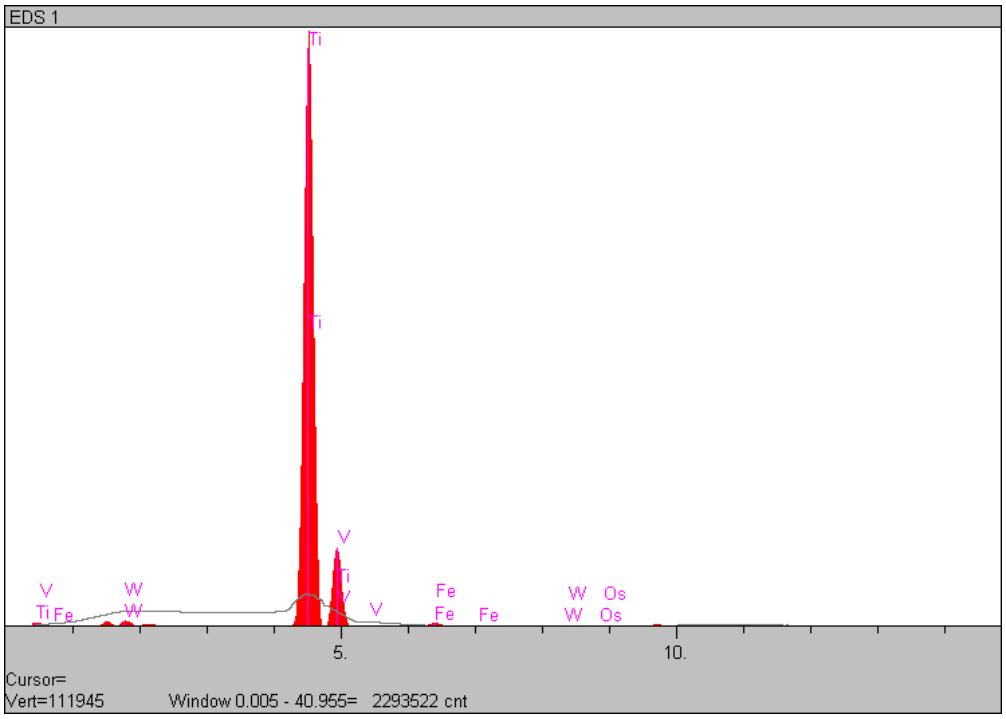
EDS 1
Ti
Ti
V
Ti
V
V
Ti Fe
W
W
Fe
Fe
Fe
W
W
Os
Os
5.
10.
Cursor=
Vert=111945
Window 0.005 - 40.955= 2293522 cnt

SEM2

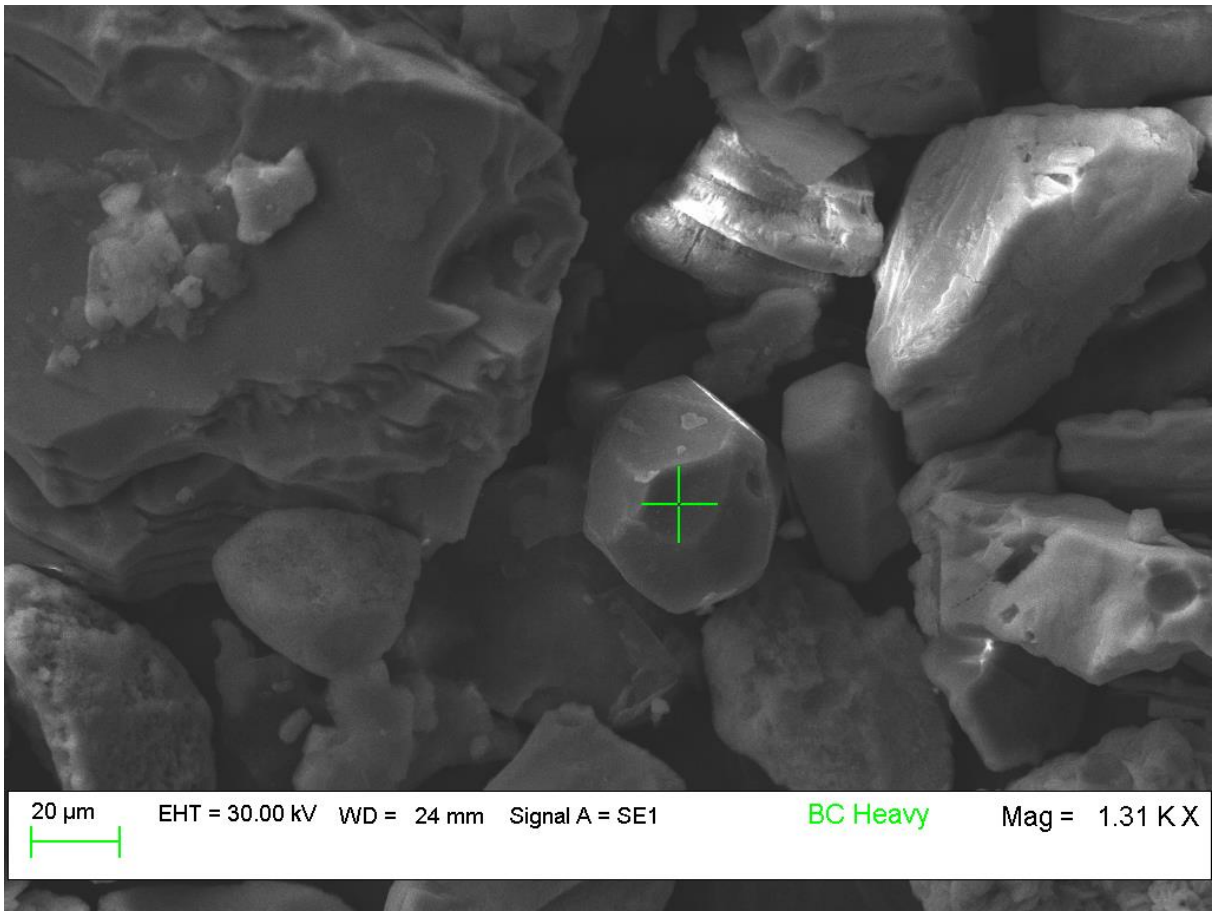
20 µm
EHT = 30.00 kV
WD = 24 mm
Signal A = SE1
BC Heavy
Mag = 1.31 K X

SEM3

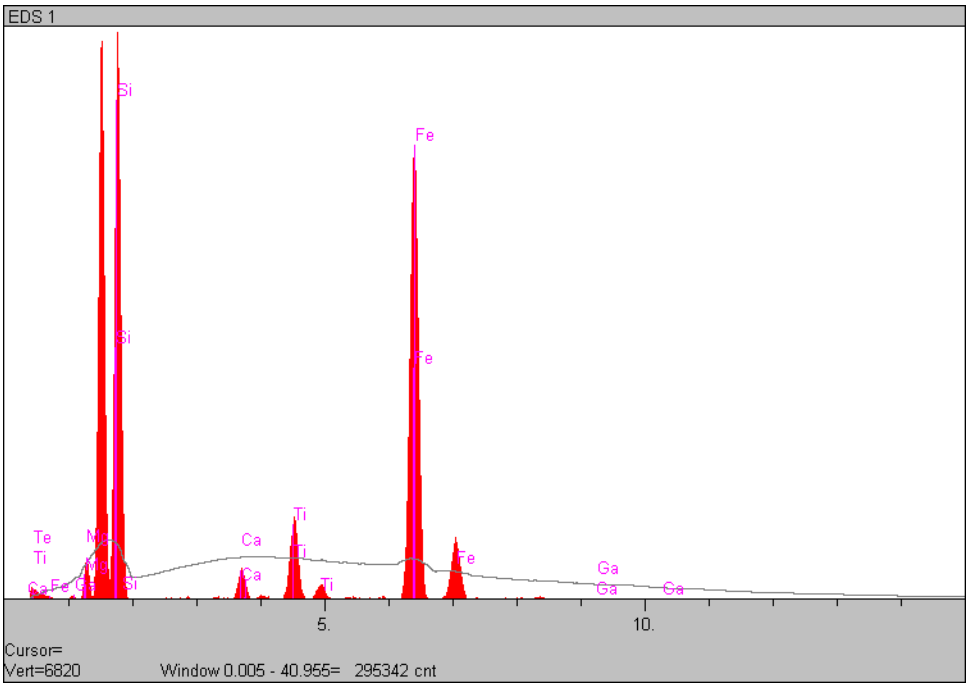
EDS 1
Si
Fe
Si
Fe
Ti
Ca
Ti
Ca
Ti
Fe
Ga
Ga
Ca
Te
Ti
5.
10.
Cursor=
Vert=6820
Window 0.005 - 40.955= 295342 cnt

SEM 3

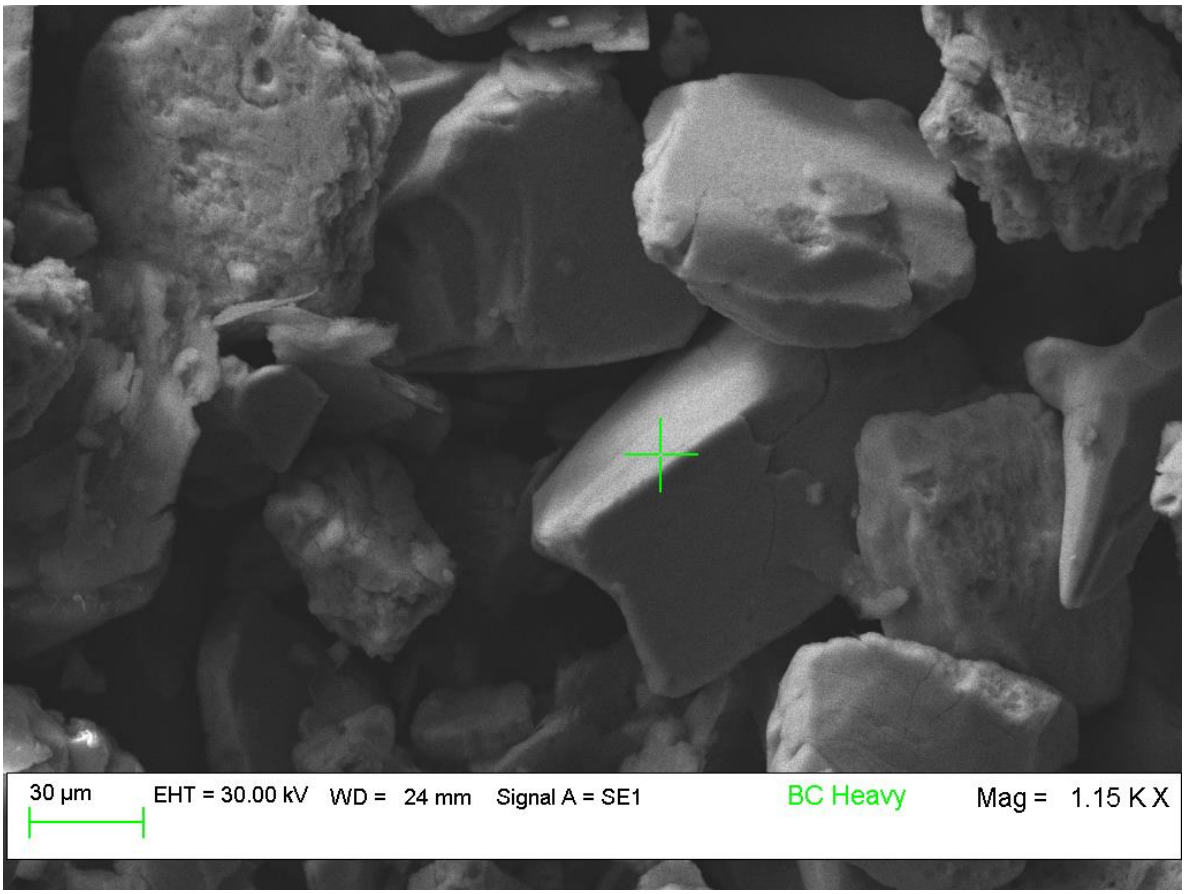
30 µm
EHT = 30.00 kV
WD = 24 mm
Signal A = SE1
BC Heavy
Mag = 1.15 K X

SEM 4

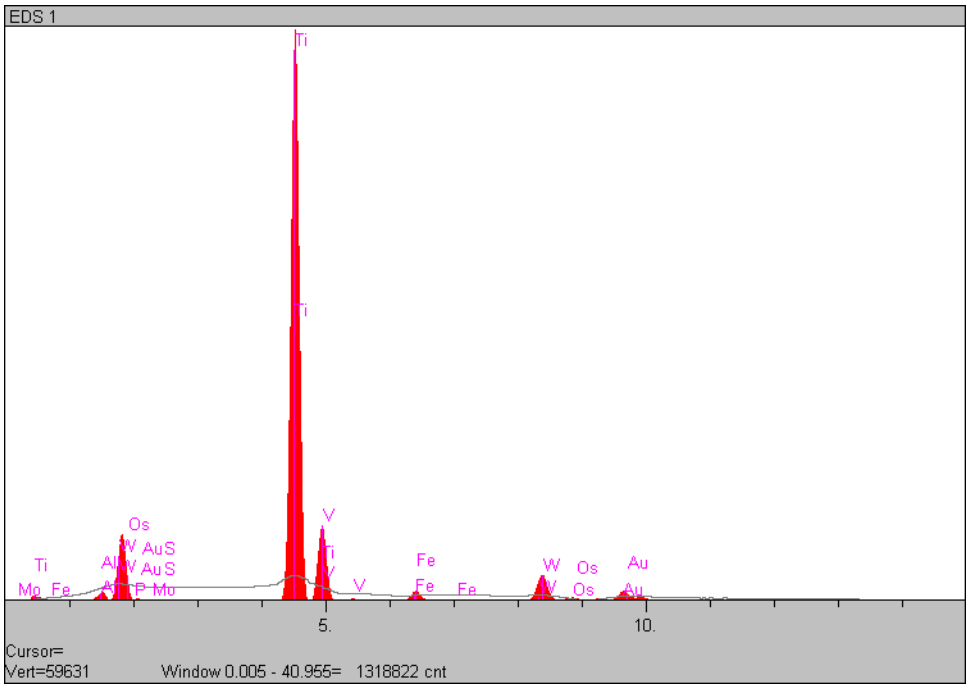
EDS 1
Ti
Ti
V
Os
W Au S
Ti
Al
W Au S
Mo Fe
Al
P Mo
Ti
V
V
Fe
Fe
Fe
W
Os
W
Os
Au
Au
5.
10.
Cursor=
Vert=59631
Window 0.005 - 40.955= 1318822 cnt

SEM 4

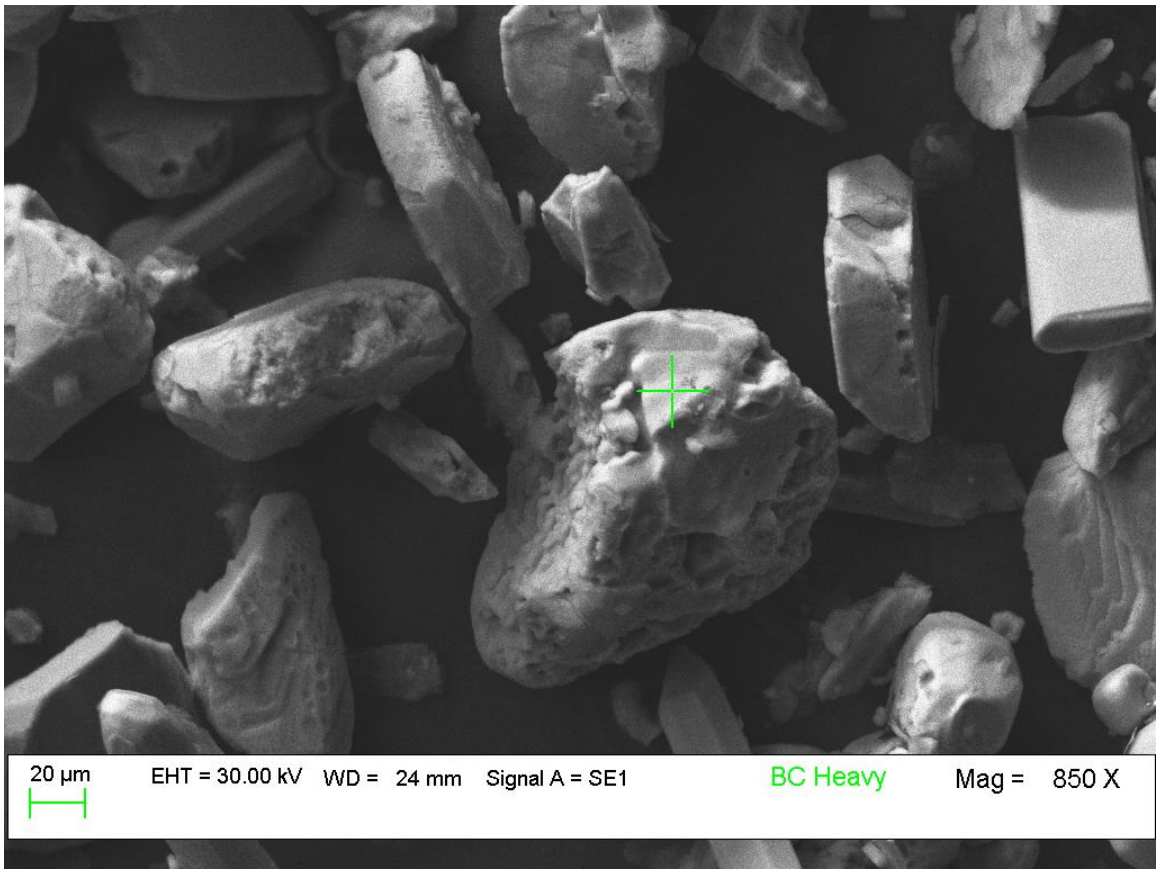
20 µm
EHT = 30.00 kV
WD = 24 mm
Signal A = SE1
BC Heavy
Mag = 850 X

SEM 5

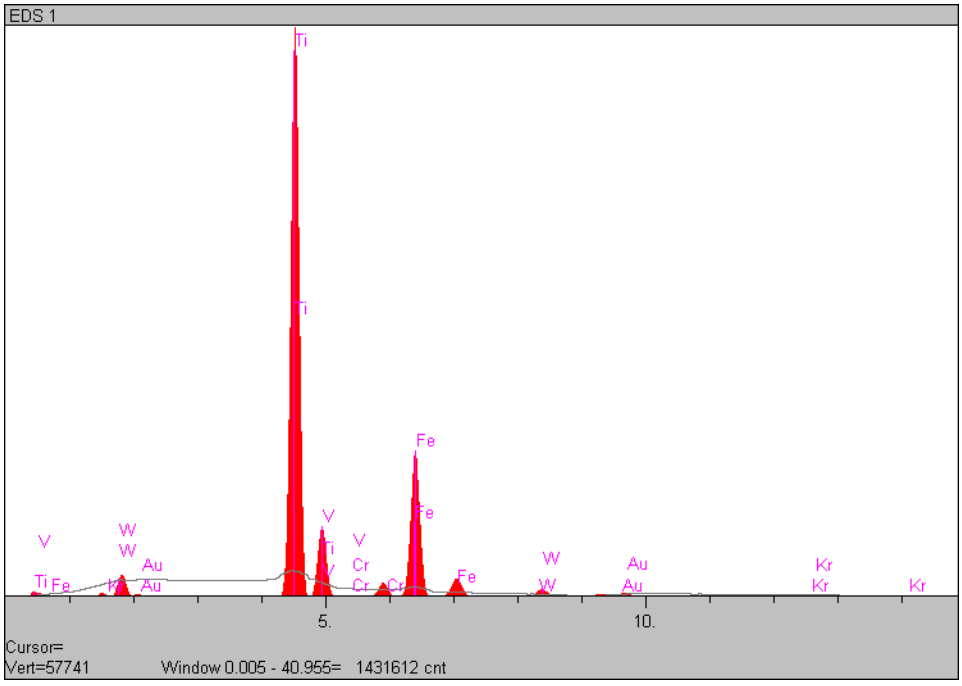
EDS 1
Ti
Fe
V
W
Au
Kr
Cr
5.
10.
Cursor=
Vert=57741
Window 0.005 - 40.955= 1431612 cnt

SEM 5

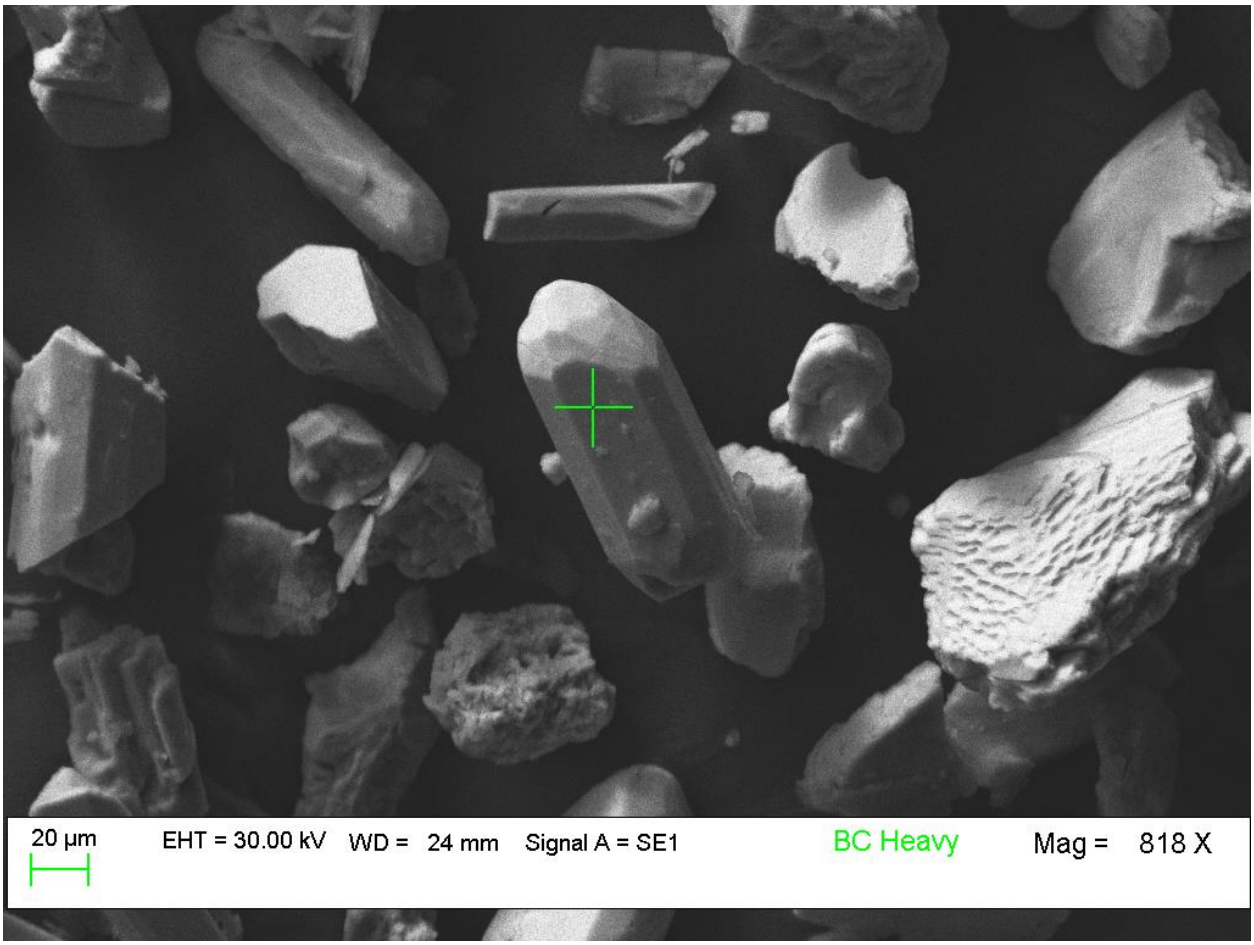
20 µm
EHT = 30.00 kV
WD = 24 mm
Signal A = SE1
BC Heavy
Mag = 818 X

SEM 6

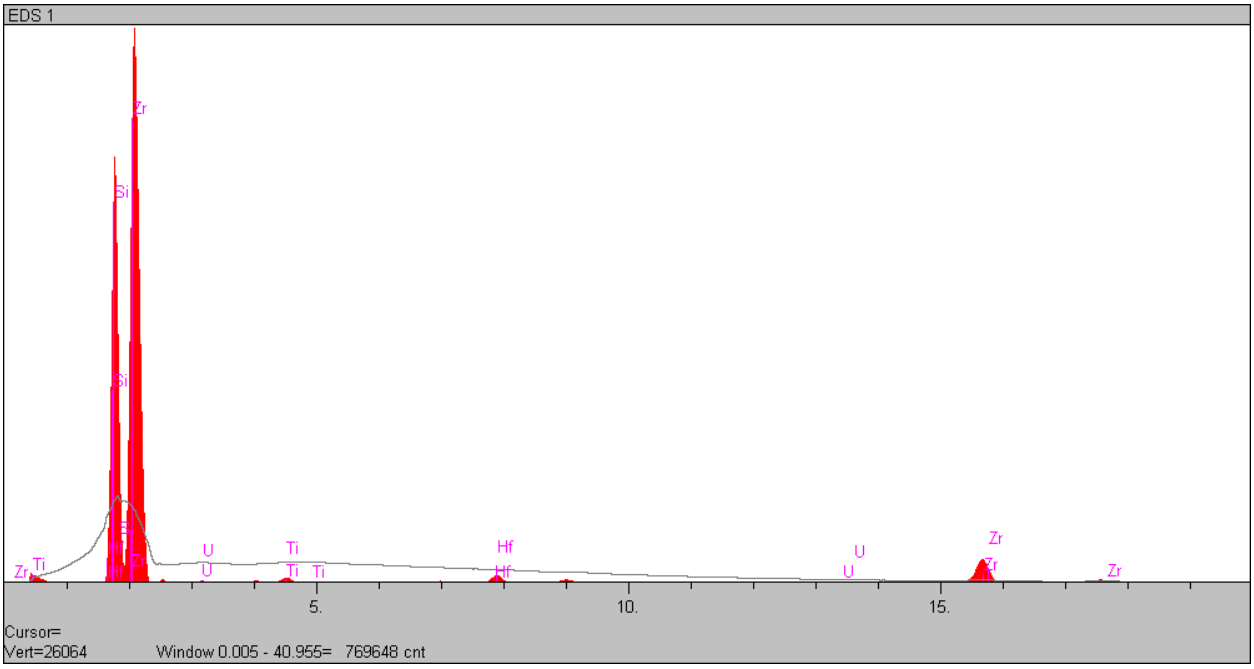
EDS 1
Zr
Si
Si
Zr
Ti
Zr
U
U
Ti
Ti
Ti
Hf
Hf
U
U
Zr
Zr
Zr
5.
10.
15.
Cursor=
Vert=26064
Window 0.005 - 40.955= 769648 cnt

SEM 6

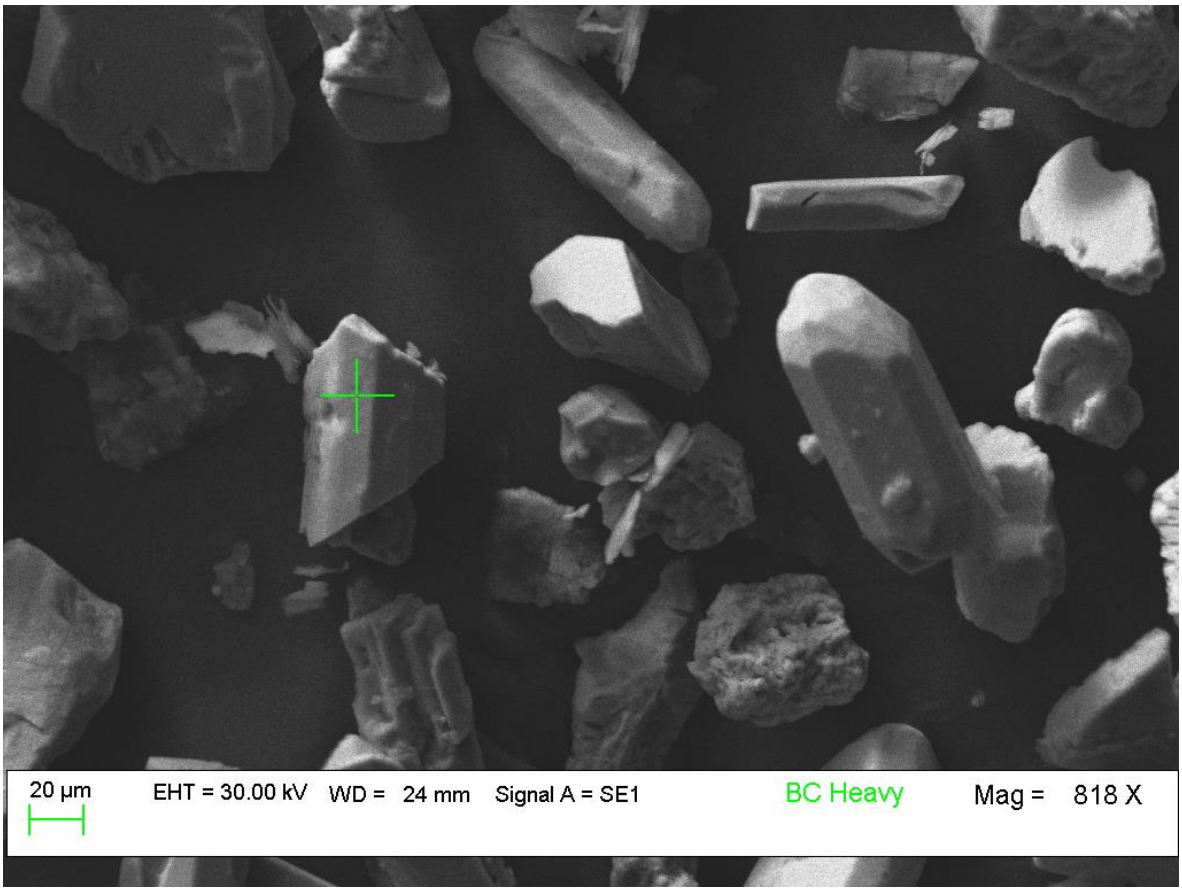
20 µm
EHT = 30.00 kV
WD = 24 mm
Signal A = SE1
BC Heavy
Mag = 818 X

SEM 7

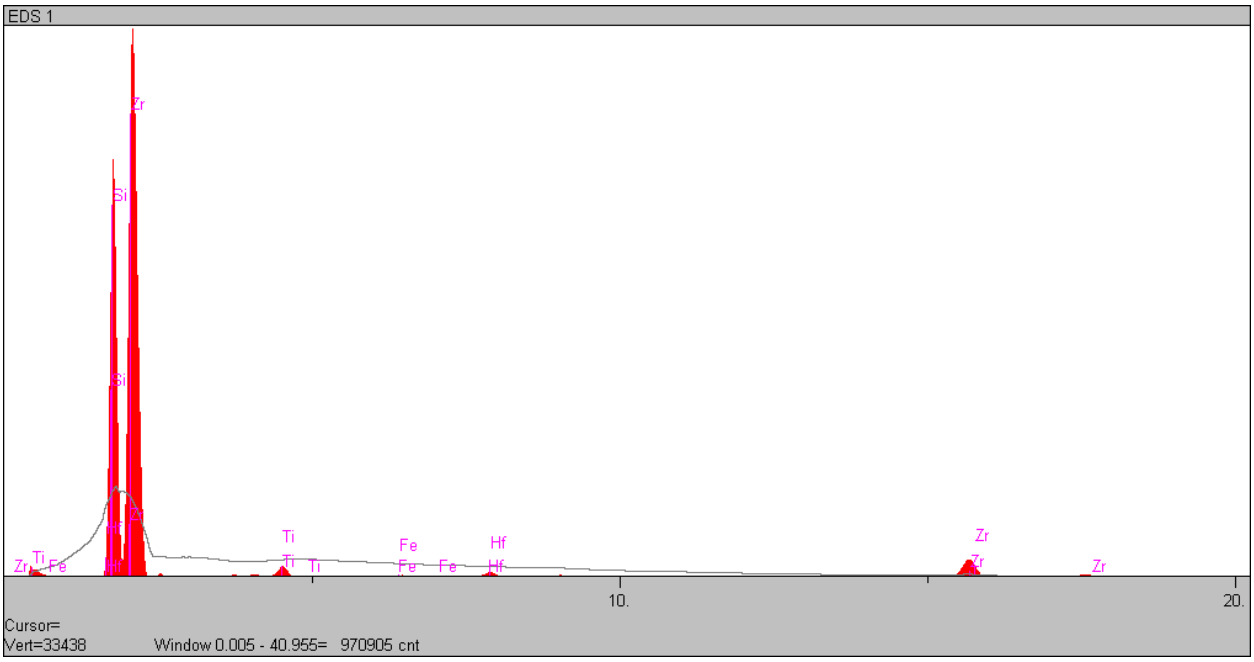
EDS 1
Zr
Si
Si
Ti
Fe
Ti
Ti
Fe
Fe
Hf
Hf
Zr
Zr
Zr
10.
20.
Cursor=
Vert=33438
Window 0.005 - 40.955= 970905 cnt

SEM 7

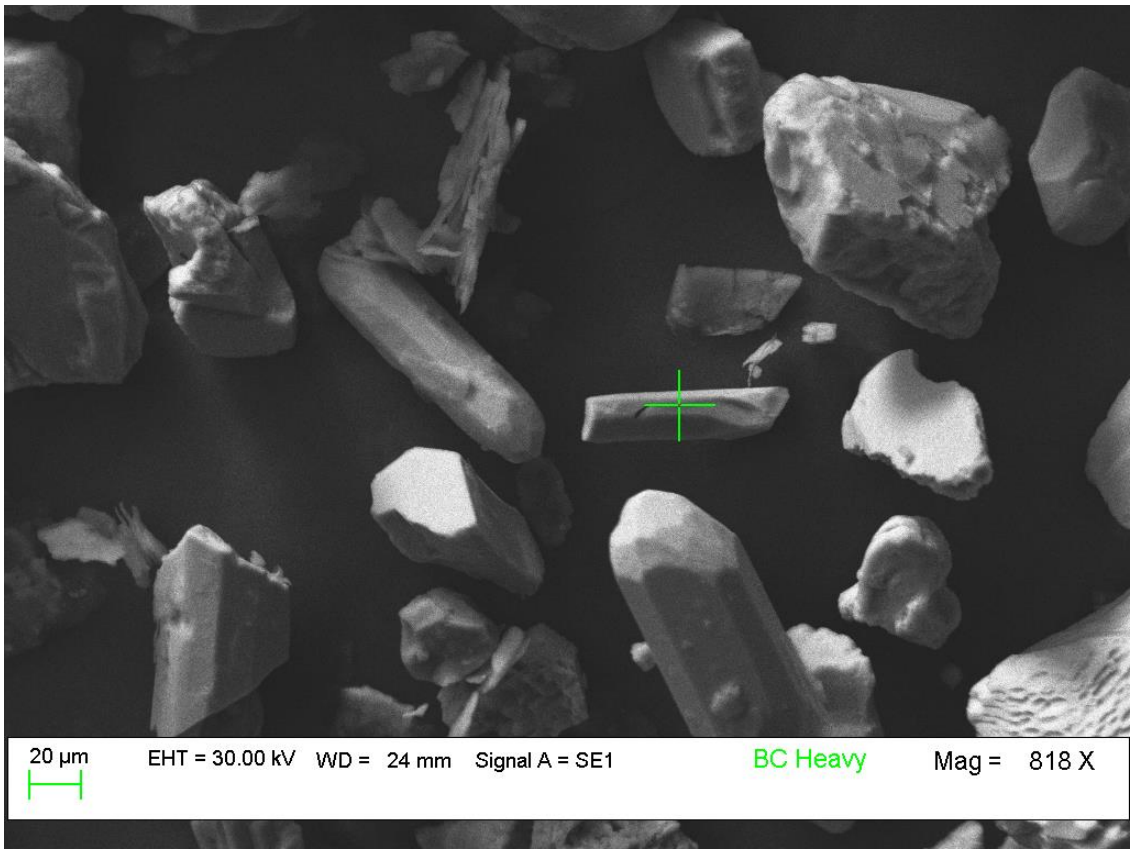
20 µm
EHT = 30.00 kV
WD = 24 mm
Signal A = SE1
BC Heavy
Mag = 818 X

SEM 8

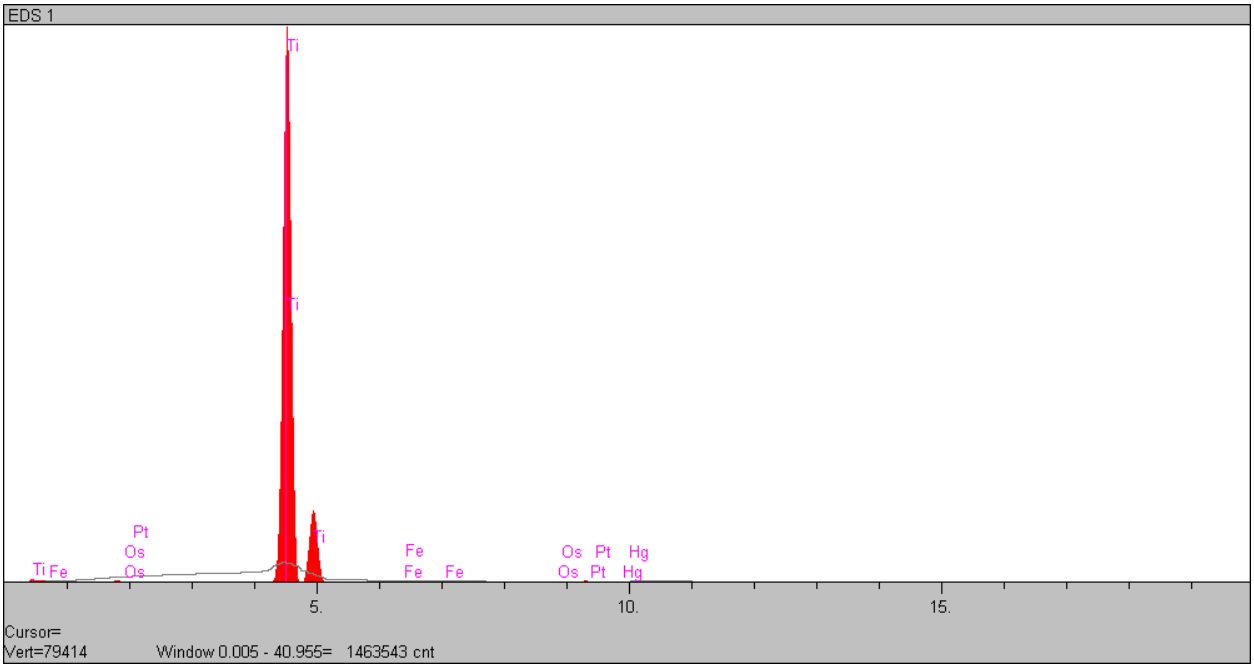
EDS 1
Ti
Ti
Ti
Pt
Os
Os
Ti Fe
Fe
Fe Fe
Os Pt Hg
Os Pt Hg
5.
10.
15.
Cursor=
Vert=79414
Window 0.005 - 40.955= 1463543 cnt

SEM 8

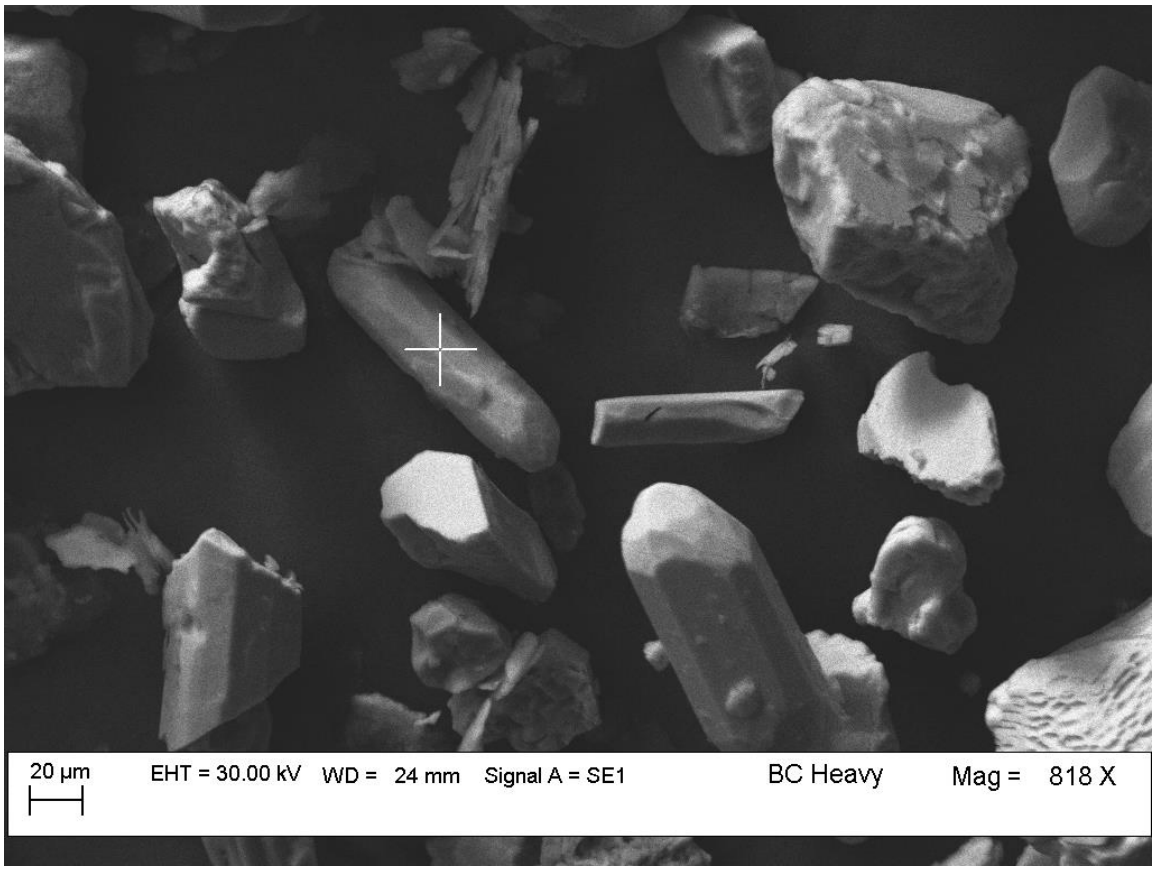
20 µm
EHT = 30.00 kV
WD = 24 mm
Signal A = SE1
BC Heavy
Mag = 818 X

SEM 9

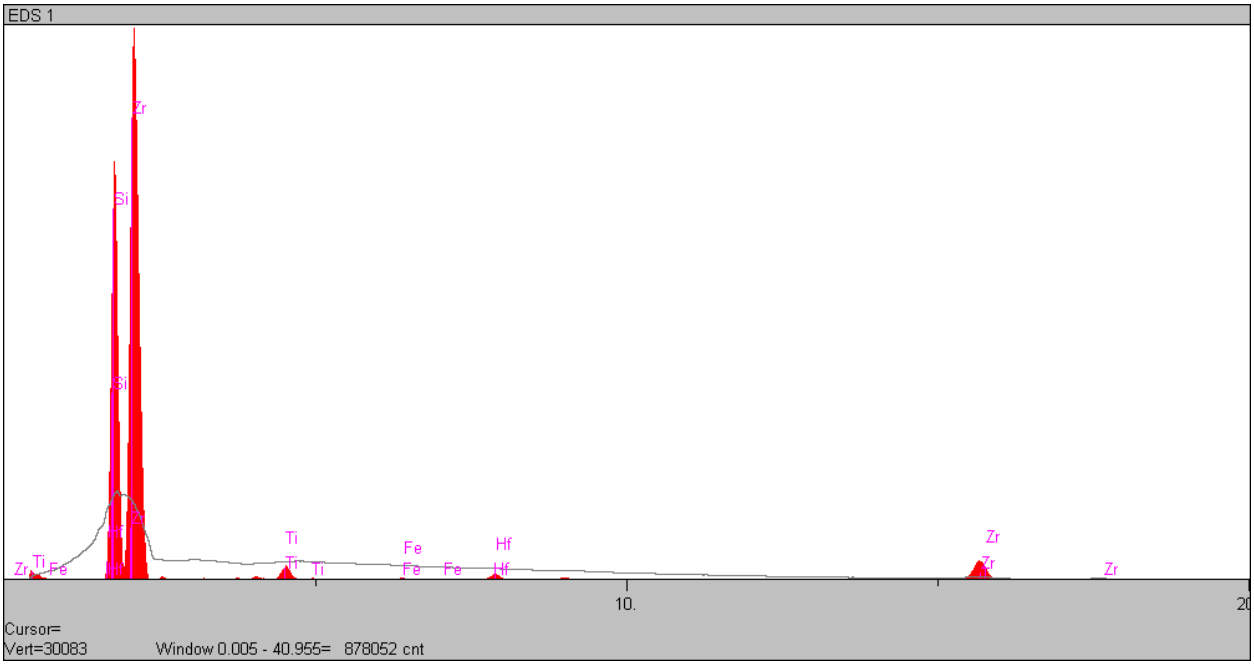
EDS 1
Zr
Si
Si
Ti
Fe
Hf
Zr
10.
Cursor=
Vert=30083
Window 0.005 - 40.955= 878052 cnt

SEM 9


20 µm
EHT = 30.00 kV
WD = 24 mm
Signal A = SE1
BC Heavy
Mag = 818 X

SEM 10

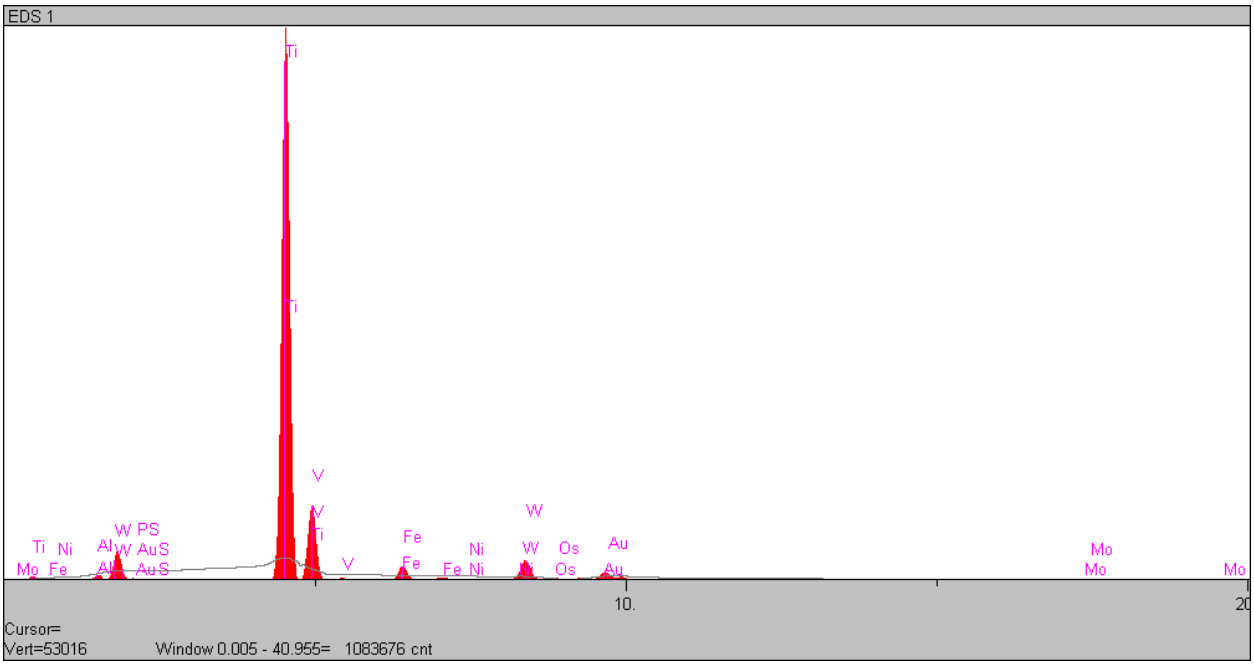
EDS 1
Ti
Ti
V
V
Ti
V
Fe
Fe
Fe
Ni
Ni
W
W
Os
Os
Au
Au
Mo
Mo
Mo
Ti
Mo
Ni
Fe
Al
W
PS
W
Au
S
Au
S
10.
Cursor=
Vert=53016
Window 0.005 - 40.955= 1083676 cnt

SEM 10

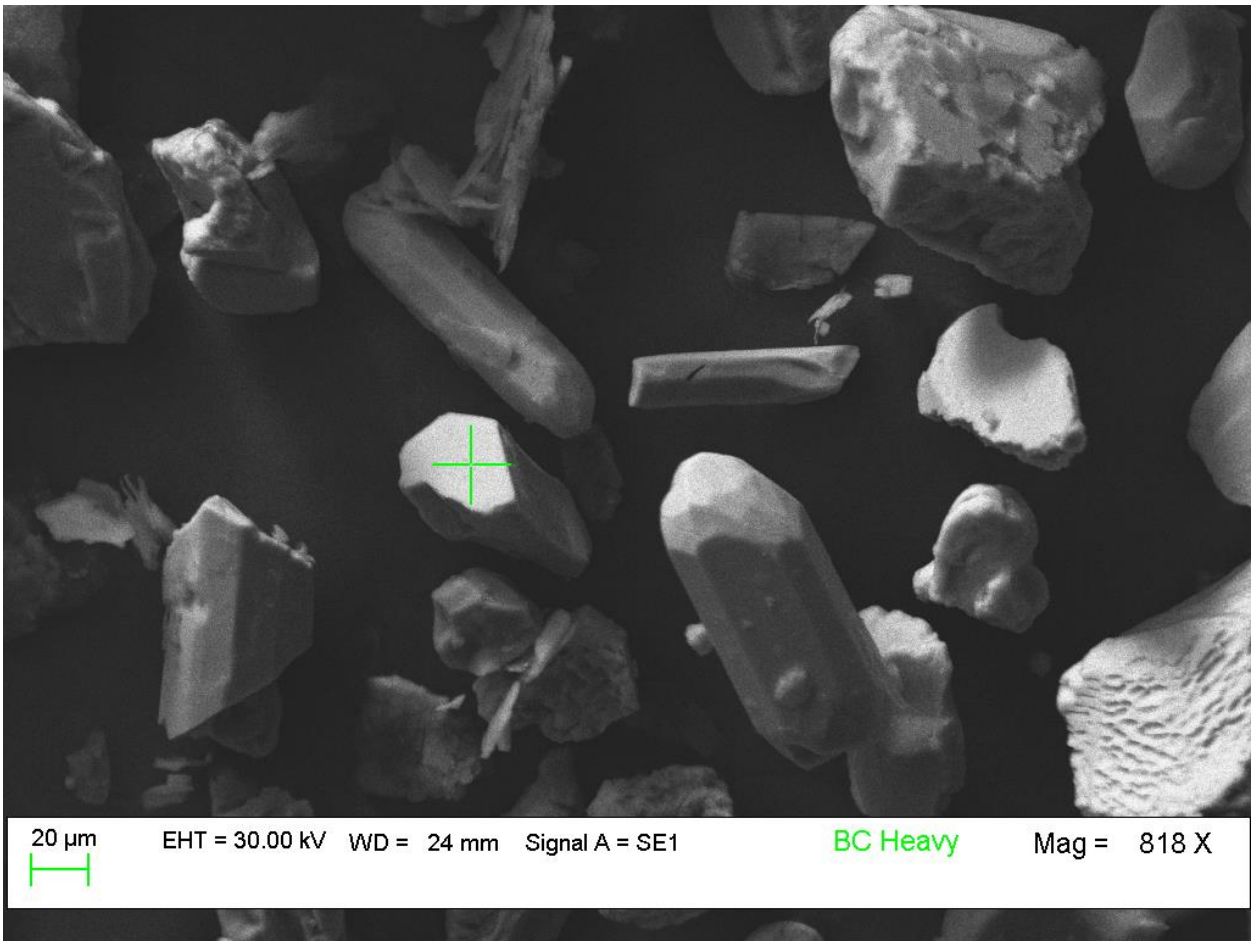
20 µm
EHT = 30.00 kV
WD = 24 mm
Signal A = SE1
BC Heavy
Mag = 818 X

SEM 11

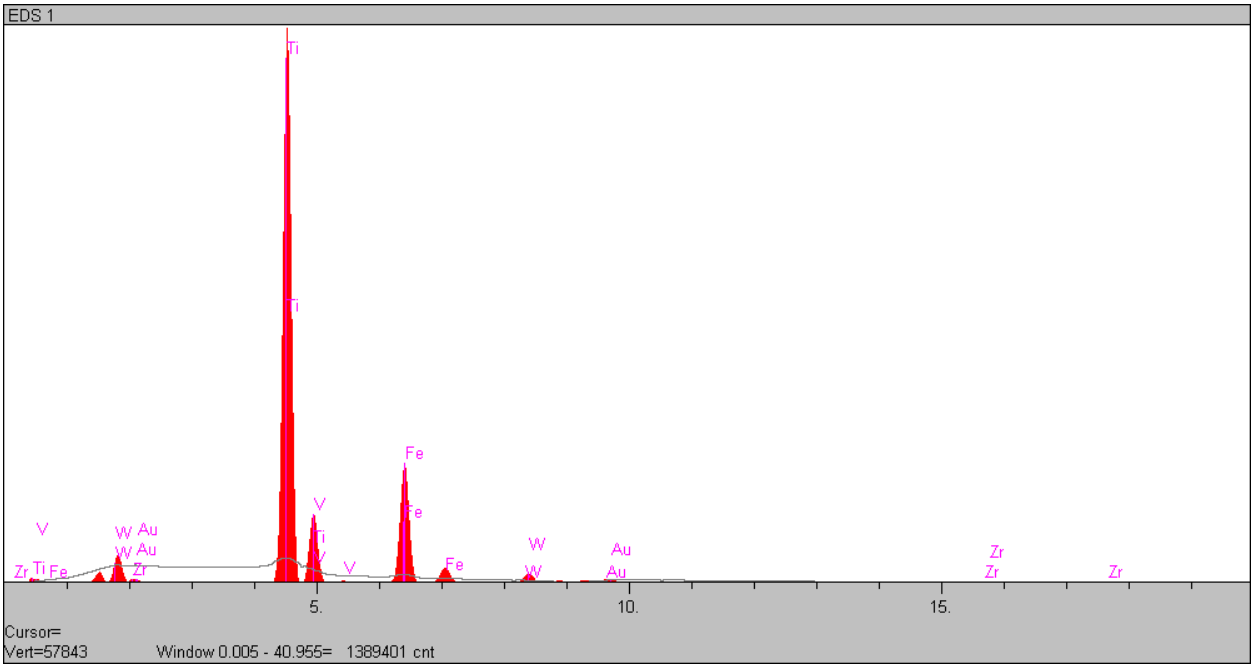
EDS 1
Ti
Ti
Fe
Fe
V
V
Ti
V
Fe
W
W
Au
Au
Au
Au
Zr
Zr
Zr
Zr
Ti
Fe
5.
10.
15.
Cursor=
Vert=57843
Window 0.005 - 40.955= 1389401 cnt

SEM 11

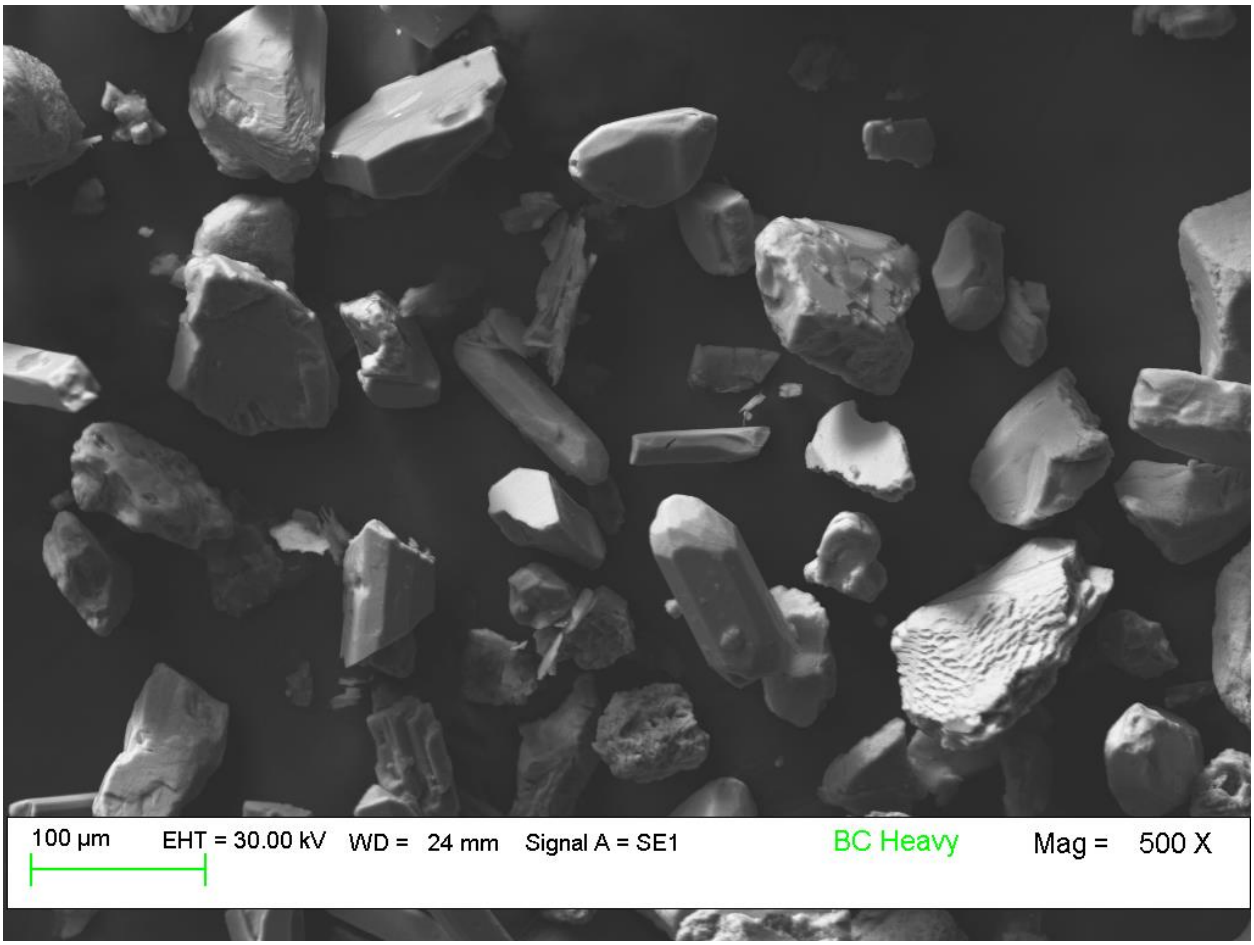

SEM 12

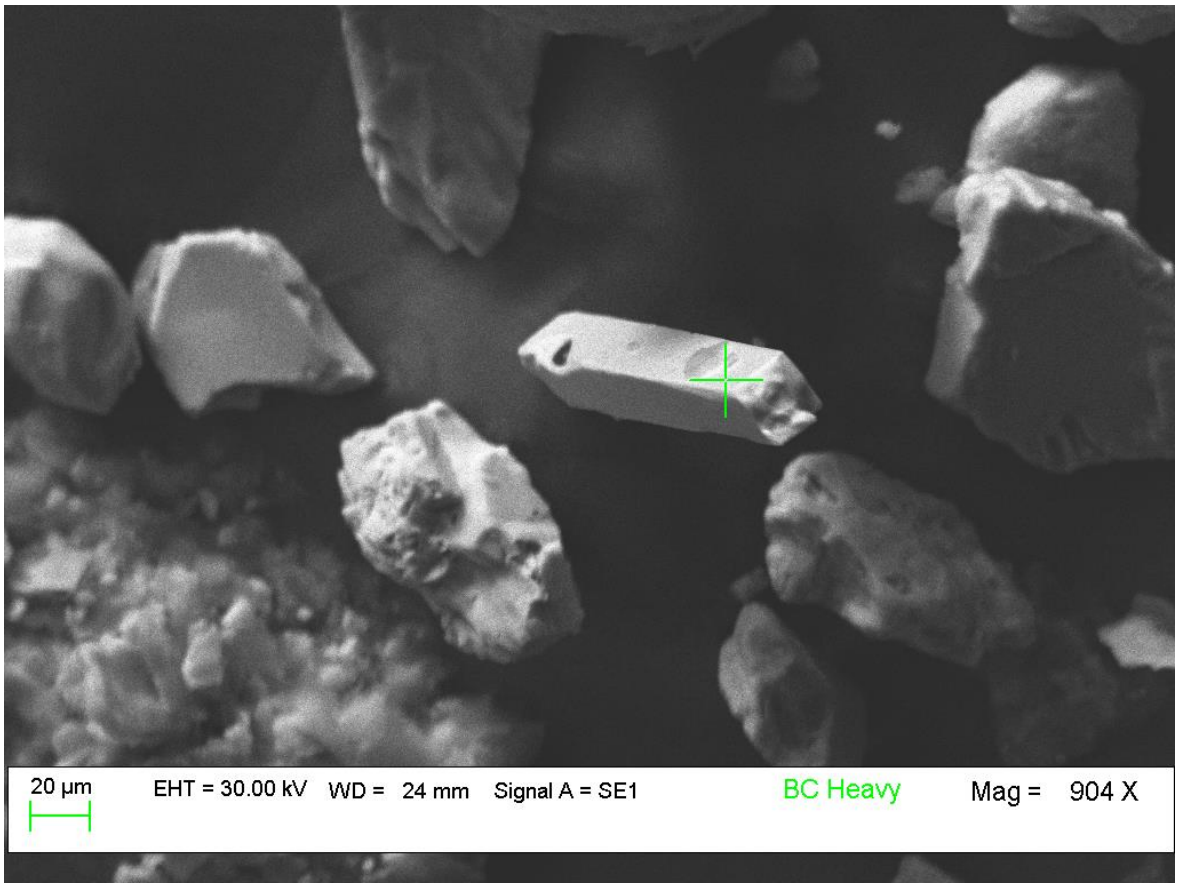
20 µm
EHT = 30.00 kV
WD = 24 mm
Signal A = SE1
BC Heavy
Mag = 904 X

SEM 13

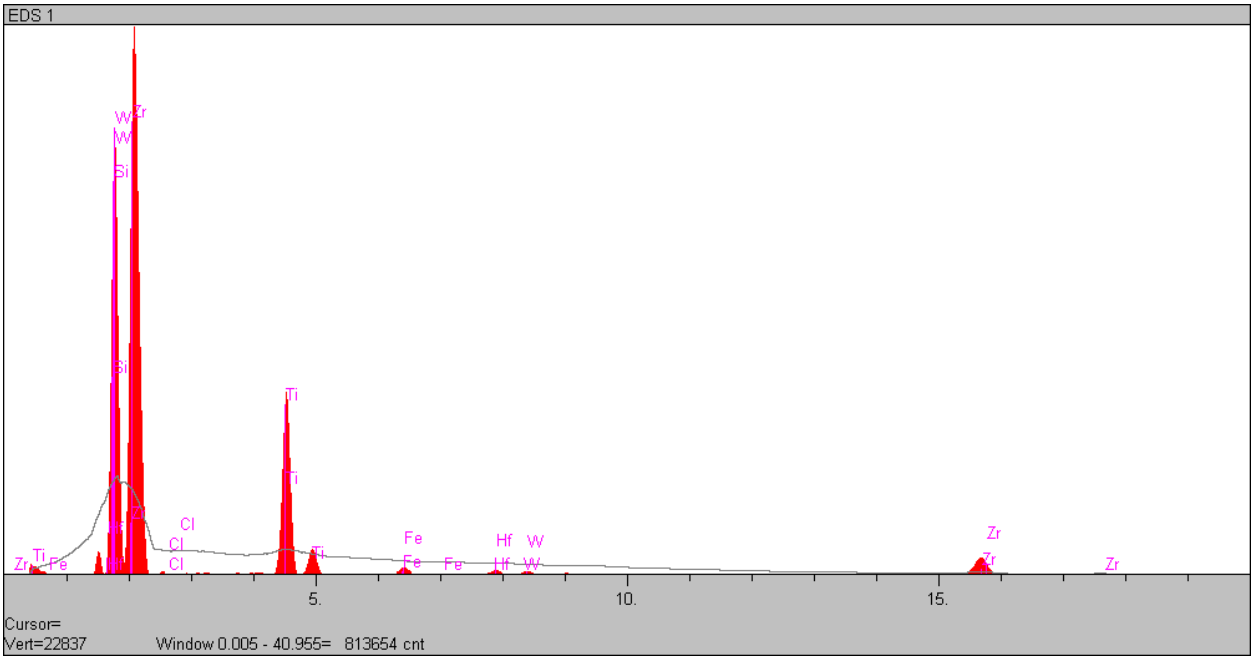
EDS 1
Zr
W
W
Si
Si
Ti
Ti
Cl
Cl
Cl
Fe
Fe
Fe
Hf
Hf
W
W
Zr
Zr
Zr
Ti
Zr
Fe
5.
10.
15.
Cursor=
Vert=22837
Window 0.005 - 40.955= 813654 cnt

SEM 13

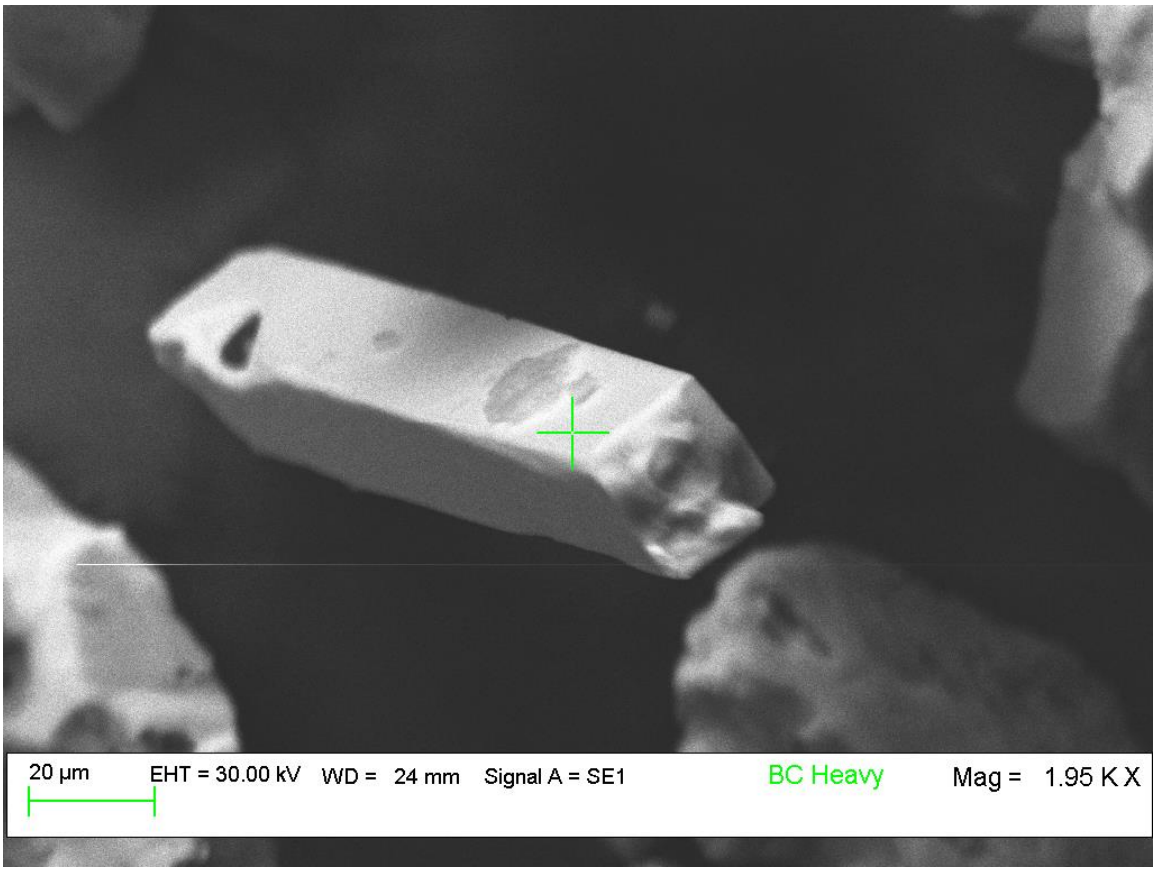
20 µm
EHT = 30.00 kV
WD = 24 mm
Signal A = SE1
BC Heavy
Mag = 1.95 K X

SEM 14

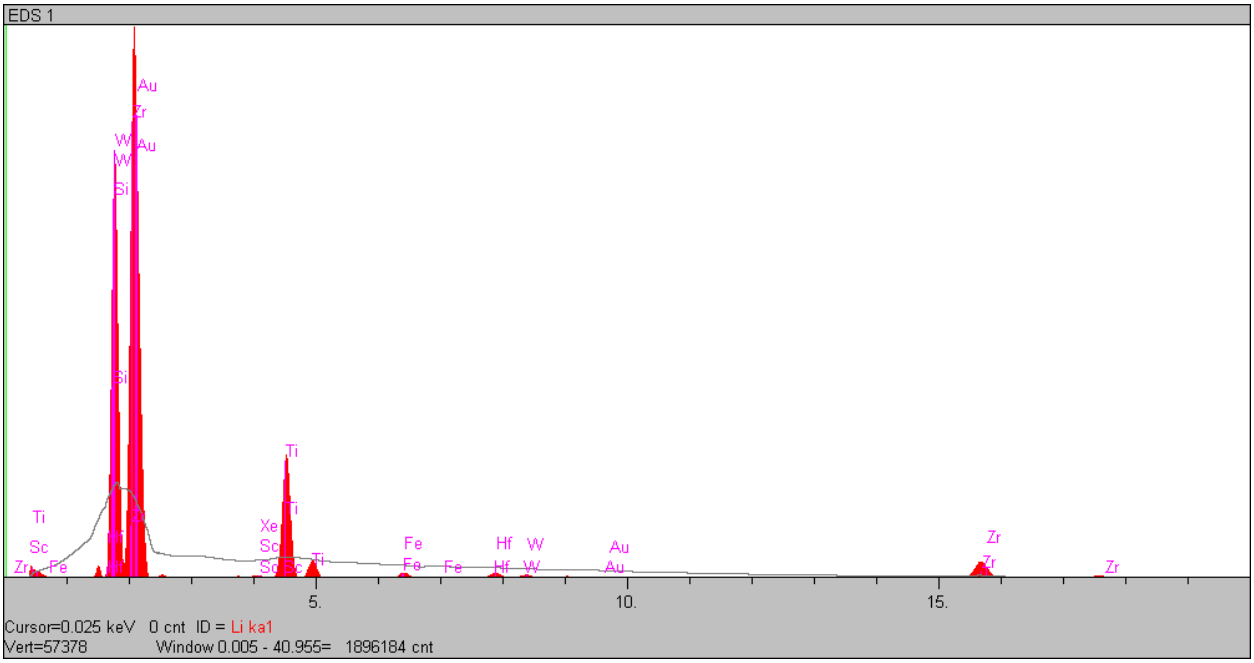
EDS 1
Au
Zr
W
Au
W
Si
Si
Ti
Ti
Sc
Zr
Pe
Xe
Sc
Ti
Fe
Fe
Fe
Hf
W
Hf
W
Au
Au
Zr
Zr
Zr
5.
10.
15.
Cursor=0.025 keV 0 cnt ID = Li ka1
Vert=57378
Window 0.005 - 40.955= 1896184 cnt

SEM 14

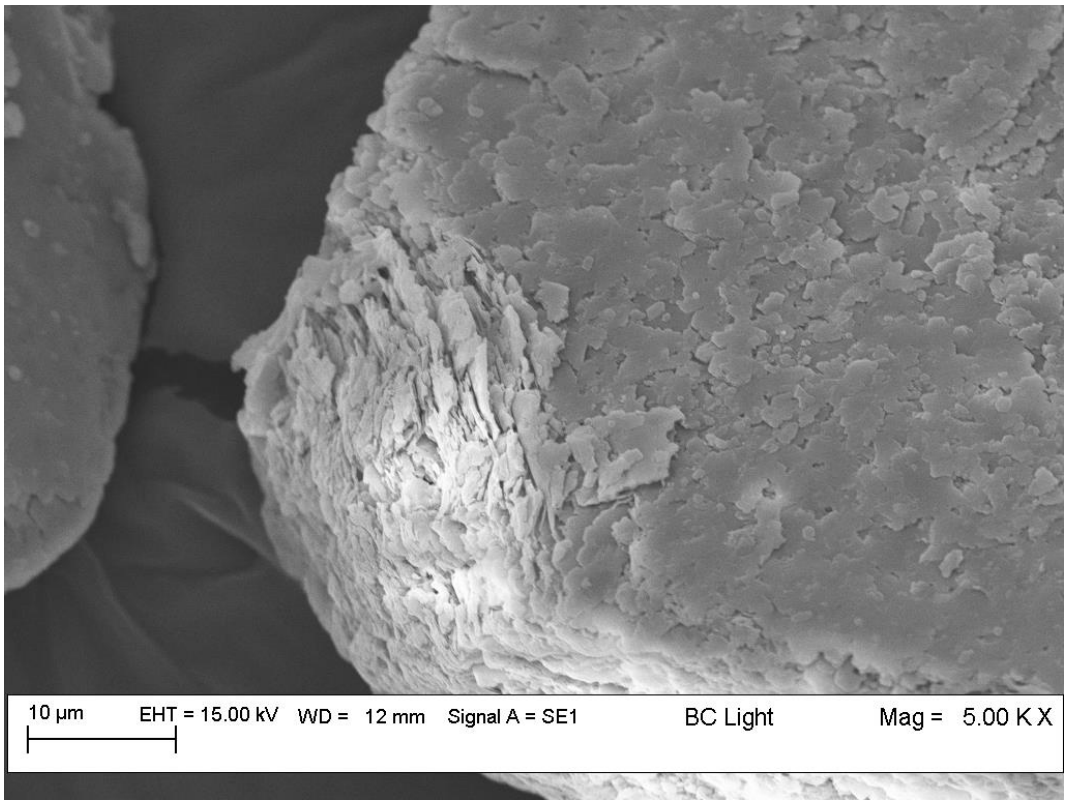

BC Light SEM 1

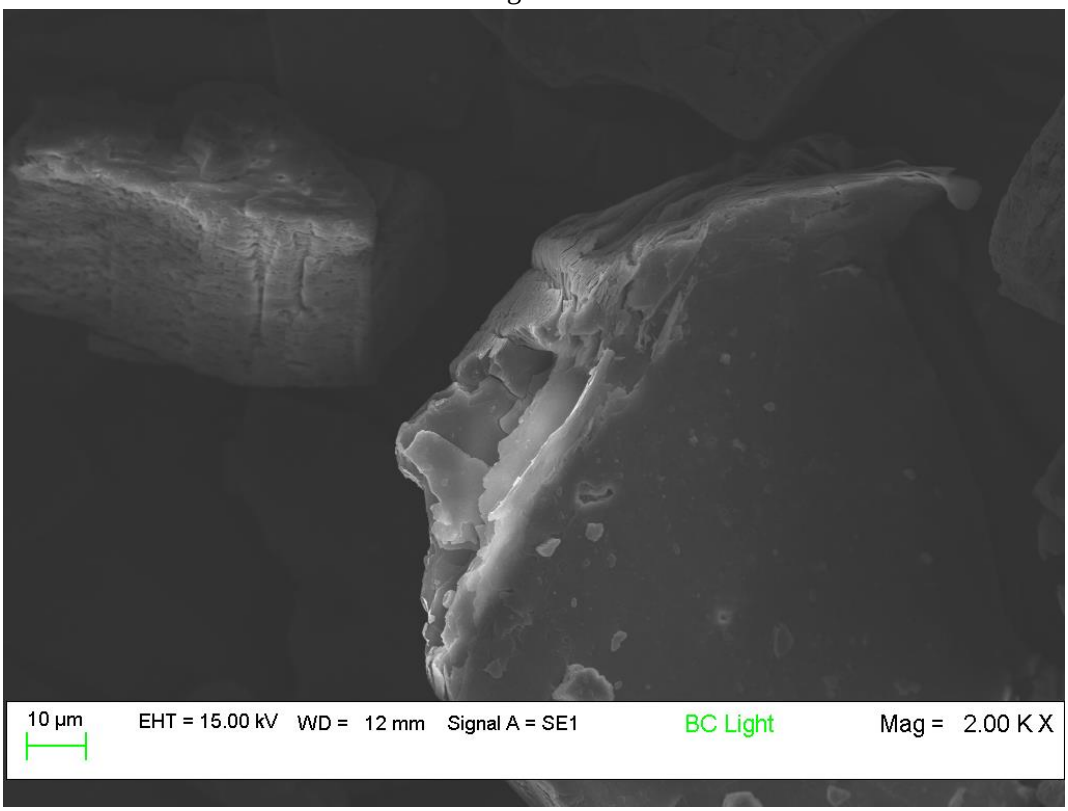

BC Light SEM 2

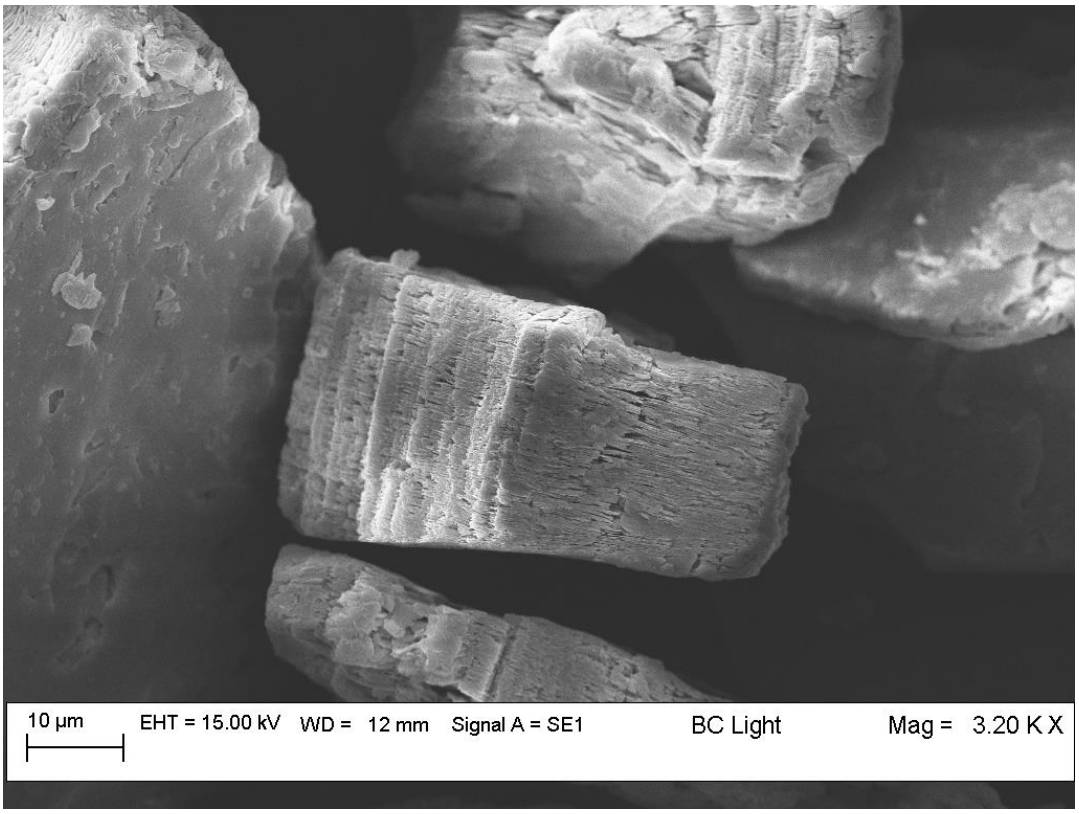

BC Light SEM 3

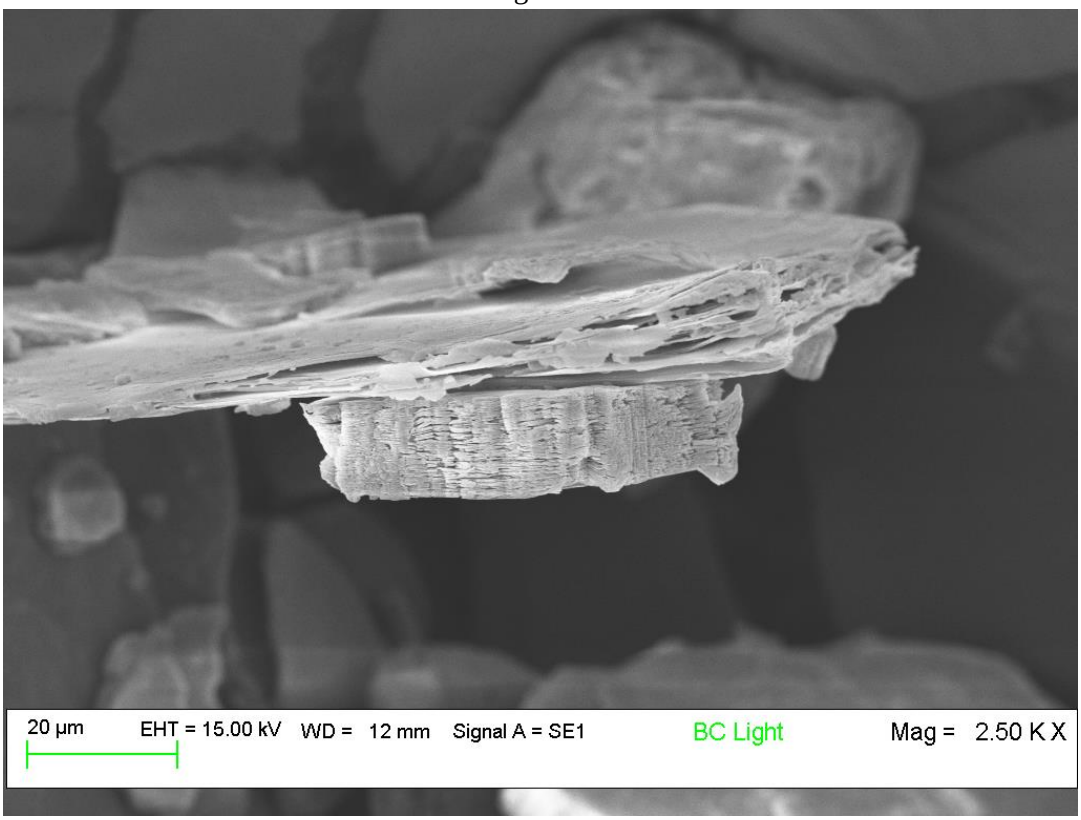

BC Light SEM 4

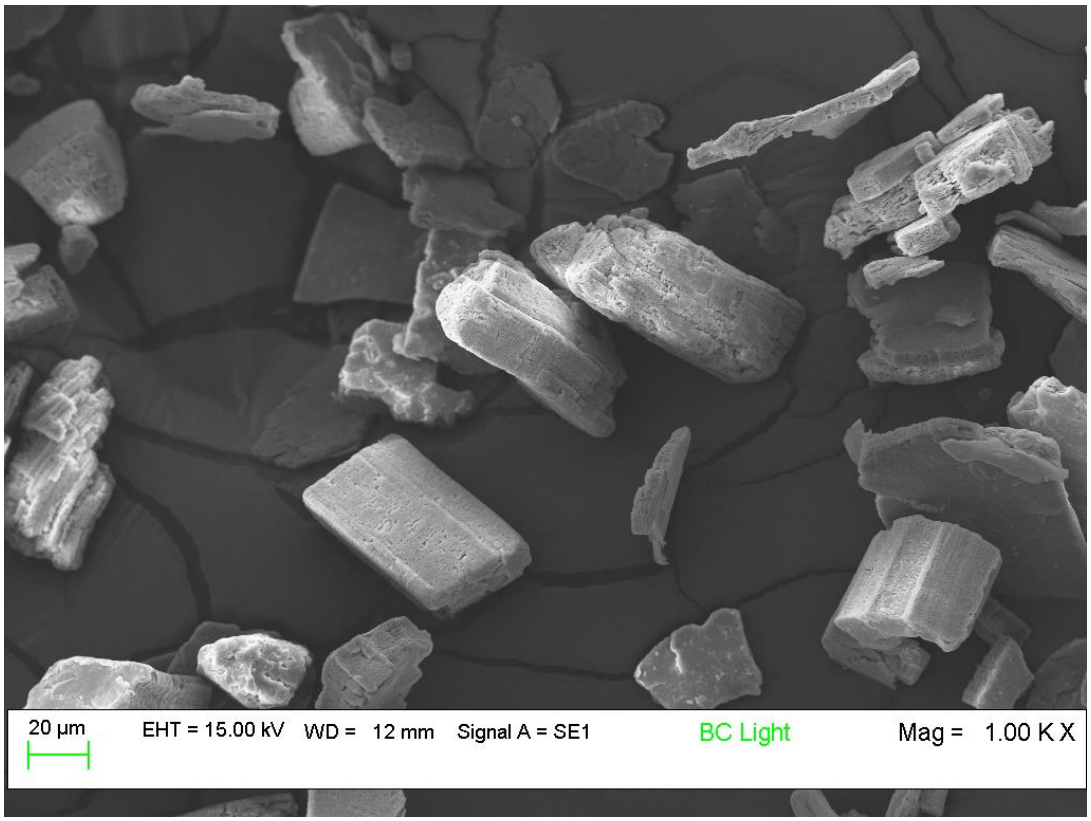

BC Light SEM 5

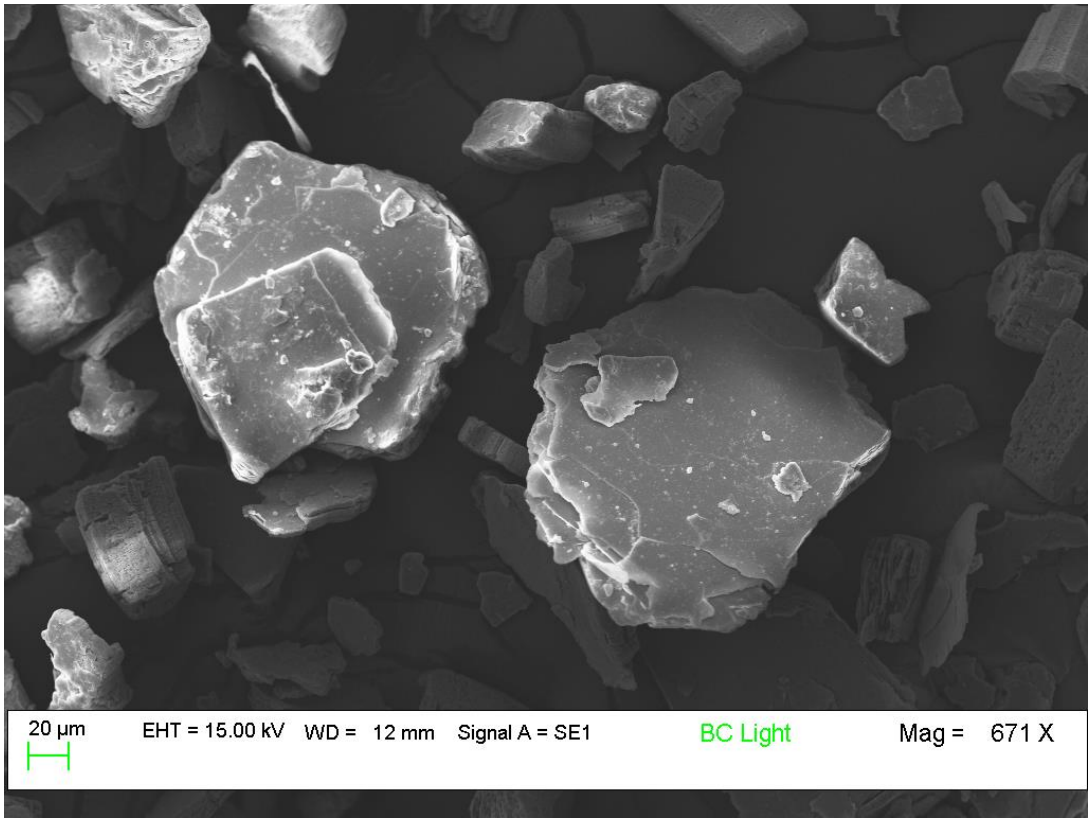

BC Light SEM 6

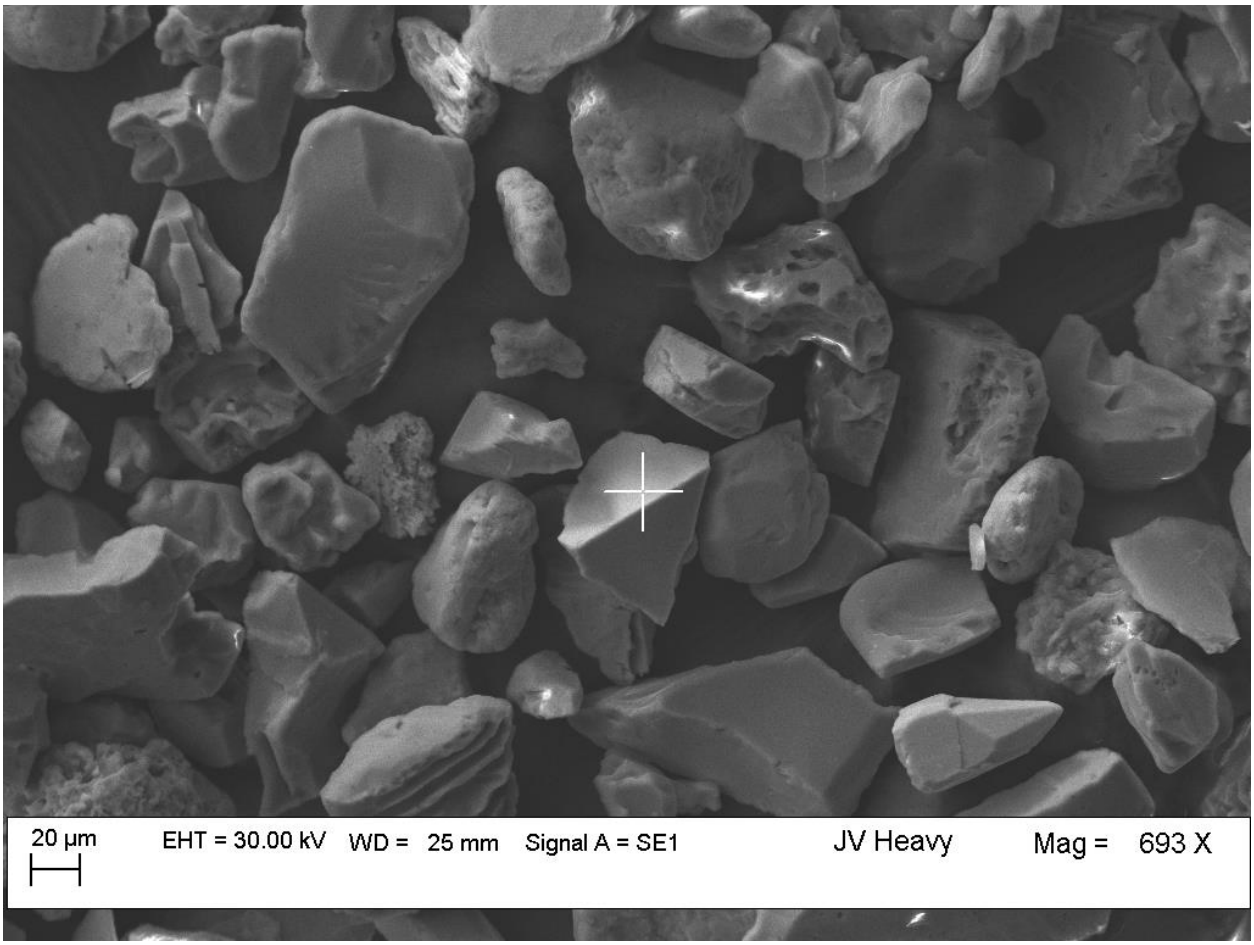

SEM JV 1

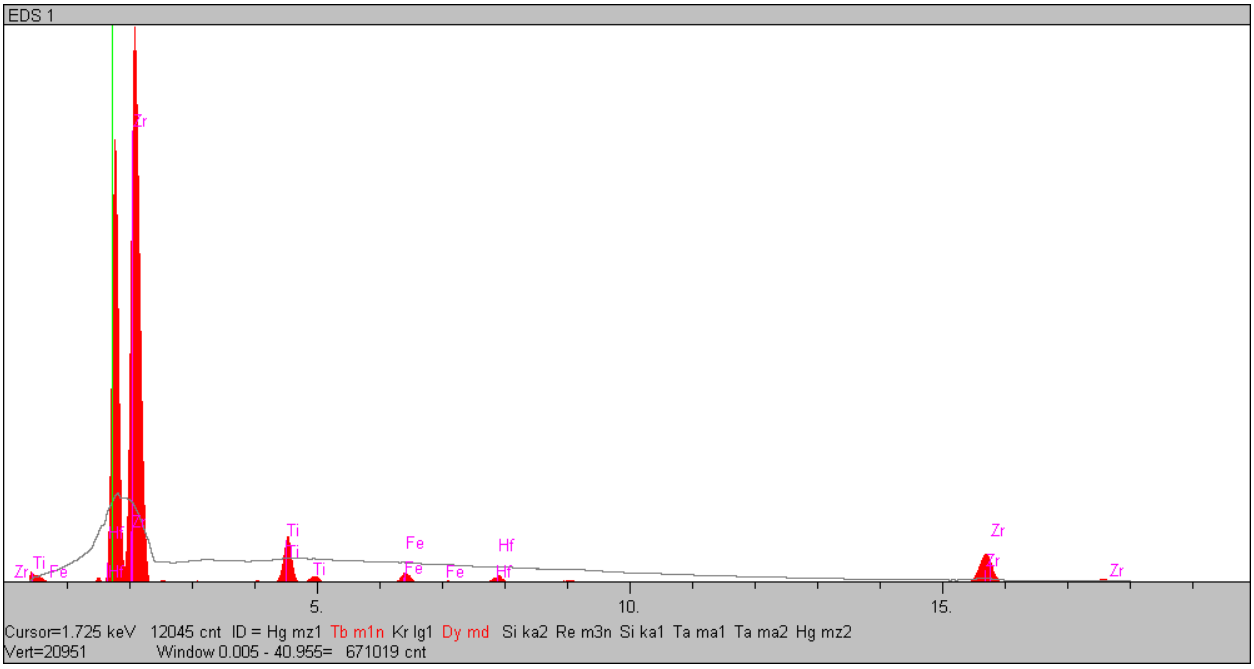

SEM JV 1

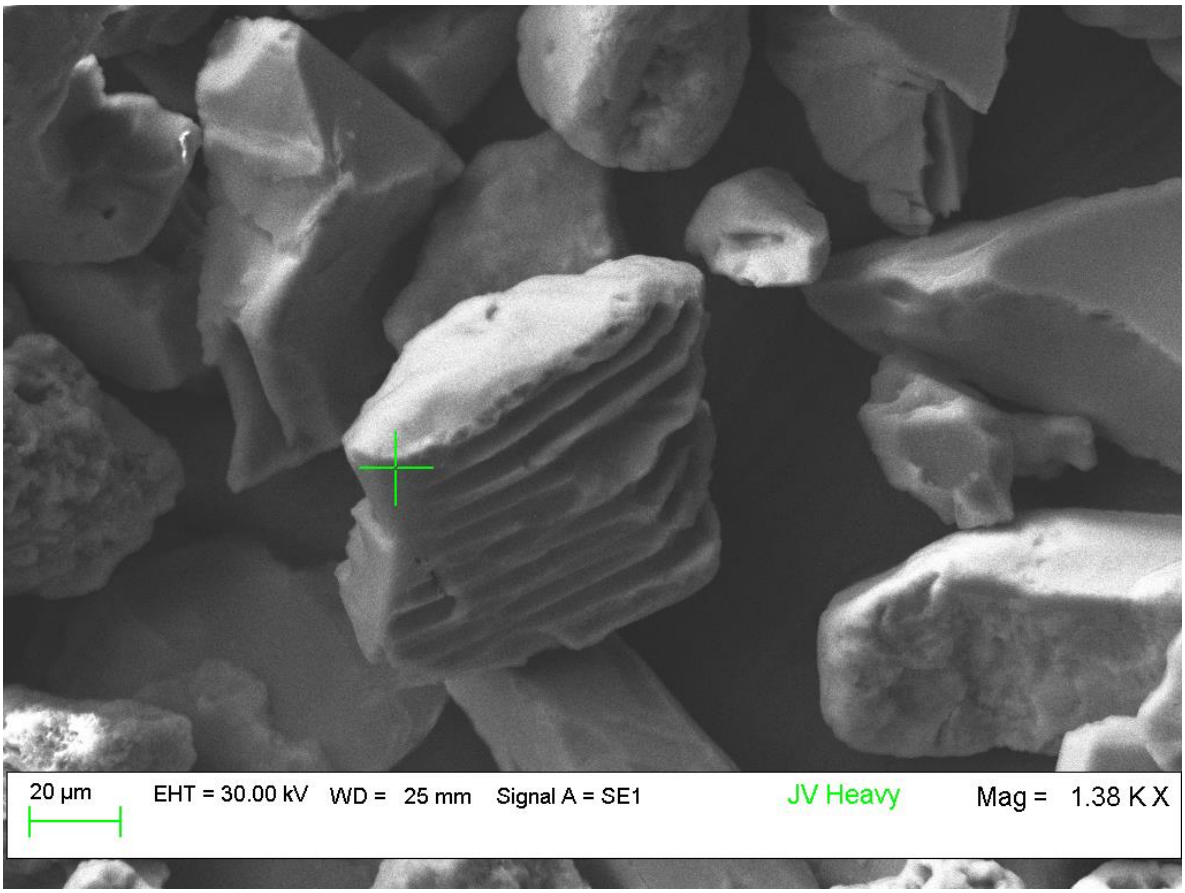

SEM JV 2

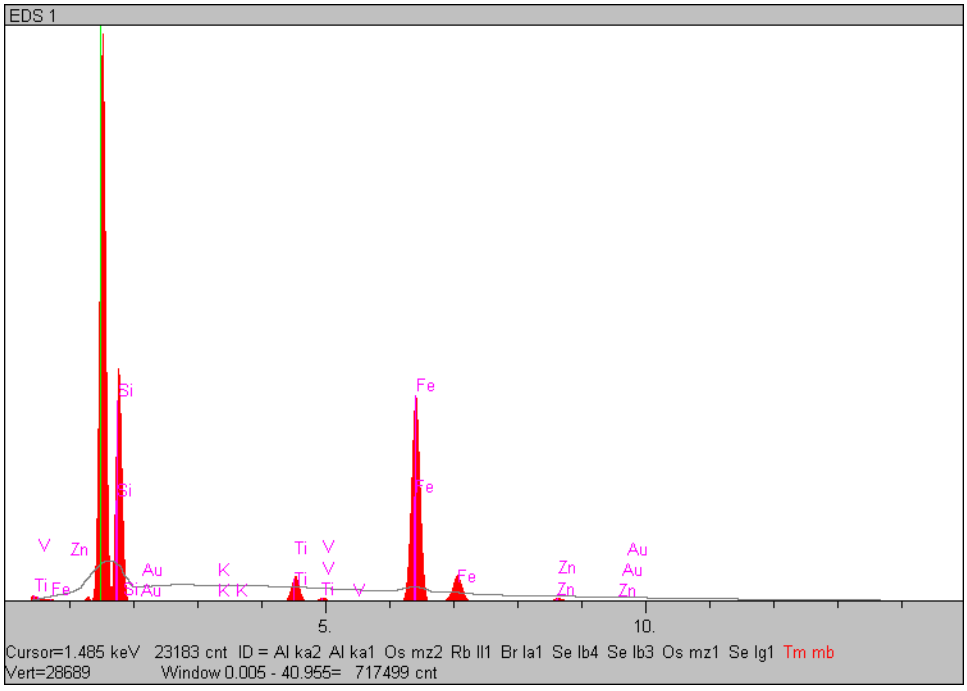

SEM JV 2

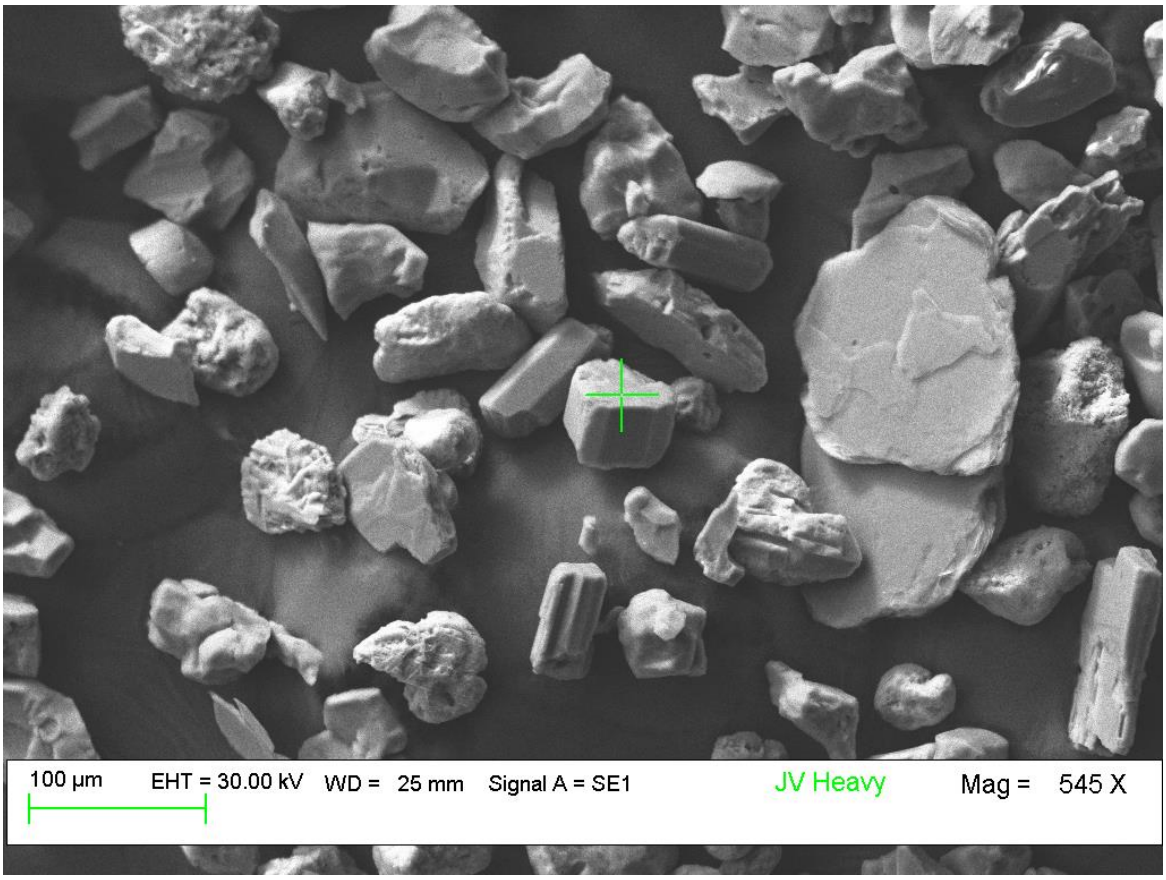

SEM JV 3

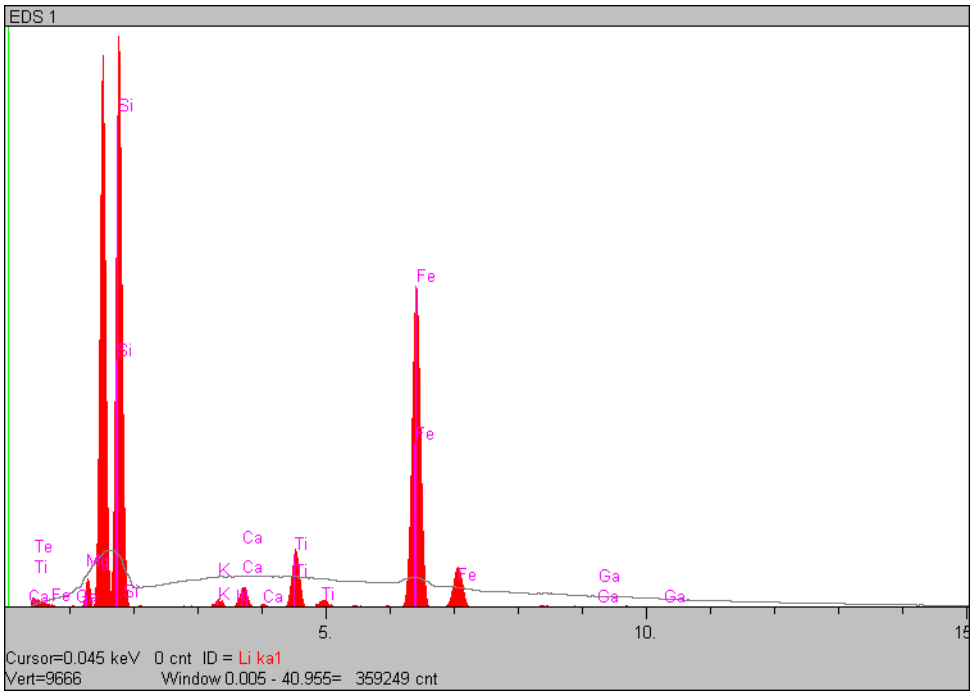

SEM JV 3

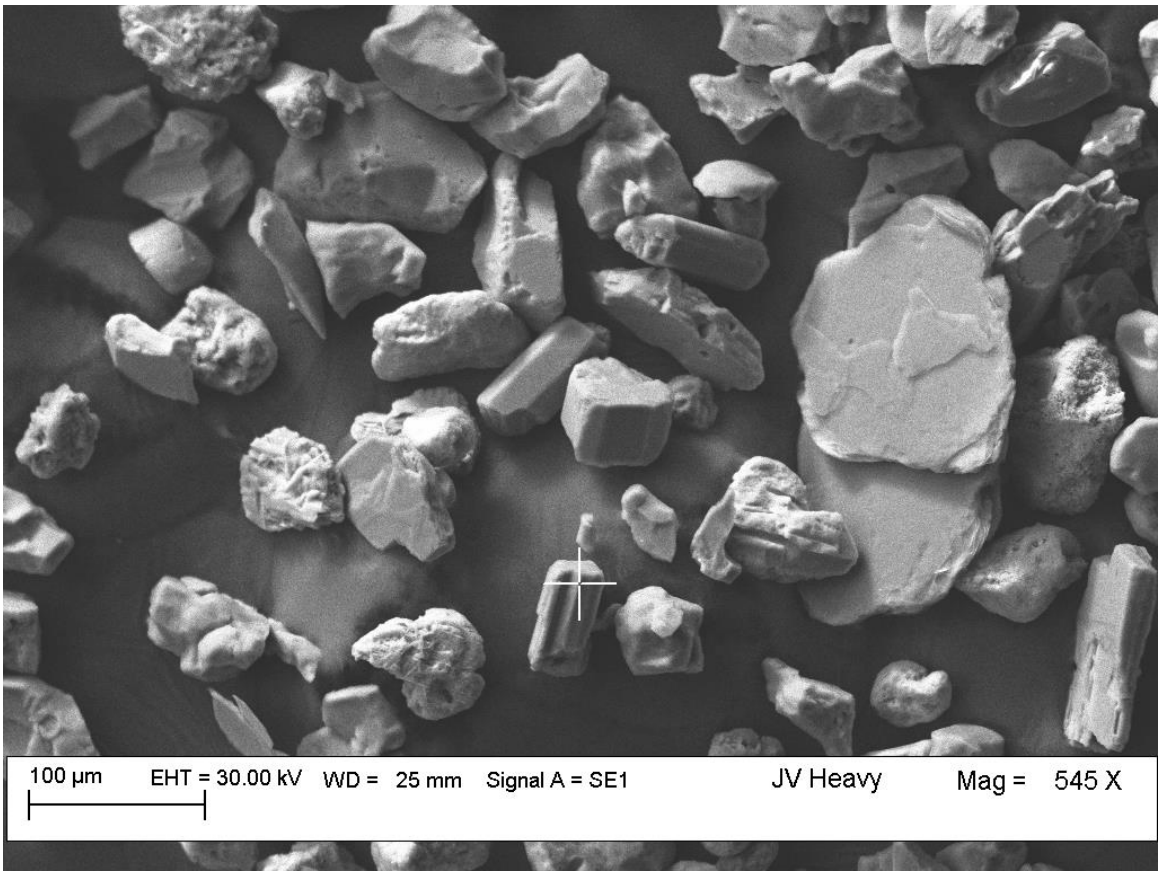

SEM JV 4

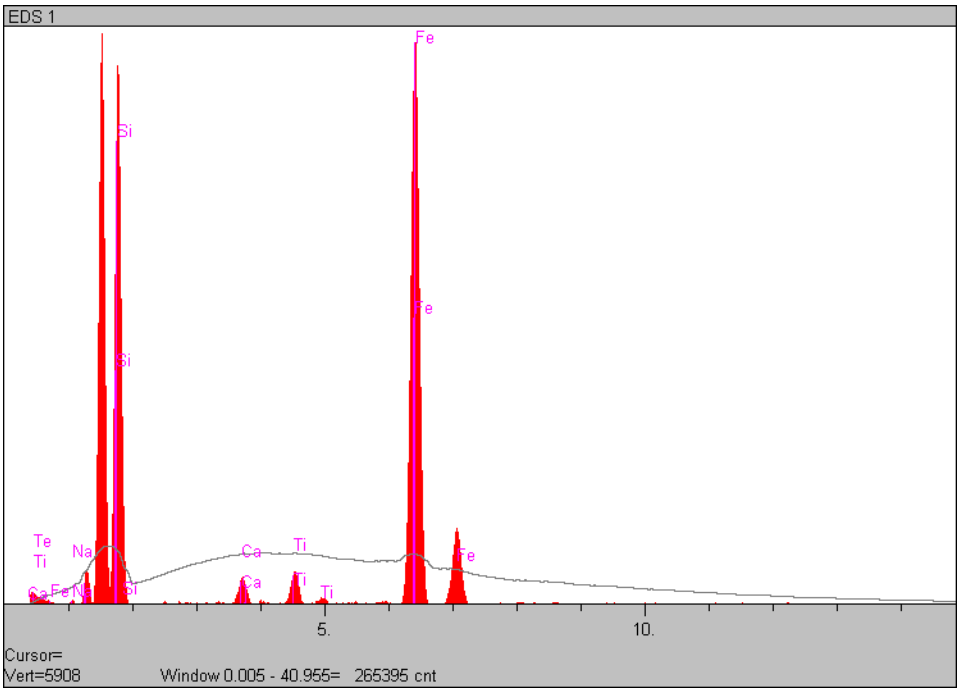

SEM JV 4

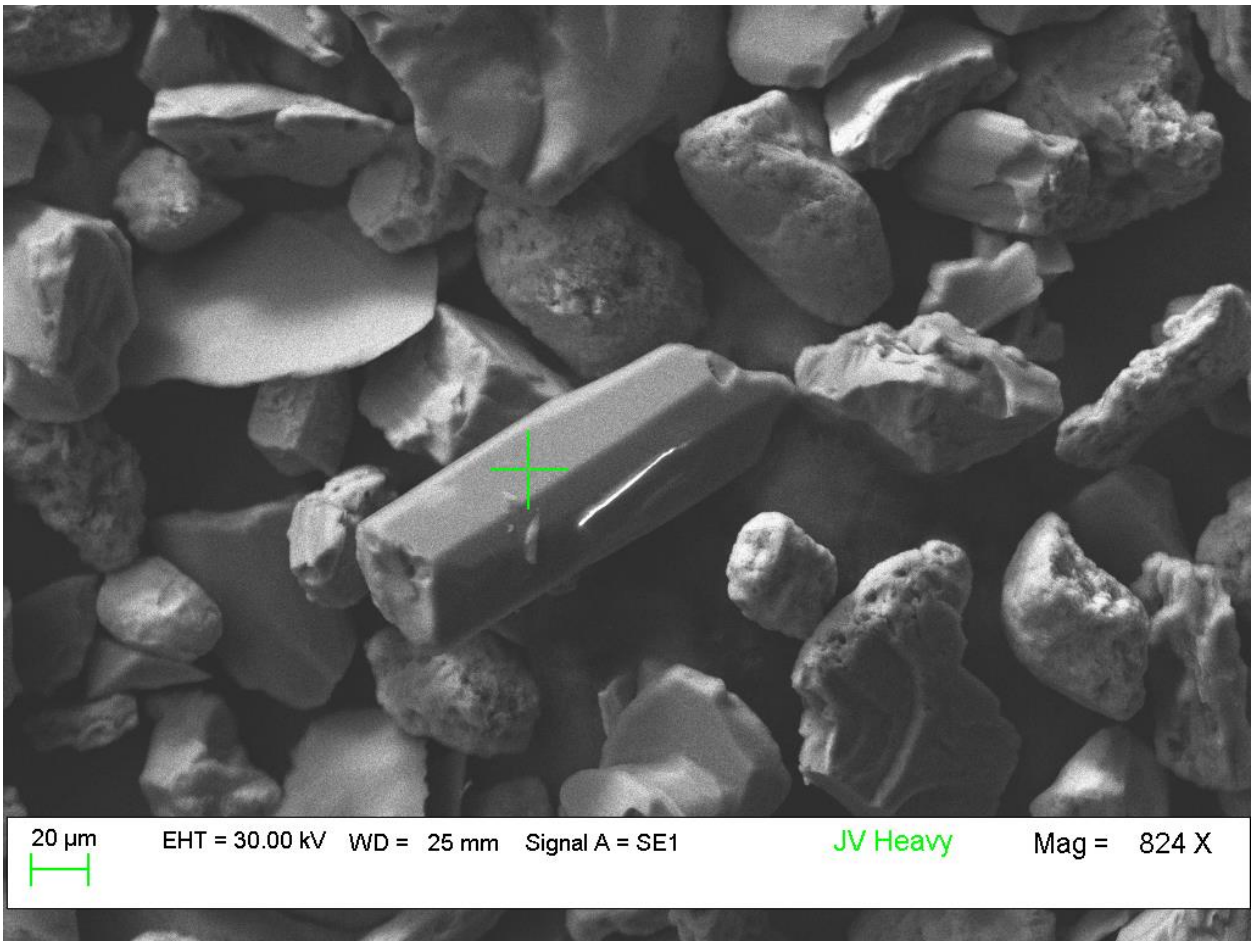

SEM JV 5

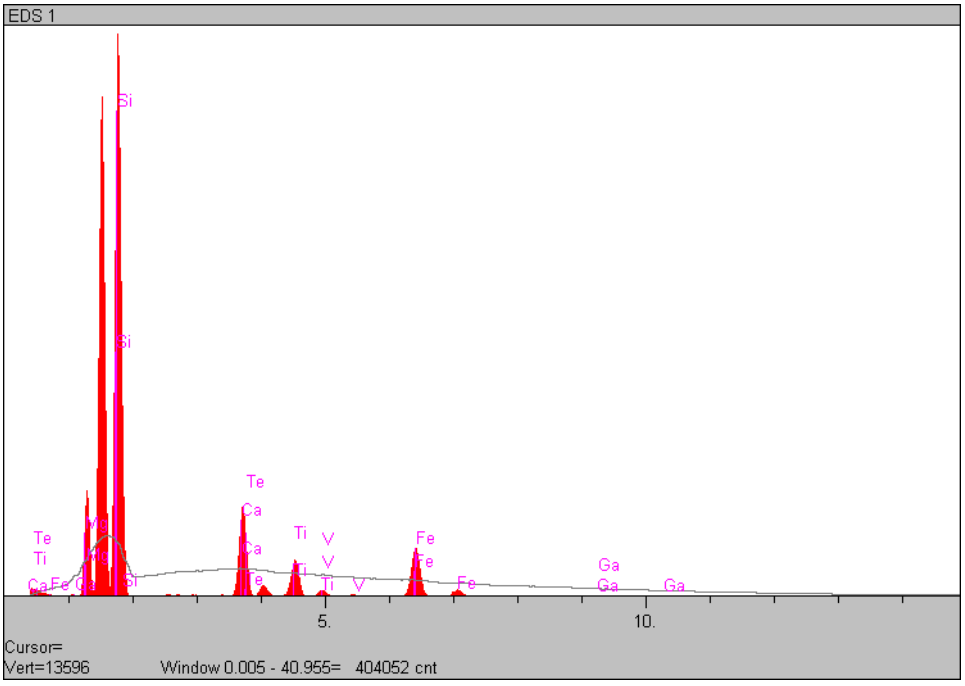

SEM JV 5

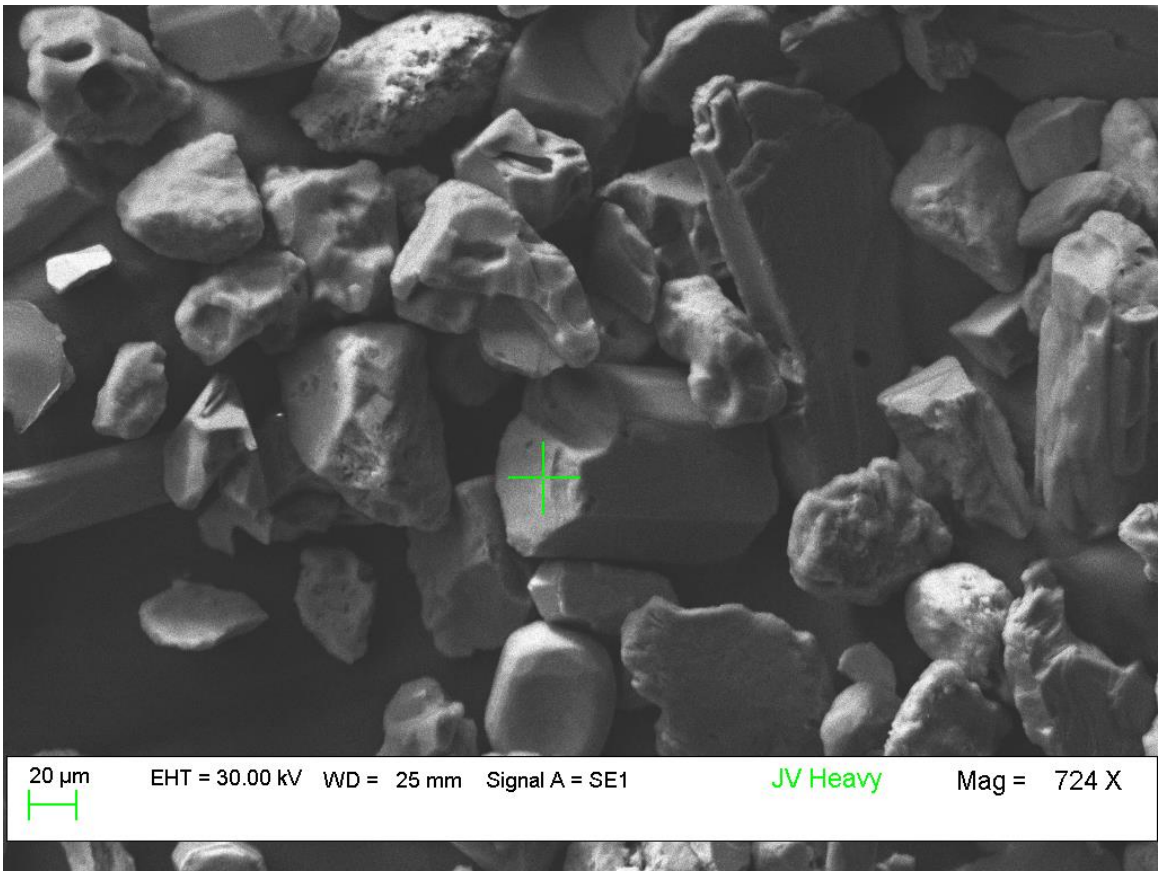

SEM JV 6

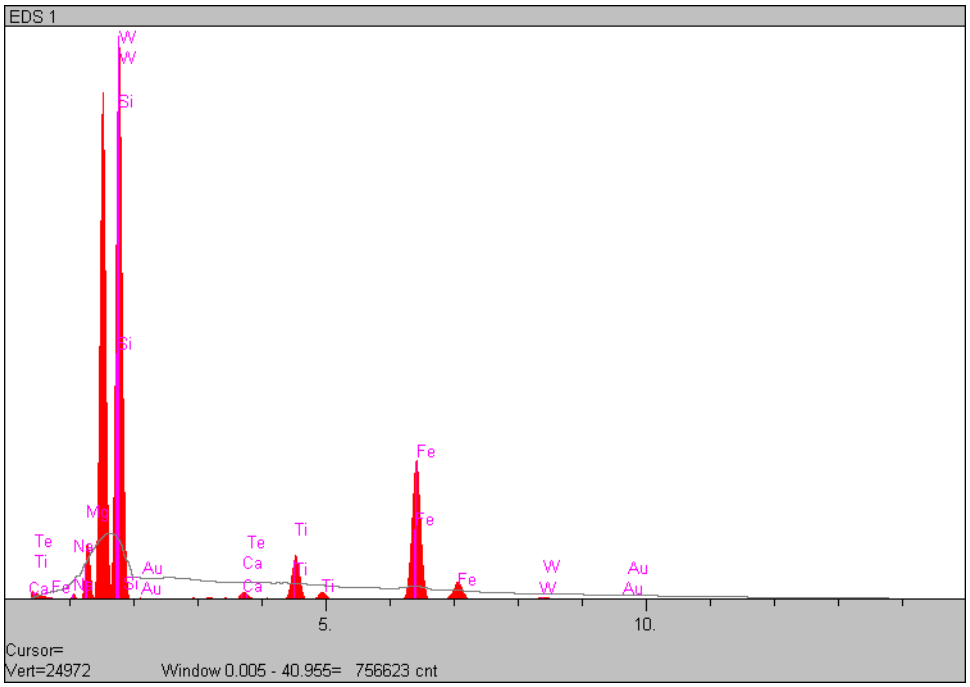

SEM JV 6

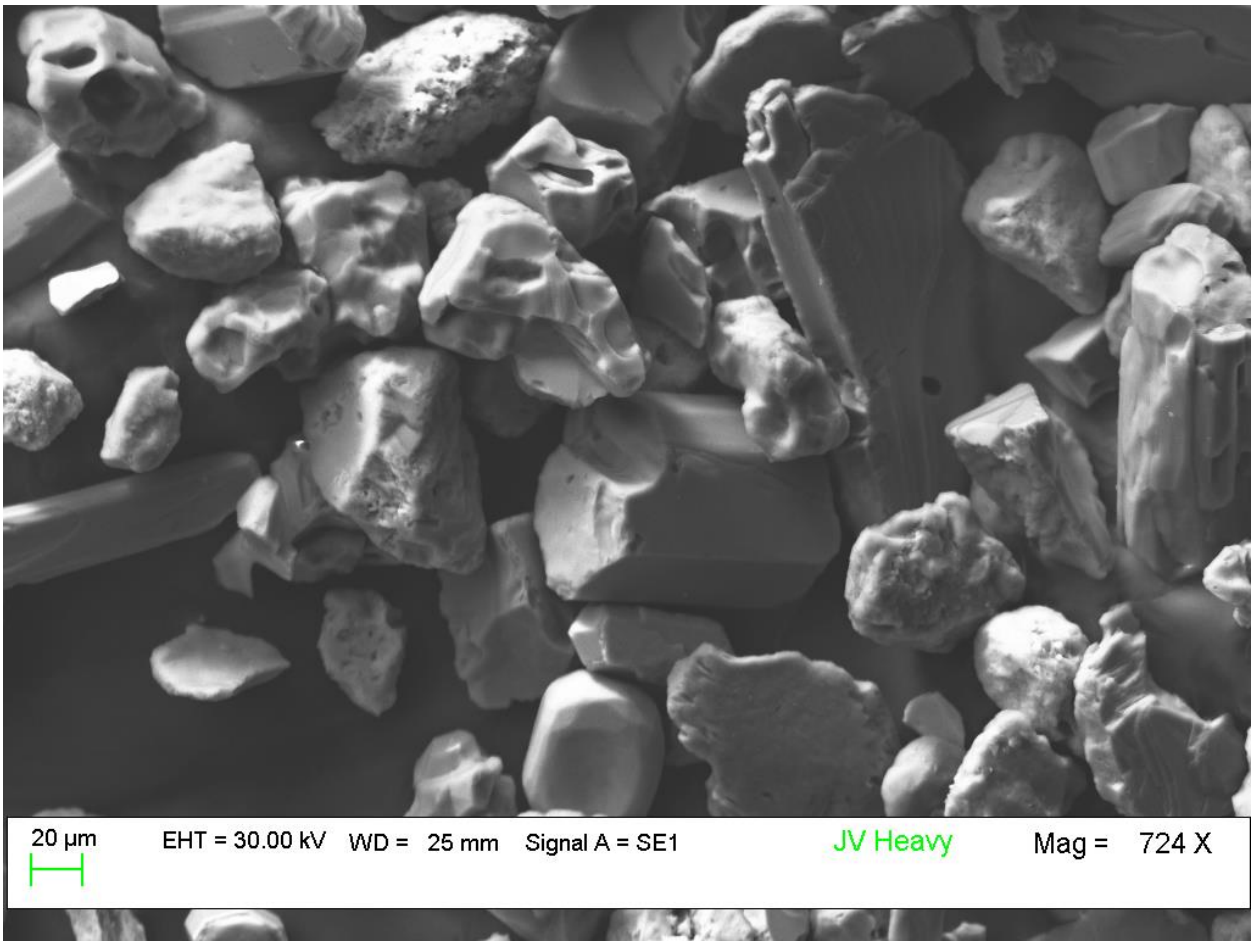

SEM JV 7

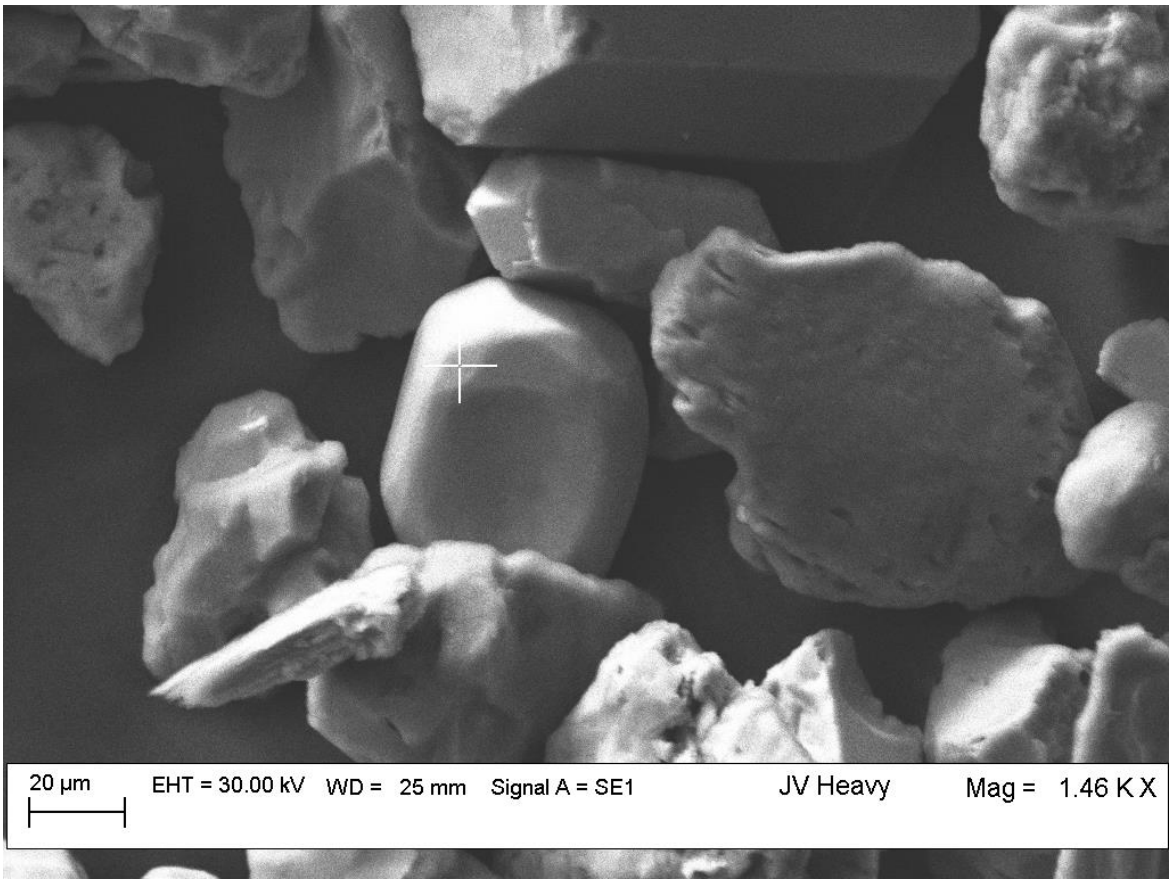

SEM JV 8

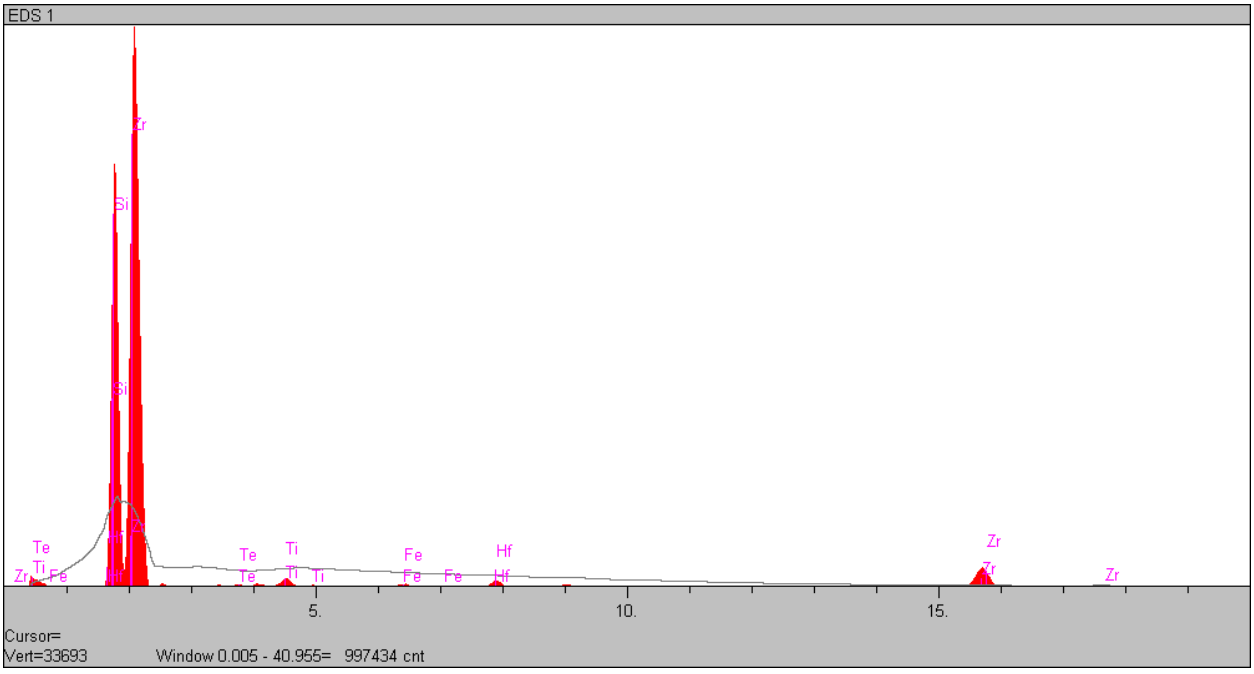

SEM JV 8

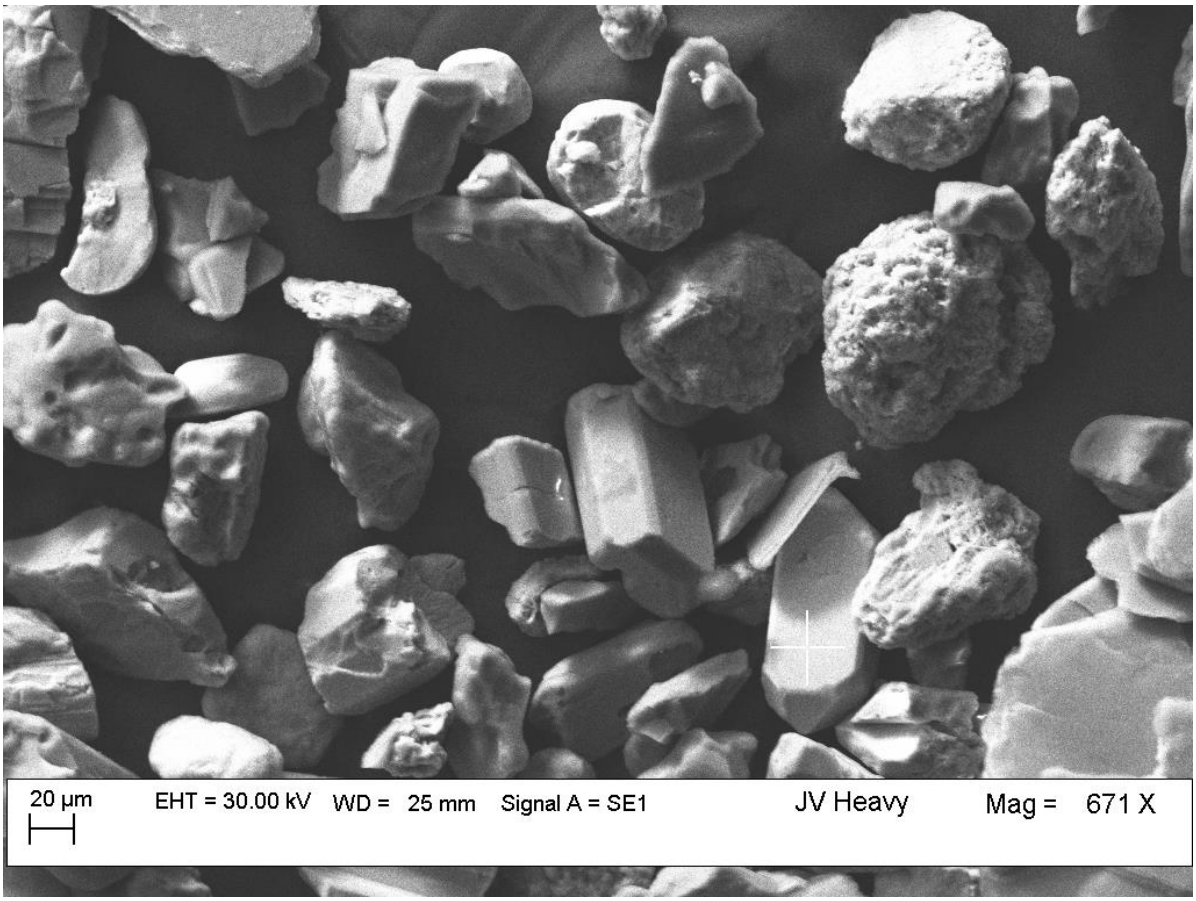

SEM JV 9

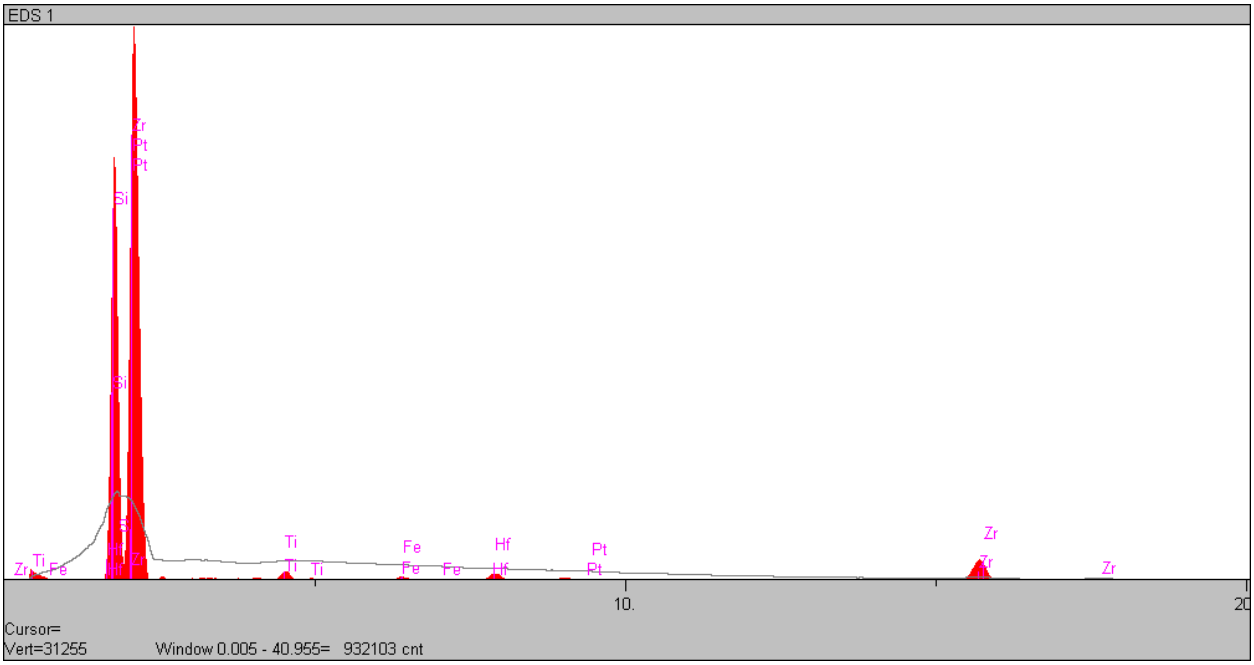

SEM JV 9

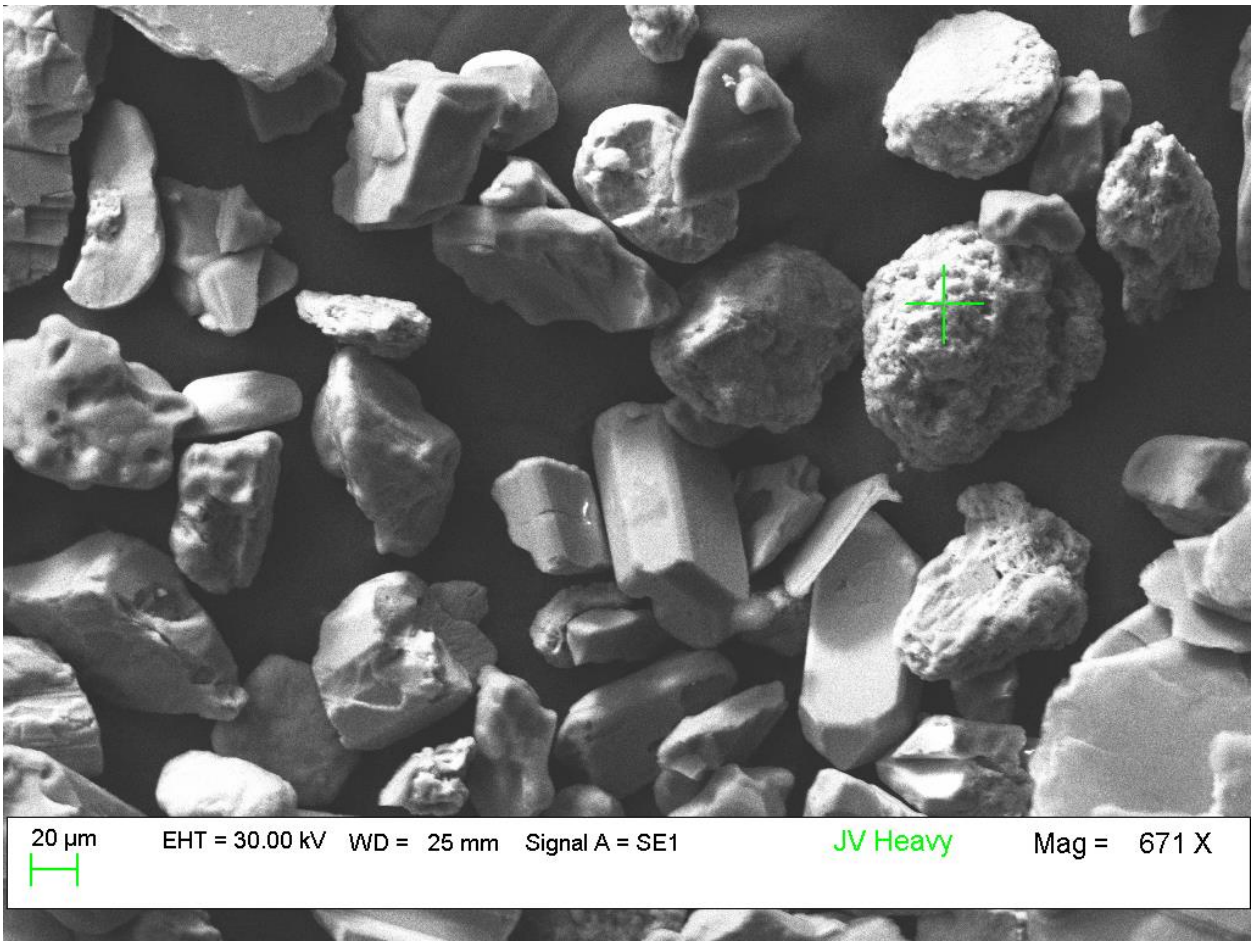

SEM JV 10

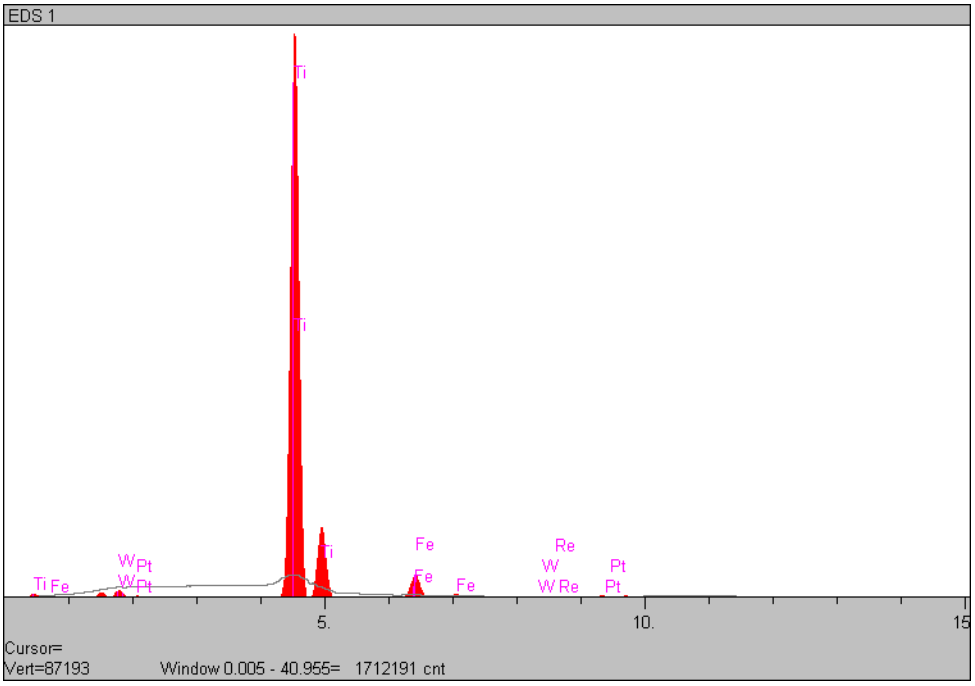

SEM JV 10

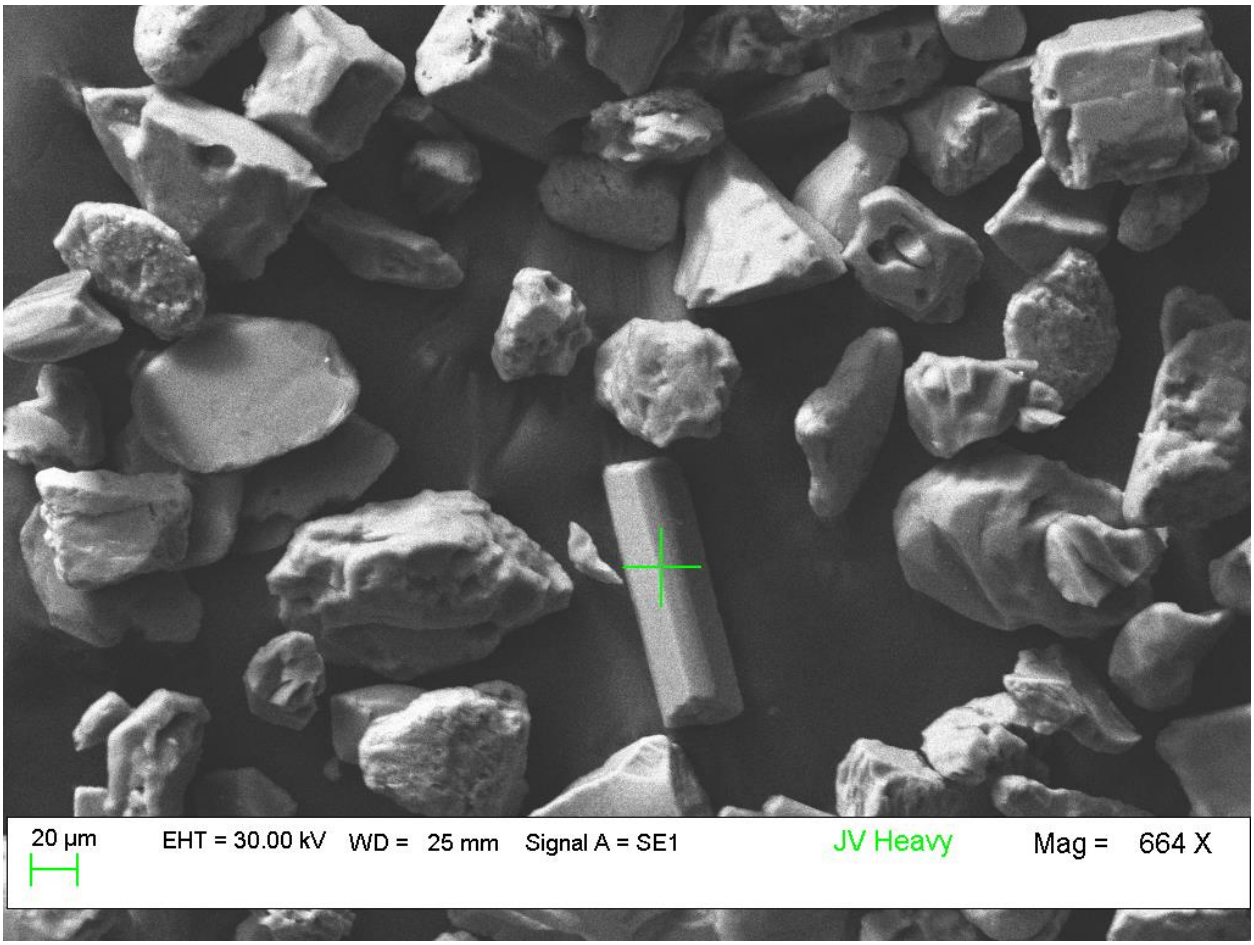

SEM JV 11

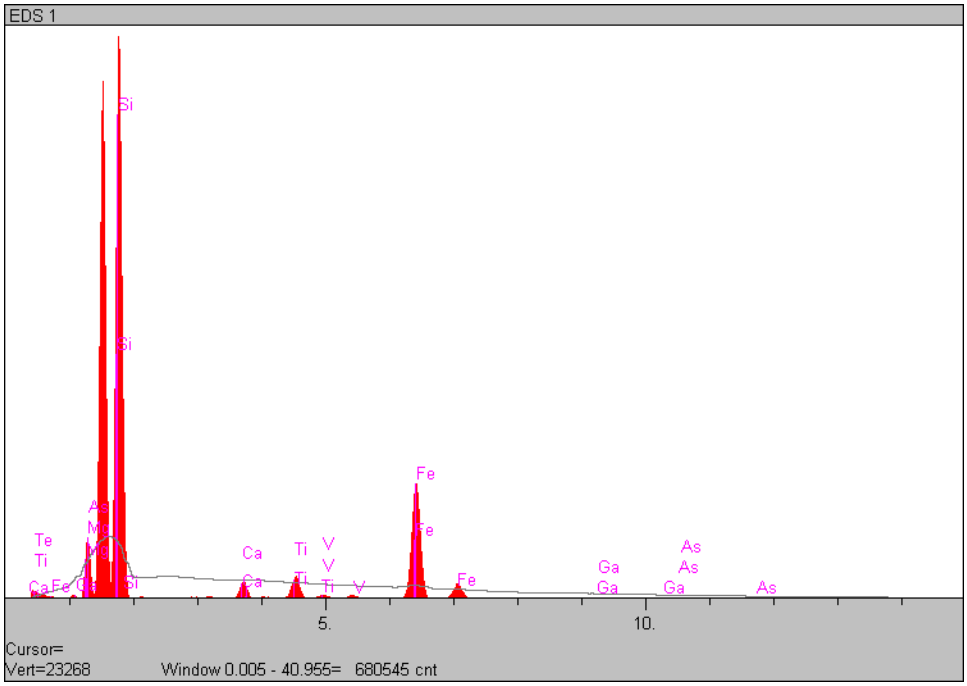

SEM JV 11

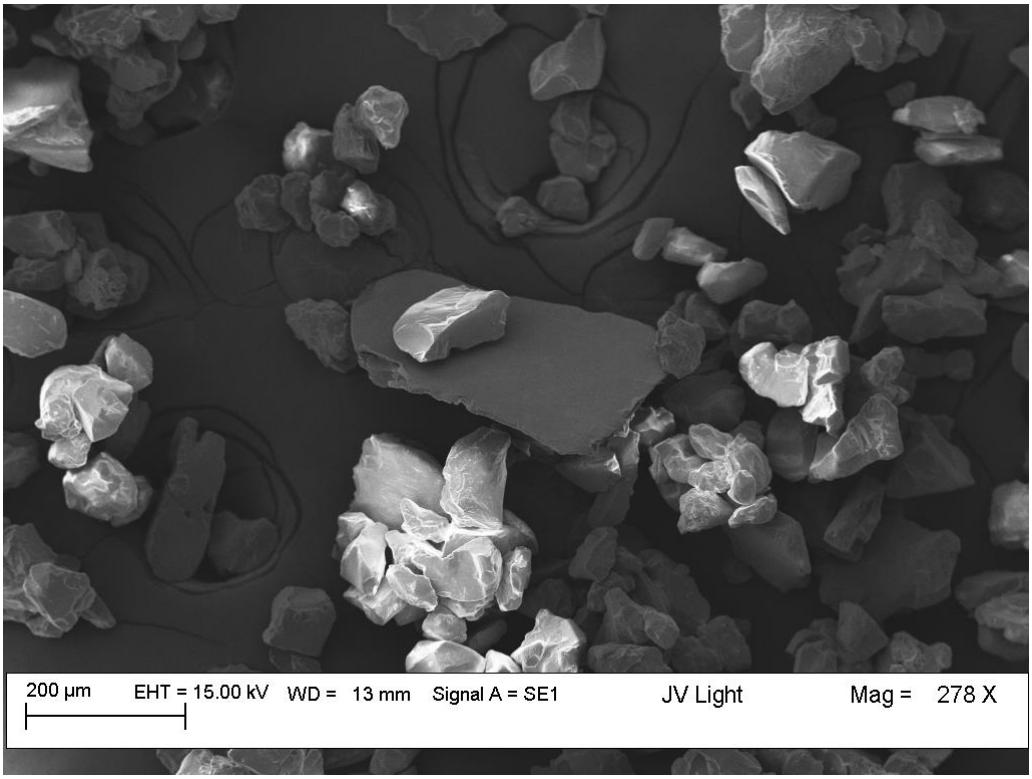

SEM JV Light 1

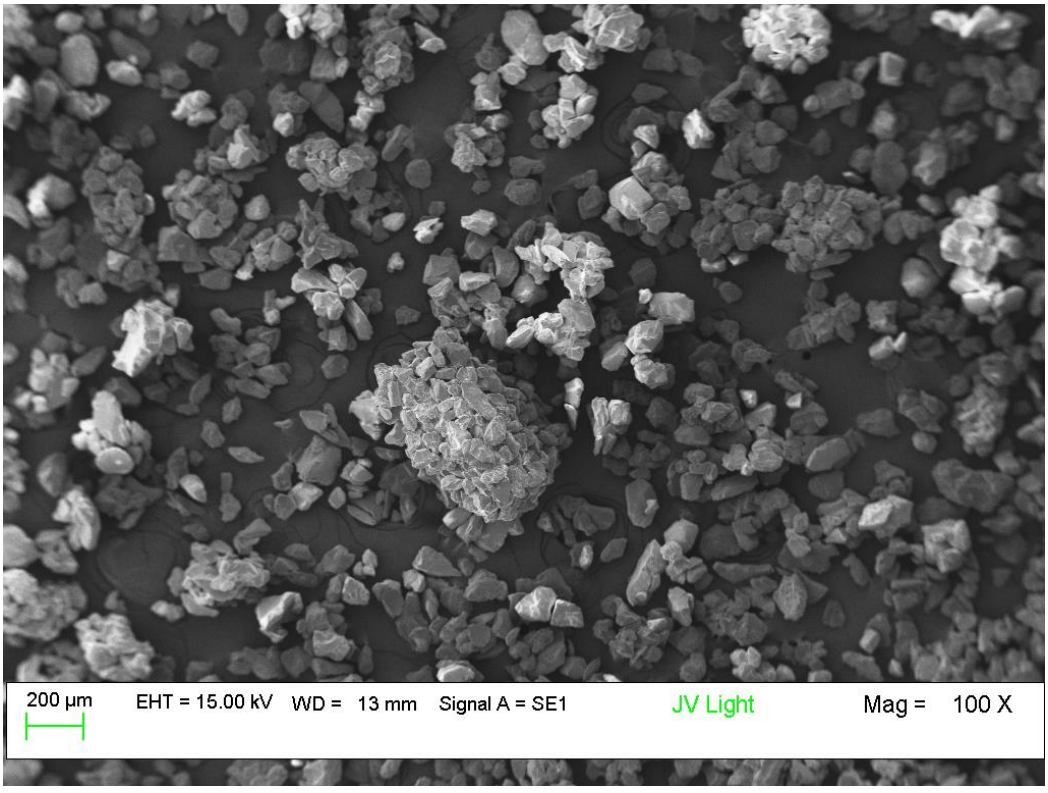

SEM JV Light 2

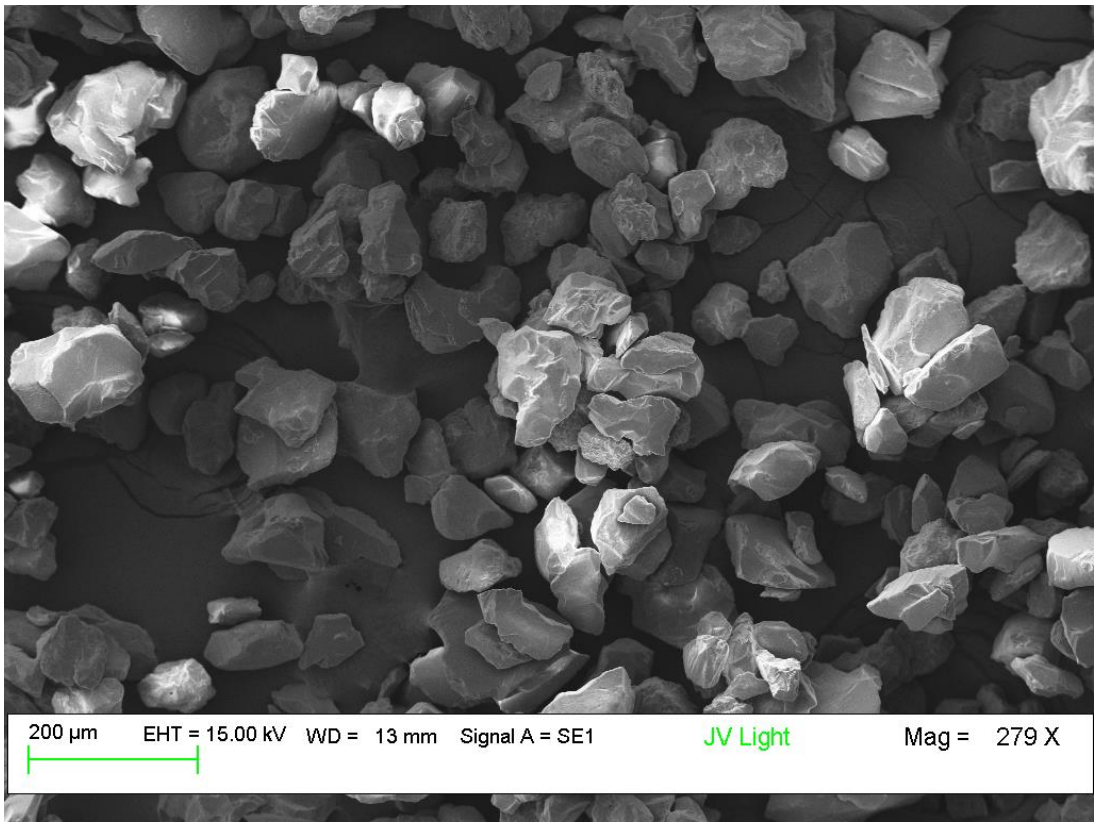

SEM JV Light 3